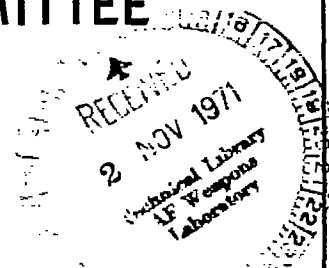# NACA

RESEARCH MEMORANDUM

CALCULATION OF FLUTTER CHARACTERISTICS FOR FINITE-SPAN

SWEPT OR UNSWEPT WINGS AT SUBSONIC AND SUPERSONIC

SPEEDS BY A MODIFIED STRIP ANALYSIS

By E. Carson Yates, Jr.

Langley Aeronautical Laboratory
Langley Field, Va.

NATIONAL ADVISORY COMMITTEE
FOR AERONAUTICS
WASHINGTON

ERRATA

NACA Research Memorandum L57L10

By E. Carson Yates, Jr.
March 1958

Page 63 (table I(a) - Concluded):

For Wing 430:
Under column heading $\frac{\omega}{\omega_\alpha}$:

Fourth row, for $M = 1.15470$, change .511 to .565
Sixth row, for $M = 1.41421$, change .680 to .696

For Wing 400:
Under column heading $\frac{V}{V_R}$:

Sixth row, for $M = 1.41421$, change 4.100 to 4.765

Under column heading $\frac{\omega}{\omega_\alpha}$:

Fourth row, for $M = 1.15470$, change .753 to .690

Corresponding to these changes in table I(a), changes in figures 10, 21, and 22 should be made as follows:

Page 76: In figure 10, the square symbol plotted for $M = 1.414$ at $V/V_R = 4.100$ should be at $V/V_R = 4.765$. (The fairing for the calculated curve would change accordingly.)

Page 87: In figure 21, the square symbol for $M = 1.155$ at $\omega/\omega_\alpha = 0.511$ should be at $\omega/\omega_\alpha = 0.565$, and the square symbol for $M = 1.414$ at $\omega/\omega_\alpha = 0.680$ should be at $\omega/\omega_\alpha = 0.696$. (The fairing for the calculated curve would change accordingly.)

Page 88: In figure 22, the square symbol plotted for $M = 1.155$ at $\omega/\omega_\alpha = 0.753$ should be at $\omega/\omega_\alpha = 0.690$. (The fairing for the calculated curve would change accordingly.)

Page 92: In figure 26, the circular (experimental) test point plotted for $M = 0.839$ at $\omega/\omega_\alpha = 0.208$ should be at $\omega/\omega_\alpha = 0.344$.

NATIONAL ADVISORY COMMITTEE FOR AERONAUTICS

RESEARCH MEMORANDUM

CALCULATION OF FLUTTER CHARACTERISTICS FOR FINITE-SPAN

SWEPT OR UNSWEPT WINGS AT SUBSONIC AND SUPERSONIC

SPEEDS BY A MODIFIED STRIP ANALYSIS

By E. Carson Yates, Jr.

SUMMARY

A method has been developed for calculating flutter characteristics of finite-span swept or unswept wings at subsonic and supersonic speeds. The method is basically a Rayleigh type analysis and is illustrated with uncoupled vibration modes although coupled modes can be used. The aerodynamic loadings are based on distributions of section lift-curve slope and local aerodynamic center calculated from three-dimensional steady-flow theory. These distributions are used in conjunction with the "effective" angle-of-attack distribution resulting from each of the assumed vibration modes in order to obtain values of section lift and pitching moment. Circulation functions modified on the basis of loadings for two-dimensional airfoils oscillating in a compressible flow are employed to account for the effects of oscillatory motion on the magnitudes and phase angles of the lift and moment vectors.

Flutter characteristics have been calculated by this method for 12 wings of varying sweep angle, aspect ratio, taper ratio, and center-of-gravity position at Mach numbers from 0 to as high as 1.75. Comparisons of the results with experimental flutter data indicate that this method gives generally good flutter results for a broad range of wings.

INTRODUCTION

Much of the difficulty encountered in attempting to predict flutter characteristics for finite-span swept and unswept wings at subsonic and supersonic speeds results from inadequate representation of the distributions of oscillating aerodynamic loads on such wings. For both subsonic and supersonic speeds a number of methods exist for evaluating three-dimensional oscillating loads (refs. 1 to 21, for example). These methods involve varying degrees of rigor, but all are characterized by

the relatively extensive amount of computation required. In all of these procedures it is necessary to recalculate the loading with each change of reduced frequency. This fact further increases the amount of computation required because in flutter prediction the reduced frequency at flutter is not usually found directly. Because the calculations are complex and lengthy and because many of the procedures have not been proved in general application, the use of these methods in flutter prediction has been limited.

A procedure commonly used in the solution of practical flutter problems involving finite wings is a modal-type analysis similar to that employed by Barmby, Cunningham, and Garrick for swept wings (ref. 22) and by Smilg and Wasserman for unswept wings (ref. 23). These methods, as presented in references 22 and 23, employ two-dimensional incompressible aerodynamic forces and moments and thus do not take into account the aerodynamic effects of finite span and compressibility.

The present report presents an approximate method of flutter calculation based on a simplified representation of the three-dimensional aerodynamic loading which is shown to be applicable to a wide variety of wing plan forms at both subsonic and supersonic speeds. The present method is also based on a modal analysis, but the aerodynamic effects of finite span, taper, and compressibility are accounted for by utilizing modified aerodynamic loadings based on spanwise distributions of section lift-curve slope and local aerodynamic center calculated from well-known subsonic (ref. 24) or supersonic (refs. 25 and 26) three-dimensional steady-flow theory for flat, rigid wings. The distributions of section lift and pitching moment on oscillating flexible wings are obtained by employing these distributions of lift-curve slope and aerodynamic center for flat rigid wings in conjunction with the "effective" angle-of-attack distribution resulting from oscillation of the wing in each of the assumed vibration modes. The effect of oscillatory motion on the magnitudes and phase angles of the lift and moment vectors is represented approximately by modifying the familiar circulation functions of Theodorsen by utilizing aerodynamic flutter coefficients given by Jordan (ref. 27) for two-dimensional airfoils oscillating in subsonic or supersonic flow. A detailed description of the procedure for making flutter calculations is given in the appendixes.

By representing the oscillating aerodynamic loads in this manner the necessity of recalculating the load distributions for each value of reduced frequency is avoided, since only the modified circulation functions vary with frequency, and these in turn are assumed not to vary along the span. The bending and twisting deformation of individual wing sections is taken into account only in terms of the "effective" angle of attack and is assumed not to affect distributions of lift-curve slope and aerodynamic center. This procedure is equivalent to neglecting the

influence of deformation on the lift-producing capacity of a given wing section.

Flutter characteristics have been calculated by the method developed herein (using three vibration modes) for wings with sweep angles from $0°$ to $52.5°$, aspect ratios from 2.4 to 7.4, taper ratios of 0.6 and 1.0, and center-of-gravity positions between 34 percent chord and 59 percent chord. The results are compared herein with experimental data obtained in the Langley 26-inch transonic blowdown tunnel (refs. 28 to 31) and in the Langley 9- by 12-inch supersonic blowdown tunnel (ref. 32).

SYMBOLS

A aspect ratio of full wing including fuselage intercept

A_p aspect ratio of wing considering side of fuselage as a reflection plane (twice the panel aspect ratio)

a nondimensional distance from midchord to elastic axis measured perpendicular to elastic axis, positive rearward, fraction of semichord b

ac nondimensional distance from leading edge to local aerodynamic center (for steady flow) measured streamwise, fraction of streamwise chord, $C_{m_\alpha}/C_{l_\alpha}$

ac_n nondimensional distance from midchord to local aerodynamic center (for steady flow) measured perpendicular to elastic axis, positive rearward, fraction of semichord b

b semichord of wing measured perpendicular to elastic axis

b_r semichord of wing measured perpendicular to elastic axis at spanwise reference station $\eta = 0.75$

s span of wing panel considering side of fuselage as a reflection plane

B ratio of local semichord b to reference semichord b_r measured perpendicular to elastic axis, b/b_r

C complex circulation function, $F + iG$

C_{l_α} local lift-curve slope for a streamwise section in steady flow

$C_{l_{\alpha,n}}$ local lift-curve slope for a section perpendicular to the elastic axis in steady flow

C_{m_α} derivative with respect to angle of attack of local pitching-moment coefficient measured about the leading edge of a streamwise section

C_p local lifting-pressure coefficient

F circulation function which modifies in-phase load components

f_h deflection function of wing in bending mode

f_θ deflection function of wing in torsion mode

G circulation function which introduces out-of-phase load components

g structural damping coefficient for wing (Subscript α denotes torsional mode; subscript h denotes bending mode.)

h local vertical translational displacement of wing at elastic axis

I_α mass moment of inertia of unit length of wing about elastic axis

i $\sqrt{-1}$

k_{nr} reduced frequency based on the spanwise reference station ($\eta = 0.75$) and on velocity component normal to elastic axis, $b_r\omega/v_n$

l length of exposed wing panel measured along elastic axis

M Mach number

M_α oscillatory moment about elastic axis per unit length of wing, positive leading edge up

m mass of wing per unit length measured along elastic axis

P oscillatory lift per unit length of wing along the elastic axis, positive downward

Q downwash expression defined by equation (5b)

r_α nondimensional radius of gyration of wing about elastic axis, $\sqrt{I_\alpha/mb^2}$

t time

V flutter speed, measured parallel to free stream (experimental values or values calculated by the method of this report)

V_R calculated reference flutter speed obtained by using $C_{l_{\alpha,n}} = 2\pi$ and $ac_n = -\frac{1}{2}$

v free-stream velocity

x streamwise coordinate measured from leading edge of wing root

x' nondimensional coordinate from midchord measured perpendicular to elastic axis, positive rearward, fraction of semichord b

x_α nondimensional distance from elastic axis to local center of gravity measured perpendicular to elastic axis, positive rearward, fraction of semichord b

y' distance along elastic axis measured from wing root, $l\eta$

α angle of attack

β $\sqrt{M^2 - 1}$ for $M > 1$; $\sqrt{1 - M^2}$ for $M < 1$

κ wing section mass-density ratio, $\pi\rho b^2/m$

Λ sweep angle; positive for sweepback

λ taper ratio of full wing including fuselage intercept

λ_p taper ratio of exposed wing panel

η nondimensional coordinate (either spanwise or along elastic axis) measured from wing root, fraction of exposed panel span s or fraction of wing length l

θ local torsional displacement of wing measured about elastic axis

ρ air density

σ local bending slope of elastic axis, $\partial h/\partial y'$

τ local rate of change of twist, $\partial \theta/\partial y'$

ω circular frequency of vibration

ω_α circular frequency of first uncoupled torsional vibration mode of wing measured about elastic axis

ω_h circular frequency of uncoupled bending vibration mode of wing (subscripts 1 and 2 denote first and second bending modes)

ξ nondimensional streamwise coordinate measured from leading edge of wing root, fraction of exposed panel span s

Subscripts:

$c/4$ quantities associated with the wing quarter-chord

ea   quantities associated with the wing elastic axis

C   circulation functions obtained from the oscillatory aerodynamic coefficients given in reference 27 for two-dimensional compressible flow

LE   quantities associated with the wing leading edge

M   quantities associated with the Mach lines originating from wing root or tip

n   quantities associated with wing sections normal to the elastic axis

I   circulation functions obtained by Theodorsen in reference 33 for two-dimensional incompressible flow

TE   quantities associated with the wing trailing edge

Dots over symbols denote derivatives with respect to time.

DESCRIPTION OF THE METHOD

General

The procedure for flutter calculation used in this report is bas-ically a Rayleigh, or modal-type, analysis and is illustrated herein with uncoupled vibration modes although coupled modes can be used. (The use of uncoupled modes in flutter calculations is discussed in detail in refs. 22 and 34.) The flutter modes of the wings studied in this inves-tigation are represented by the first and second bending and the first torsional vibration modes of uniform cantilever beams. All deformations are considered to be made up of vertical bending of an approximately straight elastic axis and rotation about that axis. The wing root is treated as though it were clamped along a line normal to the elastic axis and passing through the intersection of the elastic axis and the root chord. The dynamical equations involved in this type of analysis are obtained from Lagrange's equations of motion in which the vibration modes are used as generalized coordinates. These dynamical equations repre-senting the balance between elastic, inertial, and aerodynamic loads are derived in appendix A and are obtained (for the simple case of one bending mode and one torsion mode) in the form

$$\left\{\left[\frac{\omega_h^2}{\omega^2}(1 + ig_h) - 1\right]\int_0^l \frac{1}{\kappa}\left(\frac{b}{b_r}\right)^2 f_h^2 dy'\right\} \underline{h} + \left[-b_r\int_0^l \frac{1}{\kappa}\left(\frac{b}{b_r}\right)^3 x_\alpha f_h f_\theta \; dy'\right]\underline{\theta} - \frac{1}{\pi\rho b_r^2\omega^2}\int_0^l Pf_h \; dy' = 0 \qquad (1)$$

and

$$\left[-b_r\int_0^l \frac{1}{\kappa}\left(\frac{b}{b_r}\right)^3 x_\alpha f_h f_\theta \; dy'\right]\underline{h} + \left\{b_r^2\left[\frac{\omega_\alpha^2}{\omega^2}(1 + ig_\alpha) - 1\right]\int_0^l \frac{r_\alpha^2}{\kappa}\left(\frac{b}{b_r}\right)^4 f_\theta^2 dy'\right\} \underline{\theta} - \frac{1}{\pi\rho b_r^2\omega^2}\int_0^l M_\alpha f_\theta \; dy' = 0 \qquad (2)$$

where $\underline{h}$ and $\underline{\theta}$ are as defined in equations (A8) and (A9). These same equations in a different form were used in reference 22. The values of all geometrical, structural, and aerodynamic quantities to be used in these equations are those values associated with sections normal to the elastic axis.

The innovations of the present method consist of alterations in the expressions for section lift P, pitching moment M_α, and complex circu-lation function $C = F + iG$ in order to approximate the aerodynamic effects of finite span, taper, and compressibility. The section lift P and pitching moment M_α are expressed in terms of arbitrary section lift-curve slope and aerodynamic center which are assumed to vary along the

span of the wing. For any particular value of free-stream Mach number,
the spanwise distributions of lift-curve slope and aerodynamic center
are calculated from well-known steady-state aerodynamic theory for flat
rigid wings. The spanwise distributions of the lift and moment on the
deforming wing are then found by using the aforementioned values of
static section lift-curve slope and aerodynamic center in conjunction
with the "effective" angle-of-attack distribution resulting from oscil-
lation of the wing in each of the assumed vibration modes.[1] The values
of lift and moment thus obtained account approximately for finite span,
taper, compressibility, and deformation shape of the wing. However, it
is also necessary to take into account the effect of oscillatory motion
on the magnitudes and phase angles of the lift and moment vectors. In
the present method this is done approximately by utilizing circulation
functions (analogous to the familiar F and G functions of Theodorsen
(refs. 33 and 35)) which are modified on the basis of aerodynamic flutter
coefficients given by Jordan (ref. 27) for two-dimensional airfoils oscil-
lating in subsonic or supersonic flow. In the application of the circu-
lation functions thus obtained, the Mach number normal to the leading
edge is employed.

Formulating the aerodynamic forces and moments in this manner implies
the following assumptions:

(1) The bending and twisting deformation of individual wing sections
is accounted for in terms of the "effective" angle of attack only. The
effect of relative deformation on section lift-curve slope and aerodynamic
center can be neglected. Camber deformation of sections normal to the
elastic axis is not considered.

(2) The effect of oscillatory motion on the magnitude and phase
angles of the section lift and moment vectors is the same for each wing
section and may be represented by modified circulation functions associ-
ated with the Mach number component normal to the leading edge.

In view of the use of static lift-curve slopes and aerodynamic cen-
ters, application of this method at high values of reduced frequency
would be open to question. At low to moderate reduced frequencies, how-
ever, the approximation should be reasonable.

In the remaining sections of this description of the method are
discussed the alteration of section lift P and pitching moment M_α
by the introduction of static three-dimensional section lift-curve slopes

---

[1]The "effective" angle of attack is the downwash resulting from the
motion divided by the component of free-stream velocity normal to the
elastic axis.

and aerodynamic centers, the calculation of these static aerodynamic
parameters, and the evaluation of the complex circulation function C
by utilizing two-dimensional subsonic or supersonic oscillating-airfoil
theory.

A detailed description of the flutter calculation procedure is given
in appendix B, and expressions for the elements of the final flutter
determinant are given in appendix A.

Expressions for Section Lift and Pitching Moment

In formulating the expressions for section lift and pitching moment
the following basic assumption is made: The flow over wing sections nor-
mal to the elastic axis consists of a quasi-two-dimensional noncirculatory
flow plus a circulatory flow in which the circulation is fixed by the
component of free-stream velocity normal to the elastic axis in conjunc-
tion with downwash distributions along chord lines normal to the elastic
axis (rather than by the free-stream velocity and downwash distributions
along streamwise chord lines). In contrast to the method of reference 22
the present method does not consider the circulatory flow to be two-
dimensional and incompressible in nature. It should be observed that the
concepts of circulatory and noncirculatory flow components as developed
in references 22 and 33 appear to have little meaning for wings with
supersonic edges. Nevertheless, for convenience, these concepts have
been utilized in the present method for wings with supersonic edges since
it is believed that inclusion of the appropriate section lift-curve slopes
and aerodynamic centers represents the principal aerodynamic effects on
the calculated flutter speed of wings with supersonic edges.

The section lift P and pitching moment M_α which are used in the
present analysis may be obtained from similar expressions in reference 22
by introducing variable section lift-curve slope $C_{l_{\alpha,n}}$ and variable

aerodynamic center ac_n. The procedure for making this generalization
is as follows:

First, the expressions for P and M_α used in reference 22 are
written in the form

$$P = -\pi\rho b^2\left[\ddot{h} + v_n\dot{\theta} + v_n\dot{\sigma}\tan\Lambda_{ea} - ba\left(\ddot{\theta} + v_n\dot{\tau}\tan\Lambda_{ea}\right)\right] - \quad\left.\begin{array}{c}\\\\\end{array}\right\}\text{Noncirculatory}$$

$$2\pi\rho v_n bCQ \qquad\qquad\qquad\qquad\qquad\qquad\qquad\qquad\qquad\left.\begin{array}{c}\\\end{array}\right\}\text{Circulatory} \qquad (3)$$

and

$$
\begin{aligned}
M_\alpha = &-\pi\rho b^4\left(\frac{1}{8} + a^2\right)\left(\ddot{\theta} + v_n\dot{\tau}\ \tan\ \Lambda_{ea}\right) + \pi\rho v_n b^2\left(\dot{h} + v_n\sigma\ \tan\ \Lambda_{ea}\right) + \\[2mm]
&\pi\rho b^3 a\left(\ddot{h} + v_n\dot{\sigma}\ \tan\ \Lambda_{ea}\right) + \pi\rho v_n^2 b^2\left(\theta - ab\tau\ \tan\ \Lambda_{ea}\right) - \\[2mm]
&2\pi\rho v_n b^2\left[\frac{1}{2} - \left(a + \frac{1}{2}\right)c\right]Q
\end{aligned}
\left.\begin{array}{c} \\ \\ \\ \\ \\ \\ \\ \\ \\ \end{array}\right\}
\begin{array}{l}\text{Noncirculatory} \\[10mm] \\ \text{Circulatory} \qquad (4)\end{array}
$$

where Q is the downwash expression defined by equation (5a). These equations are, of course, based on the assumption that flow with small disturbances exists.

Circulatory components.- Only the circulatory components of these expressions are changed. In the circulatory components of equations (3) and (4) the value 2π for section lift-curve slope is replaced by the variable $C_{l_{\alpha,n}}$, and the quarter-chord aerodynamic-center position $\left(ac_n = -\frac{1}{2}\right)$ is replaced by the variable ac_n. The downwash expression Q must also be altered to include the effects of variable section lift-curve slope $C_{l_{\alpha,n}}$ and aerodynamic center ac_n.

The treatments of the circulatory components of lift and pitching moment in references 22 and 33 are based on classical two-dimensional incompressible thin-airfoil theory, which indicates a section lift-curve slope of 2π and an aerodynamic center located at the quarter-chord position. The circulation strength is therefore related to the downwash velocity at the three-quarter-chord position. This downwash as given in reference 22 is

$$
Q = \dot{h} + v_n\theta + v_n\sigma\ \tan\ \Lambda_{ea} + b\left(\frac{1}{2} - a\right)\left(\dot{\theta} + v_n\tau\ \tan\ \Lambda_{ea}\right) \qquad (5a)
$$

and the distance between the bound vortex (quarter-chord) and the point at which the downwash boundary condition is applied (three-quarter-chord) is b. For arbitrary $C_{l_{\alpha,n}}$, this distance becomes $\dfrac{C_{l_{\alpha,n}}}{2\pi}\,b$. (See ref. 24 for a detailed discussion of the application of the downwash boundary condition when $C_{l_{\alpha,n}}$ is other than 2π.) Then, if ac_n (location of bound

vortex) is also arbitrary, the downwash condition is applied at the position $b\left(\dfrac{C_{l_{\alpha,n}}}{2\pi} + ac_n\right)$ measured positive rearward from the midchord. (See fig. 1.) Then, in the expression for Q, the distance from the elastic axis to the point of application of the downwash condition $b\left(\dfrac{1}{2} - a\right)$ is replaced in the present analysis by $b\left(\dfrac{C_{l_{\alpha,n}}}{2\pi} + ac_n - a\right)$. Then for the present method,

$$Q = \dot{h} + v_n\theta + v_n\sigma \tan \Lambda_{ea} + b\left(\frac{C_{l_{\alpha,n}}}{2\pi} + ac_n - a\right)\left(\dot{\theta} + v_n\tau \tan \Lambda_{ea}\right) \quad (5b)$$

Noncirculatory components.- The noncirculatory flow components contribute to the lift and moment only a virtual mass effect which is comparatively very small except at high frequencies. Since, as mentioned previously, the present method should probably be applied only to cases involving low to moderate reduced frequencies, it appears that the noncirculatory flow terms will constitute only a small fraction of the overall section lift and moment. Now, the noncirculatory components of section lift P and moment M_α which are used in references 22 and 33 and shown in equations (3) and (4) of the present report are derived from the velocity potentials for unsteady two-dimensional incompressible flow about a flat plate. The virtual mass effects resulting from these noncirculatory flows are dependent only upon the velocity perpendicular to the wing surface and do not depend on the stream velocity as such. For low to moderate frequencies, the velocity perpendicular to the wing surface will be small compared to free-stream velocity. Therefore, for wings with all edges subsonic, any effects of compressibility on the magnitudes of the noncirculatory flow terms should be small, and the consequent effects on the section lift and moment should be of second order. It is concluded that, for wings with all edges subsonic, use of the noncirculatory components of lift and moment in essentially the two-dimensional incompressible form should result in negligible error in the calculated flutter speed.

In view of the relatively small magnitude of the noncirculatory flow components, the two-dimensional incompressible form is also used as a first approximation to virtual mass effects for wings with supersonic edges as well as for wings with all edges subsonic. At low reduced frequencies, the noncirculatory terms might even be completely neglected without introducing major errors into the calculated flutter results.

The section lift and pitching moment used throughout the present investigation are made up of circulatory components generalized as previously described and noncirculatory components used in the unaltered two-dimensional incompressible forms shown in equations (3) and (4). The resulting expressions are for the section lift

$$P = -\pi\rho b^2\left[\ddot{h} + v_n\dot{\theta} + v_n\dot{\sigma}\tan\Lambda_{ea} - ba\left(\ddot{\theta} + v_n\dot{\tau}\tan\Lambda_{ea}\right)\right] - \left.\begin{array}{c}\end{array}\right\} \text{Noncirculatory}$$

$$C_{l_{\alpha,n}}\rho v_n bCQ \qquad\qquad\qquad \left.\begin{array}{c}\end{array}\right\} \text{Circulatory} \qquad (6)$$

and for the pitching moment about the elastic axis

$$M_\alpha = -\pi\rho b^4\left(\frac{1}{8} + a^2\right)\left(\ddot{\theta} + v_n\dot{\tau}\tan\Lambda_{ea}\right) + \pi\rho b^2 v_n\left(\dot{h} + v_n\sigma\tan\Lambda_{ea}\right) +$$

$$\pi\rho b^3 a\left(\ddot{h} + v_n\dot{\sigma}\tan\Lambda_{ea}\right) + \pi\rho b^2 v_n^2\left(\theta - ab\tau\tan\Lambda_{ea}\right) - \left.\begin{array}{c}\end{array}\right\} \text{Noncirculatory}$$

$$2\pi\rho v_n b^2\left[\frac{1}{2} - \left(a - ac_n\right)C\frac{C_{l_{\alpha,n}}}{2\pi}\right]Q \qquad \left.\begin{array}{c}\end{array}\right\} \text{Circulatory} \qquad (7)$$

where the downwash expression Q is that defined in equation (5b). Note that in accordance with the discussion in reference 22 the terms of equations (3), (4), (6), and (7) associated with the variation of the velocity potential with lengthwise distance y' are omitted.

Substituting expressions (6) and (7) into the dynamical equations (1) and (2) and using equation (5b), together with the assumption of harmonic motion, yield two homogeneous flutter equations in the two unknowns h and θ. The flutter determinant resulting from these flutter equations, expressions for the elements of the determinant, and the method used in solving the determinant for the flutter condition are given in appendix A. The remainder of the description of the method is concerned with the evaluation of the static aerodynamic parameters $C_{l_{\alpha,n}}$ and ac_n and the circulation functions F and G which appear in the expressions for the determinant elements.

Static Aerodynamic Parameters

All calculations of static aerodynamic parameters are made by considering the wing to be rigid and flat.

For $M = 0$ (reference).- The reference flutter speed V_R is found for each wing by using $C_{l_{\alpha,n}} = 2\pi$ and $ac_n = -\dfrac{1}{2}$ at $M = 0$. With these values the flutter equations (A12) and (A13) reduce to those given in reference 22.

For $0 \leqq M < 1$.- At subsonic (and incompressible) speeds the spanwise distribution of C_{l_α} is found by the lifting-line method of reference 24. In reference 24 charts of the necessary influence coefficients, which facilitate rapid calculation of the loading, are presented. Although this method involves the application of boundary conditions and the evaluation of load intensity at only seven spanwise stations, the resulting accuracy is considered adequate for present purposes, and the method is used because of its simplicity. Simple sweep theory is used to relate C_{l_α} to $C_{l_{\alpha,n}}$. Thus, $C_{l_{\alpha,n}} = \dfrac{C_{l_\alpha}}{\cos \Lambda_{ea}}$. For all subsonic speeds the aerodynamic center is taken at the quarter-chord position $\left(ac_n = -\dfrac{1}{2}\right)$. However, at subsonic speeds higher than those calculated herein it may become necessary to take aerodynamic-center changes into account. Details of the loading calculations are given in appendix B.

For $M > 1$.- At supersonic speeds when the wing leading edge is swept behind the leading-edge root Mach line (subsonic leading edge), the equations of reference 25 are used to calculate the static distributions of $C_{l_{\alpha,n}}$ and ac_n. The method of reference 25 is based on a superposition of conical flows, and relatively simple formulas are given for calculating the loading. When the leading edge lies ahead of the leading-edge root Mach line (supersonic leading edge), the equations of reference 26 are used. Reference 26 is also based on conical-flow concepts. These equations for lifting pressure have been used in integrals which yield section-lift and pitching-moment coefficients C_{l_α} and C_{m_α} (and hence ac). The resulting expressions and details of their application are given in appendix B. The equations for C_{l_α} and C_{m_α} given in appendix B make it unnecessary to refer to references 25 and 26 for present purposes.

Circulation Functions

The complex circulation function

$$C = C(M, k_{nr}) = F(M, k_{nr}) + iG(M, k_{nr})$$

appearing in equations (6) and (7) and in the expressions of appendix A, modifies the otherwise-static circulatory components of lift and pitching moment to account for the effect of oscillation. The F function modifies the load component which is in phase with angle of attack, and the G function introduces out-of-phase load components. Values of the F and G functions used in reference 22 were those developed by Theodorsen (ref. 33) for two-dimensional incompressible flow about an oscillating airfoil. In the present investigation these values are again used for M = 0, but the functions must be modified to account for compressibility effects at M > 0. The modification used herein is based on loading functions for two-dimensional subsonic or supersonic flow about an oscillating airfoil as given by Jordan in reference 27. The relations between these loading functions and the F and G circulation functions are derived in appendix B. Although the flutter calculation is based on a consideration of sections normal to the elastic axis, the governing Mach number for the determination of the circulation functions is taken to be that normal to the leading edge. This choice of governing Mach number arises from the fact that the nature of the flow over a section of wing is influenced by whether the leading edge is subsonic or supersonic.

Although it would seem straightforward to use the appropriate F_C and G_C functions directly in the flutter calculations, this procedure gives poor results in comparison with experiment. (See figs. 3 and 9, for example.) The large phase angles $\left(\tan^{-1} \dfrac{G_C}{F_C}\right)$ of the complex circulation functions associated with two-dimensional compressible flow were found to be inappropriate for three-dimensional wings. It was anticipated that if phase angles remained moderately small (i.e., if G remained fairly small relative to F)[1], the calculated flutter speed would be relatively insensitive to changes in the magnitude of G. That is, if G is not large relative to F, the actual value of G is unimportant. The

---

[1]The assumption of small phase angles implies an upper bound on the values of reduced frequency k_{nr} for which the present method can be used. However, as previously mentioned the use of statically based load distributions also restricts the method to moderately small frequency values, so the present assumption imposes no further limitation.

predominant effect on the loading of changing Mach number would then lie in changing the magnitude of the in-phase component associated with F. The form of the complex function C which is used in the present calculations is therefore taken to be

$$C = C\left(M_{LE}, k_{nr}\right) = F + iG = \frac{F_C}{F_I}\left(F_I + iG_I\right)$$

This function contains an in-phase component which is the same as that derived from reference 27 for two-dimensional compressible flow, but the associated phase angle is independent of Mach number. Hence, the phase angle is the same as that given by Theodorsen in reference 33.

In order to investigate the validity of this reasoning some calculations were also made by using

$$C = C\left(M_{LE}, k_{nr}\right) = F_C + i0$$

Also, to investigate the sensitivity of the flutter calculations to different forms of circulation-function representation, some calculations at the higher Mach numbers were made by using

$$C = C\left(M_{LE}, k_{nr}\right) = \frac{\sqrt{F_C^2 + G_C^2}}{\sqrt{F_I^2 + G_I^2}}\left(1 + i0\right)$$

This function has zero phase angle, and its amplitude is the ratio of the magnitudes of the resultant vectors for compressible and incompressible flow.

Further details of the circulation-function calculation are given in appendix B. The method for solving the final flutter determinant is given in appendix A.

RESULTS AND DISCUSSION

Presentation of Results

Flutter characteristics have been calculated by the present method (using three vibration modes) for wings with sweep angles from 0° to 52.5°, aspect ratios from 2.4 to 7.4, taper ratios of 0.6 and 1.0, and center-of-gravity positions between 34 percent chord and 59 percent chord. The plan forms of these wings are shown in figure 2. The calculated results are compared with experimental data obtained in the Langley 26-inch transonic blowdown tunnel (refs. 28 to 31) and in the Langley 9- by 12-inch supersonic blowdown tunnel (ref. 32).

Unless otherwise indicated the subsequent discussion deals entirely with calculated results obtained by using the complex circulation function

$$C = \frac{F_C}{F_I}\left(F_I + iG_I\right)$$

Wing designation.- The three-digit system used to identify the wings with taper ratio of 0.6 is the same as that used in reference 30. The first digit in this system is the aspect ratio of the full wing to the nearest integer. The second and third digits give the quarter-chord sweep angle to the nearest degree. For example, wing 445 has an aspect ratio of 4, a sweep angle of 45°, and a full-wing taper ratio of 0.6. Since some of the wings discussed in this paper have identical plan forms but different center-of-gravity positions (ref. 31), a single letter is appended to the plan-form designation to signify a shifted center of gravity. For example, wing 445 has a center of gravity at approximately 46 percent chord, whereas the center of gravity of wing 445F is at about 34 percent chord, and that of wing 445R is at about 58 percent chord. Wing 400 has a center of gravity at approximately 45 percent chord, but wing 400R has a center of gravity at about 59 percent chord.

For the wings with taper ratio of 1.0, the same system is used, except that a fourth digit 1 is added to distinguish the taper ratio. For example, wing 4451 has a full-wing aspect ratio of 4, a sweep angle of 45°, and a taper ratio of 1.0.

Flutter characteristics.- Calculated flutter characteristics V/V_R, ω/ω_α, and k_{nr} and the associated values of V_R, M, ω_α, and ρ are given in table I for several wings (see fig. 2) at several Mach numbers. The calculated values of V/V_R and ω/ω_α are compared with experimental

data in figures 3 to 14 and 15 to 26, respectively. The experimental
flutter points shown were obtained at various values of density ρ;
whereas, for a particular wing, all of the points calculated by the pres-
ent method were obtained at a constant value of ρ which represented
approximately an average of the experimental densities. For each experi-
mental point, however, the normalizing V_R was calculated by using the
appropriate experimental density. On the basis of previous experience,
it is believed that normalizing the experimental flutter speeds in this
manner essentially accounts for density effects so that the resulting
$\left(V/V_R\right)_{exp}$ is considered to be nearly independent of ρ, at least over
the range of density variation which occurs herein.

The static distributions of $C_{l_{\alpha,n}}$ and ac_n used in obtaining the
calculated flutter characteristics are shown in figures 27 to 35. For
all of the flutter calculations presented in this report, the flutter
modes of the wings were represented by a combination of the first torsion
mode shape and first and second bending mode shapes of a uniform cantilever
beam.

The reference flutter speeds V_R used in references 28, 30, and 32
for wings 430, 245, 400, 4001, and 7001 were calculated by employing
only two degrees of freedom (first bending and first torsion). Since
three-degree-of-freedom calculations yield values of V_R which are
slightly lower than the two-degree-of-freedom values, the experimental
V/V_R values for these wings have been multiplied by the ratio
$\dfrac{V_R \text{ for two degrees of freedom}}{V_R \text{ for three degrees of freedom}}$ so that both calculated and experimental
flutter-speed ratios as presented herein are normalized by V_R for three
degrees of freedom.

Flutter Speeds

As shown in figures 3 to 14, the flutter speeds calculated by the
present method for all wings demonstrate a characteristic decrease as
Mach number increases from 0 to near 1.0. This decrease is the result
of increasing C_{l_α} which is caused by compressibility at high subsonic
speeds. It should be noted that at $M = 0$ the differences between the
V/V_R values shown and the value 1.0 result solely from the effect of
finite aspect ratio. As Mach number increases above 1.0, decreasing
C_{l_α} and rearward shifting ac cause a rapid rise in the flutter speed.
In the immediate vicinity of $M = 1.0$ the flutter-speed curves are shown
dashed to indicate that this region is inaccessible to the present

calculations. This inaccessibility results from the breakdown of both subsonic and supersonic three-dimensional steady-flow wing theories near $M = 1.0$. It should be noted that the minimum value of V/V_R will generally occur within this inaccessible region, and, hence, $\left(\dfrac{V}{V_R}\right)_{min}$ cannot usually be calculated by use of theoretical static aerodynamic coefficients obtained from the wing theories employed herein. It is possible, however, to fair a reasonable curve through the neighborhood of $M = 1.0$ by making use of the adjacent subsonic and supersonic calculated points. The extent shown for the dashed portion of the curves should not, of course, be interpreted as representing the limits of the inaccessible region. No attempt has been made to evaluate these limits, and the range shown in the figures is only illustrative.

For all of the swept wings the calculated flutter-speed curves of figures 3 to 14 are in very good agreement with the experimental data at all Mach numbers. In general, the calculated curves actually lie within the scatter of the experimental data. For wing 445 (fig. 3) there are no experimental data in the range $1.4 < M < 1.75$. However, the leveling-off tendency demonstrated by the calculated flutter-speed curve in this Mach number range is in qualitative agreement with data for other similar wings.

Comparison of the flutter-speed curves for wings 445, 445F, and 445R (figs. 3, 4, and 5) shows that the rather large differences between the center-of-gravity positions for these wings cause only very slight differences in V/V_R at subsonic speeds. At supersonic Mach numbers, however, the data show that the characteristic rise of flutter speed with increasing Mach number becomes more rapid as the center of gravity is moved progressively forward. This behavior is also predicted by the calculated curves.

The close agreement between calculated and experimental flutter speeds for wing 245 (fig. 6) is rather surprising in view of the small aspect ratio of this wing. In general, the use of a strip-theory type of analysis and uncoupled vibration modes for a wing of such small aspect ratio (panel aspect ratio = 0.91) would be open to question. The agreement in the present case may, therefore, be fortuitous.

For most of the wings shown in this report no tip correction was applied to ac_n to account for the forward shift of aerodynamic center within the tip Mach cone. (See discussion of tip corrections in appendix B.) For wing 430, however, the tip Mach cone covered so large a portion of the wing that it was considered necessary to apply a tip correction to ac_n. (See figs. 28(d) and (e).) At $M = 1.15470$, this correction appears to be rather large. However, a preliminary calculation

at this Mach number without the correction to ac_n yielded a value of flutter speed only 13 percent higher than that shown. It appears, therefore, that unless the tip Mach cone covers a large portion of the wing, the application of a tip correction to ac_n is not necessary.

For the low-aspect-ratio unswept wings (figs. 10, 11, and 13) agreement between calculated and experimental flutter speeds is not as good as for the swept wings. For wing 400 (fig. 10) the agreement is fair up to about $M = 1.0$, but the calculated values overpredict the flutter speed by as much as $2\frac{1}{2}$ times at $M = \sqrt{2}$. The magnitude of this error is believed to be related to the proximity of the local aerodynamic centers to the local centers of gravity and the fact that linear theory predicts an aerodynamic center that is too far rearward. This hypothesis is supported by the results obtained for wing 400 with its center of gravity shifted from about 45 percent chord to about 59 percent chord (wing 400R). Figure 11 shows that for wing 400R at supersonic speeds the calculated curve overpredicts the mean experimental values by only about 13 percent. The erroneous results obtained for wing 400 should probably not be interpreted as indicating a limitation on the present method of flutter calculation. Rather, these errors appear to arise from the well-known limitations on the use of linearized flow theory to calculate load distributions on wings of finite thickness. Wing 400 at supersonic speeds seems to constitute a very sensitive case in which a small inaccuracy in the location of the aerodynamic center leads to large errors in calculated flutter speed. In the case of wing 4001 (fig. 13) the calculated and experimental values are in very good agreement up to about $M = 1.0$. At supersonic speeds, where the local aerodynamic centers are shifted rearward toward the local centers of gravity, the theory again overpredicts the experimental values, this time by up to 37 percent. This deviation is not surprising in view of the fact that wing 4001 is not greatly different from wing 400.

The calculated flutter speeds for the high-aspect-ratio unswept wing (wing 7001, fig. 14) are in good agreement with experiment throughout the Mach number range. The improved agreement for this wing as compared with that for the low-aspect-ratio unswept wings may be caused to some extent by the decreased thickness of wing 7001 near the tip. Wing 7001 was tapered in thickness from 4 percent at the root to 2 percent at the tip, whereas wings 400, 400R, and 4001 were of constant 4-percent thickness.

The flutter-speed curves shown in figures 3 to 14 were calculated by using the complex circulation function

$$C = \frac{F_C}{F_I}\left(F_I + iG_I\right)$$

as described previously. The few points obtained by using the function

$$C = F_C + i0$$

differ from the curves by no more than 7 percent. This close agreement supports the previously stated contention that if phase angles $\left(\tan^{-1} \frac{G}{F}\right)$ are moderately small,[1] the calculated flutter speed will be relatively insensitive to changes in G. Figures 3 to 14 also show that flutter speeds at the higher Mach numbers calculated by using the function

$$C = \frac{\sqrt{F_C{}^2 + G_C{}^2}}{\sqrt{F_I{}^2 + G_I{}^2}}(1 + i0)$$

differ from the curves by no more than 10 or 11 percent. Although, as expected, the points calculated in this manner do not agree with experiment as well as the curves $\left(\text{obtained with}\quad C = \frac{F_C}{F_I}\left(F_I + iG_I\right)\right)$, the small differences between them do point out the relative insensitivity of the calculated flutter speed to the form of circulation-function representation used.

In making the flutter calculations presented herein it was observed that for all but the highest subsonic speeds the circulation functions F_C and G_C are not greatly different from the functions F_I and G_I of Theodorsen. At $M = 0.75$ for the wings shown in figure 2, the use of $C = F_I + iG_I$ instead of $C = \frac{F_C}{F_I}\left(F_I + iG_I\right)$ changes the flutter speed by only about 4 percent or less. It would seem, therefore, that the modified circulation functions need be employed only at high subsonic and supersonic speeds.

---

[1]It should be clearly understood that the quantity $\tan^{-1} \frac{G}{F}$ is the phase angle of the complex circulation function $C = F + iG$ and should not be confused with any phase angles associated with the wing displacements.

Flutter Frequencies

The calculated curves $\left(\text{with } C = \dfrac{F_C}{F_I}\left(F_I + iG_I\right)\right)$ of flutter frequency (figs. 15 to 26) indicate that for all of the swept wings the frequency is well predicted at subsonic speeds. At supersonic speeds the usual rise in frequency is predicted by the theory, but it occurs at Mach numbers higher than those indicated by the test results. In general, the agreement between calculated and experimental flutter frequencies is not as good as the agreement between calculated and experimental flutter speeds. The frequencies calculated for the swept wings by using

$$C = \frac{\sqrt{F_C{}^2 + G_C{}^2}}{\sqrt{F_I{}^2 + G_I{}^2}}(1 + i0)$$

are all excessively high, except at Mach numbers where the leading edge is supersonic or nearly so. At these higher Mach numbers the frequencies thus obtained are generally in better agreement with the experimental

values than are the values obtained with $C = \dfrac{F_C}{F_I}\left(F_I + iG_I\right)$.

For unswept wing 4001 (fig. 25), the number of calculated points is not sufficient to indicate whether the pronounced dip in frequency, which occurs at high subsonic Mach numbers, is predicted by the theory. At low

supersonic speeds the calculated curves $\left(\text{with } C = \dfrac{F_C}{F_I}\left(F_I + iG_I\right)\right)$ over-

predict flutter frequencies by a substantial amount. However, the differences between theory and experiment become much smaller at the higher supersonic speeds, except in the case of wing 400 (fig. 22). The frequencies as well as the flutter speeds of wing 400 are overpredicted by a factor of nearly $2\frac{1}{2}$. As in the case of the swept wings the frequencies for the unswept wings obtained by using

$$C = \frac{\sqrt{F_C{}^2 + G_C{}^2}}{\sqrt{F_I{}^2 + G_I{}^2}}(1 + i0)$$

are all excessively high.

Limitations of the Method

Although the limitations of this method have not been fully evaluated, some of the more important restrictions may be qualitatively discussed.

Frequency range.- As stated previously, the use of spanwise load distributions based on lift-curve slopes and aerodynamic centers calculated from steady-flow wing theory imposes an upper bound on reduced-frequency values for which the method can reasonably be used. No attempt has been made to determine the upper limits of reduced frequency for which the method is usable, but good results for values of k_{nr} up to 0.2 are shown herein.

Mach number range.- The nature of the equations for the circulation functions (eqs. (B38) and (B39) or (B40) and (B41)) shows that at $M_{LE} = 1$, the circulation functions become $F_C = G_C = 0$. This implies that a small range of Mach number in the immediate vicinity of $M_{LE} = 1$ is inaccessible to the present method. This is not a serious limitation, however, because a curve of flutter speed or frequency can be reasonably faired through this inaccessible region by making use of adjacent points. For the wings calculated in this report, there appear to be no sudden or extreme fluctuations of flutter speed or frequency in this region.

The limitations on Mach number range appertaining to the particular steady-flow wing theories used are, of course, carried over to the flutter calculation. In general, this carried-over restriction will exclude free-stream Mach numbers in the immediate vicinity of 1.0, as was mentioned previously.

Flutter modes.- The use of uncoupled modes in combination with a strip theory involving strips normal to the elastic axis is not an essential requirement of the present method of flutter calculation. An analogous calculation procedure would result from the use of coupled modes together with streamwise strips. Flutter modes which involve significant amounts of camber deformation obviously cannot be treated by the method in its present form. As mentioned previously, all flutter calculations presented herein were made by using the mode shapes of a uniform cantilever beam. Since the results of the flutter analysis are not very sensitive to slight changes in mode shape, such a procedure is reasonable as long as aspect ratio and especially taper ratio are not too small.

Plan-form range.- The strip-theory concepts which are employed in the present method also impose plan-form limitations. When aspect ratio or taper ratio or both become so small that the variables (notably herein, aerodynamic loading and circulation functions) associated with a given

section of the wing cannot be treated by strip theory, then the present method is no longer usable.

Center-of-gravity position.- Although the influence of different center-of-gravity positions was investigated for only two plan forms (wings 445 and 400), it appears that, in cases for which the local centers of gravity are located close to the local aerodynamic centers, linearized flow theory should be employed only with great caution. This limitation is not peculiar to the present method. It would apply to any flutter calculation for which the aerodynamic loadings are obtained from linear theory.

At subsonic speeds, neither the swept nor the unswept wings demonstrate any appreciable sensitivity of V/V_R to center-of-gravity position. This result would be expected since at subsonic speeds local aerodynamic centers are at or near the quarter-chord position and are not in proximity to the local centers of gravity.

CONCLUDING REMARKS

A method has been developed for calculating flutter characteristics of finite-span swept or unswept wings at subsonic and supersonic speeds. The method is basically a Rayleigh type analysis and is illustrated herein with uncoupled vibration modes although coupled modes can be used. The aerodynamic loadings are based on distributions of section lift-curve slope and local aerodynamic centers calculated from three-dimensional steady-flow theory. These distributions are used in conjunction with the "effective" angle-of-attack distribution resulting from each of the assumed vibration modes in order to obtain values of section lift and pitching moment. Circulation functions modified on the basis of loadings for two-dimensional airfoils oscillating in a compressible flow are employed to account for the effects of oscillatory motion on the magnitudes and phase angles of the lift and moment vectors.

Calculation of subsonic and supersonic flutter characteristics for 12 wings of varying sweep angle, aspect ratio, taper ratio, and center-of-gravity position and comparison of the results with experimental flutter data indicate that the present method gives generally good flutter results for a wide variety of wings. The method is, however, subject to the following limitations:

(1) It is probably not applicable at high values of reduced frequency, although good results are shown for values of reduced frequency up to about 0.2.

(2) It cannot be used at free-stream Mach numbers in the immediate vicinity of 1.0 nor in the immediate vicinity where the Mach number component normal to the leading edge is 1.0. However, flutter speeds and frequencies may be interpolated through these regions.

(3) The use of a strip-theory approach and the absence of camber flexibility preclude treatment of wings with low aspect ratio and low taper ratio (e.g., delta wings). Good results have been obtained, however, for a 45° swept wing with a panel aspect ratio of 0.91.

(4) Caution must be used when applying the method to wings for which the local aerodynamic centers are close to the local centers of gravity.

Langley Aeronautical Laboratory,
    National Advisory Committee for Aeronautics,
        Langley Field, Va., November 26, 1957.

APPENDIX A

DERIVATION OF THE FLUTTER EQUATIONS AND FLUTTER DETERMINANT

Flutter Equations

Basic assumptions.- The dynamical equations used in the present method are essentially the same as those derived in reference 22, except for changes in the expressions for lift P, pitching-moment M_α, and circulation functions F and G. The general assumptions appertaining to the method of reference 22 thus apply herein also. Briefly, the assumptions made with regard to the equations of motion are as follows:

(1) The elastic axis of the wing is approximately straight and the oscillatory motion may be represented by a combination of the uncoupled bending and twisting vibration modes of the wing with respect to this elastic axis.

(2) The wing root is treated as though it were clamped along a line normal to the elastic axis and passing through the intersection of the elastic axis and the root chord.

(3) The analysis is based on geometric, structural, and aerodynamic quantities associated with sections normal to the elastic axis. These assumptions are discussed in detail in reference 22.

Application of Lagrange's equations.- The dynamical equations result from the application of Lagrange's equations of motion to the flutter problem. For simplicity, the flutter equations are derived herein for the case of one bending mode and one torsion mode. Generalization to an arbitrary number of modes is easily accomplished in the flutter determinant as will be illustrated. (The notation of of ref. 22 has been followed where possible.) In the present method the appropriate expressions for kinetic energy

$$T = \frac{1}{2} \dot{h}^2 \int_0^l m\left[f_h(y')\right]^2 dy' + \frac{1}{2} \dot{\theta}^2 \int_0^l I_\alpha\left[f_\theta(y')\right]^2 dy' +$$

$$\dot{h}\dot{\theta} \int_0^l mx_\alpha b\left[f_h(y')\right]\left[f_\theta(y')\right] dy' \tag{A1}$$

potential energy

$$U = \frac{1}{2}\omega_h^2 \underline{h}^2 \int_0^l m f_h^2 dy' + \frac{1}{2}\omega_\alpha^2 \underline{\theta}^2 \int_0^l I_\alpha f_\theta^2 dy' \tag{A2}$$

and virtual work

$$\delta W = Q_h \delta \underline{h} + Q_\theta \delta \underline{\theta} \tag{A3}$$

are the same as those of reference 22. The generalized forces are left in the form

$$Q_h = \int_0^l \left(P - m\omega_h^2 \frac{g_h}{\omega} f_h \underline{\dot{h}}\right) f_h dy' \tag{A4}$$

and

$$Q_\theta = \int_0^l \left(M_\alpha - I_\alpha \omega_\alpha^2 \frac{g_\alpha}{\omega} f_\theta \underline{\dot{\theta}}\right) f_\theta dy' \tag{A5}$$

Substituting these expressions into Lagrange's equations

$$\frac{d}{dt}\left(\frac{\partial T}{\partial \underline{\dot{h}}}\right) - \frac{\partial T}{\partial \underline{h}} + \frac{\partial U}{\partial \underline{h}} = Q_h \tag{A6}$$

and

$$\frac{d}{dt}\left(\frac{\partial T}{\partial \underline{\dot{\theta}}}\right) - \frac{\partial T}{\partial \underline{\theta}} + \frac{\partial U}{\partial \underline{\theta}} = Q_\theta \tag{A7}$$

and assuming harmonic oscillations

$$h = \left[f_h(y')\right]\underline{h} = \left[f_h(y')\right]h_0 e^{i\omega t} \tag{A8}$$

and

$$\theta = \left[f_\theta(y')\right]\underline{\theta} = \left[f_\theta(y')\right]\theta_0 e^{i\omega t} \tag{A9}$$

lead to the equations of flutter

$$\left\{\left[\frac{\omega_h^2}{\omega^2}(1 + ig_h) - 1\right]\int_0^l \frac{1}{\kappa}\left(\frac{b}{b_r}\right)^2 f_h^2 dy'\right\}\underline{h} + \left[-b_r \int_0^l \frac{1}{\kappa}\left(\frac{b}{b_r}\right)^3 x_\alpha f_h f_\theta dy'\right]\underline{\theta} - \frac{1}{\pi\rho b_r^2\omega^2}\int_0^l Pf_h dy' = 0 \tag{A10}$$

and

$$\left[-b_r \int_0^l \frac{1}{\kappa}\left(\frac{b}{b_r}\right)^3 x_\alpha f_h f_\theta dy'\right]\underline{h} + \left\{b_r^2\left[\frac{\omega_\alpha^2}{\omega^2}(1 + ig_\alpha) - 1\right]\int_0^l \frac{r_\alpha^2}{\kappa}\left(\frac{b}{b_r}\right)^4 f_\theta^2 dy'\right\}\underline{\theta} - \frac{1}{\pi\rho b_r^2\omega^2}\int_0^l M_\alpha f_\theta dy' = 0 \tag{A11}$$

In the calculations of the present report, uncoupled beam bending and torsional mode shapes h_i and α_j are used for the flutter deflection functions f_h and f_θ. The introduction of uncoupled modes into the flutter equations is discussed in detail in references 22 and 34.

Expressions for the elements of the flutter determinant resulting from equations of the type (A10) and (A11) are given in the following section both for the case of an arbitrary number of vibration modes and for the case of one torsion and two bending vibration modes as used in the present analysis.

The Flutter Determinant

Inserting equations (6) and (7) into equations (A10) and (A11) and using equations (A8), (A9), and (5b) yield two homogeneous equations in the two unknowns $\underline{h}$ and $\underline{\theta}$, which may be written in the form

$$\left.\begin{array}{l} A\underline{h} + B\underline{\theta} = 0 \\ D\underline{h} + E\underline{\theta} = 0 \end{array}\right\} \tag{A12}$$

and for a nontrivial solution to exist,

$$\begin{vmatrix} A & B \\ D & E \end{vmatrix} = 0 \tag{A13}$$

Now if u bending modes and v torsion modes are employed, the elements of the flutter determinant (A13) will become matrices A_{ij}, B_{ij}, D_{ij}, and E_{ij}, such that

$$\begin{vmatrix} A_{ij} & B_{ij} \\ D_{ij} & E_{ij} \end{vmatrix} = 0 \qquad (A14)$$

The solution of equation (A14) gives the conditions of flutter (flutter speed and frequency). The procedure for solving this determinant is given at the end of this appendix. Expressions for typical elements in the matrices A_{ij}, B_{ij}, D_{ij}, and E_{ij} are as follows:

$$A_{ii} = \left[\left(\frac{\omega_{h_i}}{\omega}\right)^2 \left(1 + ig_{h_i}\right) - 1\right] l \int_0^1 \frac{1}{\kappa} B^2 h_i^2 d\eta - l \int_0^1 B^2 h_i^2 d\eta +$$

$$i \frac{l}{\pi} \frac{C}{k_{nr}} \int_0^1 C_{l_{\alpha,n}} B h_i^2 d\eta + \frac{b_r \tan \Lambda_{ea}}{\pi} \frac{C}{k_{nr}^2} \int_0^1 C_{l_{\alpha,n}} B \frac{dh_i}{d\eta} h_i d\eta +$$

$$i \frac{b_r \tan \Lambda_{ea}}{k_{nr}} \int_0^1 B^2 \frac{dh_i}{d\eta} h_i d\eta \qquad\qquad (i = 1, 2, 3, \ldots u)$$

$$A_{ij} = -l \int_0^1 B^2 h_i h_j d\eta + i \frac{l}{\pi} \frac{C}{k_{nr}} \int_0^1 C_{l_{\alpha,n}} B h_i h_j d\eta +$$

$$\frac{b_r \tan \Lambda_{ea}}{\pi} \frac{C}{k_{nr}^2} \int_0^1 C_{l_{\alpha,n}} B \frac{dh_j}{d\eta} h_i d\eta + i \frac{b_r \tan \Lambda_{ea}}{k_{nr}} \int_0^1 B^2 \frac{dh_j}{d\eta} h_i d\eta$$

$$\begin{pmatrix} i = 1, 2, 3, \ldots u \\ j = 1, 2, 3, \ldots u \\ i \neq j \end{pmatrix}$$

$$B_{ij} = -b_r l \int_0^1 \frac{x_\alpha}{\kappa} B^3 h_i \alpha_j d\eta + \frac{b_r l}{\pi} \frac{c}{k_{nr}^2} \int_0^1 C_{l_{\alpha,n}} B h_i \alpha_j d\eta +$$

$$i \frac{b_r l}{\pi} \frac{c}{k_{nr}} \int_0^1 C_{l_{\alpha,n}} B^2 \left(\frac{C_{l_{\alpha,n}}}{2\pi} + ac_n - a \right) h_i \alpha_j d\eta + b_r l \int_0^1 B^3 a h_i \alpha_j d\eta +$$

$$i \frac{b_r l}{k_{nr}} \int_0^1 B^2 h_i \alpha_j d\eta + \frac{b_r^2 \tan \Lambda_{ea}}{\pi} \frac{c}{k_{nr}^2} \int_0^1 C_{l_{\alpha,n}} B^2 \left(\frac{C_{l_{\alpha,n}}}{2\pi} + ac_n - a \right) \frac{d\alpha_j}{d\eta} h_i d\eta -$$

$$i \frac{b_r^2 \tan \Lambda_{ea}}{k_{nr}} \int_0^1 B^3 a \frac{d\alpha_j}{d\eta} h_i d\eta \qquad\qquad \begin{pmatrix} i = 1,\, 2,\, 3,\, \ldots u \\ j = 1,\, 2,\, 3,\, \ldots v \end{pmatrix}$$

$$D_{ij} = -b_r l \int_0^1 \frac{x_\alpha}{\kappa} B^3 h_j \alpha_i d\eta + b_r l \int_0^1 B^3 a h_j \alpha_i d\eta -$$

$$i \frac{b_r l}{\pi} \frac{c}{k_{nr}} \int_0^1 C_{l_{\alpha,n}} B^2 (a - ac_n) h_j \alpha_i d\eta -$$

$$\frac{b_r^2 \tan \Lambda_{ea}}{\pi} \frac{c}{k_{nr}^2} \int_0^1 C_{l_{\alpha,n}} B^2 (a - ac_n) \frac{dh_j}{d\eta} \alpha_i d\eta -$$

$$i \frac{b_r^2 \tan \Lambda_{ea}}{k_{nr}} \int_0^1 B^3 a \frac{dh_j}{d\eta} \alpha_i d\eta \qquad\qquad \begin{pmatrix} i = 1,\, 2,\, 3,\, \ldots v \\ j = 1,\, 2,\, 3,\, \ldots u \end{pmatrix}$$

$$E_{ii} = \left[\left(\frac{\omega_{\alpha_i}}{\omega}\right)^2\left(1 + ig_{\alpha_i}\right) - 1\right]b_r^2 l \int_0^1 \frac{r_\alpha^2}{\kappa} B^4 \alpha_i^2 d\eta -$$

$$\frac{b_r^2 l}{\pi} \frac{c}{k_{nr}^2} \int_0^1 C_{l_{\alpha,n}} B^2\left(a - ac_n\right)\alpha_i^2 d\eta - b_r^2 l \int_0^1 B^4\left(\frac{1}{8} + a^2\right)\alpha_i^2 d\eta -$$

$$i \frac{b_r^2 l}{\pi} \frac{c}{k_{nr}} \int_0^1 C_{l_{\alpha,n}} B^3\left(\frac{C_{l_{\alpha,n}}}{2\pi} + ac_n - a\right)\left(a - ac_n\right)\alpha_i^2 d\eta +$$

$$i \frac{b_r^2 l}{k_{nr}} \int_0^1 B^3\left(\frac{C_{l_{\alpha,n}}}{2\pi} + ac_n - a\right)\alpha_i^2 d\eta -$$

$$\frac{b_r^3 \tan \Lambda_{ea}}{\pi} \frac{c}{k_{nr}^2} \int_0^1 C_{l_{\alpha,n}} B^3\left(\frac{C_{l_{\alpha,n}}}{2\pi} + ac_n - a\right)\left(a - ac_n\right)\frac{d\alpha_i}{d\eta} \alpha_i d\eta +$$

$$\frac{b_r^3 \tan \Lambda_{ea}}{k_{nr}^2} \int_0^1 B^3\left(\frac{C_{l_{\alpha,n}}}{2\pi} + ac_n\right)\frac{d\alpha_i}{d\eta} \alpha_i d\eta +$$

$$i \frac{b_r^3 \tan \Lambda_{ea}}{k_{nr}} \int_0^1 B^4\left(\frac{1}{8} + a^2\right)\frac{d\alpha_i}{d\eta} \alpha_i d\eta \qquad\qquad (i = 1, 2, 3, \ldots v)$$

$$E_{ij} = - \frac{b_r^2 l}{\pi} \frac{c}{k_{nr}^2} \int_0^1 C_{l_{\alpha,n}} B^2\left(a - ac_n\right)\alpha_i \alpha_j d\eta - b_r^2 l \int_0^1 B^4\left(\frac{1}{8} + a^2\right)\alpha_i \alpha_j d\eta -$$

$$i \frac{b_r^2 l}{\pi} \frac{c}{k_{nr}} \int_0^1 C_{l_{\alpha,n}} B^3\left(\frac{C_{l_{\alpha,n}}}{2\pi} + ac_n - a\right)\left(a - ac_n\right)\alpha_i \alpha_j d\eta +$$

$$i \frac{b_r^2 l}{k_{nr}} \int_0^1 B^3 \left(\frac{C_{l_{\alpha,n}}}{2\pi} + ac_n - a\right) \alpha_i \alpha_j d\eta -$$

$$\frac{b_r^3 \tan \Lambda_{ea}}{\pi} \frac{C}{k_{nr}^2} \int_0^1 C_{l_{\alpha,n}} B^3 \left(\frac{C_{l_{\alpha,n}}}{2\pi} + ac_n - a\right)\left(a - ac_n\right) \frac{d\alpha_j}{d\eta} \alpha_i d\eta +$$

$$\frac{b_r^3 \tan \Lambda_{ea}}{k_{nr}^2} \int_0^1 B^3 \left(\frac{C_{l_{\alpha,n}}}{2\pi} + ac_n\right) \frac{d\alpha_j}{d\eta} \alpha_i d\eta +$$

$$i \frac{b_r^3 \tan \Lambda_{ea}}{k_{nr}} \int_0^1 B^4 \left(\frac{1}{8} + a^2\right) \frac{d\alpha_j}{d\eta} \alpha_i d\eta \qquad \left(\begin{matrix} i = 1, 2, 3, \ldots v \\ j = 1, 2, 3, \ldots v \\ i \neq j \end{matrix}\right)$$

In the special case of three degrees of freedom (first and second bending and first torsion modes) used throughout the present investigation, the flutter determinant (eq. (A14)) becomes

$$\begin{vmatrix} A_{11} & A_{12} & B_{11} \\ A_{21} & A_{22} & B_{21} \\ D_{11} & D_{12} & E_{11} \end{vmatrix} = 0 \qquad (A15)$$

The elements of this determinant can be conveniently expressed in the forms

$$A_{11} = \left(a_1 + a_2 \frac{G}{k_{nr}} + a_3 \frac{F}{k_{nr}^2}\right) + i\left(\frac{a_4}{k_{nr}} - a_2 \frac{F}{k_{nr}} + a_3 \frac{G}{k_{nr}^2}\right) - R_1 Z$$

$$A_{12} = \left(b_1 + b_2 \frac{G}{k_{nr}} + b_3 \frac{F}{k_{nr}^2}\right) + i\left(\frac{b_4}{k_{nr}} - b_2 \frac{F}{k_{nr}} + b_3 \frac{G}{k_{nr}^2}\right)$$

$$B_{11} = \left(c_1 + c_2 \frac{G}{k_{nr}} + c_3 \frac{F}{k_{nr}{}^2} \right) + i \left(\frac{c_4}{k_{nr}} - c_2 \frac{F}{k_{nr}} + c_3 \frac{G}{k_{nr}{}^2} \right)$$

$$A_{21} = \left(d_1 + d_2 \frac{G}{k_{nr}} + d_3 \frac{F}{k_{nr}{}^2} \right) + i \left(\frac{d_4}{k_{nr}} - d_2 \frac{F}{k_{nr}} + d_3 \frac{G}{k_{nr}{}^2} \right)$$

$$A_{22} = \left(e_1 + e_2 \frac{G}{k_{nr}} + e_3 \frac{F}{k_{nr}{}^2} \right) + i \left(\frac{e_4}{k_{nr}} - e_2 \frac{F}{k_{nr}} + e_3 \frac{G}{k_{nr}{}^2} \right) - R_2 Z$$

$$B_{21} = \left(f_1 + f_2 \frac{G}{k_{nr}} + f_3 \frac{F}{k_{nr}{}^2} \right) + i \left(\frac{f_4}{k_{nr}} - f_2 \frac{F}{k_{nr}} + f_3 \frac{G}{k_{nr}{}^2} \right)$$

$$D_{11} = \left(g_1 + g_2 \frac{G}{k_{nr}} + g_3 \frac{F}{k_{nr}{}^2} \right) + i \left(\frac{g_4}{k_{nr}} - g_2 \frac{F}{k_{nr}} + g_3 \frac{G}{k_{nr}{}^2} \right)$$

$$D_{12} = \left(h_1 + h_2 \frac{G}{k_{nr}} + h_3 \frac{F}{k_{nr}{}^2} \right) + i \left(\frac{h_4}{k_{nr}} - h_2 \frac{F}{k_{nr}} + h_3 \frac{G}{k_{nr}{}^2} \right)$$

$$E_{11} = \left(m_1 + m_2 \frac{G}{k_{nr}} + m_3 \frac{F}{k_{nr}{}^2} + \frac{m_5}{k_{nr}{}^2} \right) + i \left(\frac{m_4}{k_{nr}} - m_2 \frac{F}{k_{nr}} + m_3 \frac{G}{k_{nr}{}^2} \right) - R_3 Z$$

where

$$C = F + iG \qquad\qquad k_{nr} = \frac{b_r \omega}{v_n} = \frac{b_r \omega}{v \cos \Lambda_{ea}} \qquad\qquad Z = \left(\frac{\omega_\alpha}{\omega} \right)^2 (1 + ig)$$

and

$$a_1 = \frac{-l}{\pi \rho b_r{}^2} \, \textcircled{1} - l \, \textcircled{2} \qquad\qquad\qquad a_2 = \frac{-l}{\pi} \, \textcircled{3}$$

$$a_3 = \frac{b_r \tan \Lambda_{ea}}{\pi} \quad \text{④} \qquad\qquad a_4 = b_r \tan \Lambda_{ea} \quad \text{⑤}$$

$$b_1 = -l \quad \text{⑥} \qquad\qquad b_2 = \frac{-l}{\pi} \quad \text{⑦}$$

$$b_3 = \frac{b_r \tan \Lambda_{ea}}{\pi} \quad \text{⑧} \qquad\qquad b_4 = b_r \tan \Lambda_{ea} \quad \text{⑨}$$

$$c_1 = \frac{-l}{\pi \rho b_r} \quad \text{⑩} \;+\; b_r l \quad \text{⑬} \qquad\qquad c_2 = \frac{-b_r l}{\pi} \quad \text{⑫}$$

$$c_3 = \frac{b_r l}{\pi} \quad \text{⑪} \;+\; \frac{b_r^2 \tan \Lambda_{ea}}{\pi} \quad \text{⑮} \qquad\qquad c_4 = b_r l \quad \text{⑭} \;-\; b_r^2 \tan \Lambda_{ea} \quad \text{⑯}$$

$$d_1 = -l \quad \text{⑥} \qquad\qquad d_2 = \frac{-l}{\pi} \quad \text{⑦}$$

$$d_3 = \frac{b_r \tan \Lambda_{ea}}{\pi} \quad \text{⑧} \qquad\qquad d_4 = b_r \tan \Lambda_{ea} \quad \text{⑨}$$

$$e_1 = \frac{-l}{\pi \rho b_r^2} \quad \text{①} \;-\; l \quad \text{②} \qquad\qquad e_2 = \frac{-l}{\pi} \quad \text{③}$$

$$e_3 = \frac{b_r \tan \Lambda_{ea}}{\pi} \quad \text{④} \qquad\qquad e_4 = b_r \tan \Lambda_{ea} \quad \text{⑤}$$

$$f_1 = \frac{-l}{\pi \rho b_r} \quad \text{⑩} \;+\; b_r l \quad \text{⑬} \qquad\qquad f_2 = \frac{-b_r l}{\pi} \quad \text{⑫}$$

$$f_3 = \frac{b_r l}{\pi} \quad \text{⑪} \;+\; \frac{b_r^2 \tan \Lambda_{ea}}{\pi} \quad \text{⑮} \qquad\qquad f_4 = b_r l \quad \text{⑭} \;-\; b_r^2 \tan \Lambda_{ea} \quad \text{⑯}$$

$$g_1 = \frac{-l}{\pi \rho b_r} \quad \text{⑩} \;+\; b_r l \quad \text{⑬} \qquad\qquad g_2 = \frac{b_r l}{\pi} \quad \text{⑰}$$

$$g_3 = \frac{-b_r^2 \tan \Lambda_{ea}}{\pi} \;\; ⑱ \qquad\qquad g_4 = -b_r^2 \tan \Lambda_{ea} \;\; ⑲$$

$$h_1 = \frac{-l}{\pi\rho b_r} \;\; ⑩\!\!\!\diagup + b_r l \;\; ⑬\!\!\!\diagup \qquad\qquad h_2 = \frac{b_r l}{\pi} \;\; ⑰\!\!\!\diagup$$

$$h_3 = \frac{-b_r^2 \tan \Lambda_{ea}}{\pi} \;\; ⑱\!\!\!\diagup \qquad\qquad h_4 = -b_r^2 \tan \Lambda_{ea} \;\; ⑲\!\!\!\diagup$$

$$m_1 = \frac{-l}{\pi\rho} \;\; ⑳ - b_r^2 l \;\; ㉒ \qquad\qquad m_2 = \frac{b_r^2 l}{\pi} \;\; ㉓$$

$$m_3 = \frac{-b_r^2 l}{\pi} \;\; ㉑ - \frac{b_r^3 \tan \Lambda_{ea}}{\pi} \;\; ㉕ \qquad m_4 = b_r^2 l \;\; ㉔ + b_r^3 \tan \Lambda_{ea} \;\; ㉗$$

$$m_5 = b_r^3 \tan \Lambda_{ea} \;\; ㉖$$

$$R_1 = \frac{-l}{\pi\rho b_r^2}\left(\frac{\omega_{h_1}}{\omega_\alpha}\right)^2 \;\; ① \qquad R_2 = \frac{-l}{\pi\rho b_r^2}\left(\frac{\omega_{h_2}}{\omega_\alpha}\right)^2 \;\; ①\!\!\!\diagup \qquad R_3 = \frac{-l}{\pi\rho} \;\; ⑳$$

and the circled numbers represent the following integrals:

$$① = \int_0^1 mh_1^2 d\eta \qquad\qquad ①\!\!\!\diagup = \int_0^1 mh_2^2 d\eta$$

$$② = \int_0^1 B^2 h_1^2 d\eta \qquad\qquad ②\!\!\!\diagup = \int_0^1 B^2 h_2^2 d\eta$$

$$③ = \int_0^1 C_{l_{\alpha,n}} B h_1^2 d\eta \qquad\qquad ③\!\!\!\diagup = \int_0^1 C_{l_{\alpha,n}} B h_2^2 d\eta$$

$$\text{④} = \int_0^1 C_{l_{\alpha,n}} B \frac{dh_1}{d\eta} h_1 d\eta \qquad\qquad \text{④}' = \int_0^1 C_{l_{\alpha,n}} B \frac{dh_2}{d\eta} h_2 d\eta$$

$$\text{⑤} = \int_0^1 B^2 \frac{dh_1}{d\eta} h_1 d\eta \qquad\qquad \text{⑤}' = \int_0^1 B^2 \frac{dh_2}{d\eta} h_2 d\eta$$

$$\text{⑥} = \int_0^1 B^2 h_1 h_2 d\eta \qquad\qquad\qquad \text{⑥}' = \text{⑥}$$

$$\text{⑦} = \int_0^1 C_{l_{\alpha,n}} B h_1 h_2 d\eta \qquad\qquad \text{⑦}' = \text{⑦}$$

$$\text{⑧} = \int_0^1 C_{l_{\alpha,n}} B \frac{dh_1}{d\eta} h_2 d\eta \qquad\qquad \text{⑧}' = \int_0^1 C_{l_{\alpha,n}} B \frac{dh_2}{d\eta} h_1 d\eta$$

$$\text{⑨} = \int_0^1 B^2 \frac{dh_1}{d\eta} h_2 d\eta \qquad\qquad \text{⑨}' = \int_0^1 B^2 \frac{dh_2}{d\eta} h_1 d\eta$$

$$\text{⑩} = \int_0^1 mB x_\alpha h_1 \alpha d\eta \qquad\qquad \text{⑩}' = \int_0^1 mB x_\alpha h_2 \alpha d\eta$$

$$\text{⑪} = \int_0^1 C_{l_{\alpha,n}} B h_1 \alpha d\eta \qquad\qquad \text{⑪}' = \int_0^1 C_{l_{\alpha,n}} B h_2 \alpha d\eta$$

$$\text{⑫} = \int_0^1 C_{l_{\alpha,n}} B^2 \left(\frac{C_{l_{\alpha,n}}}{2\pi} + ac_n - a \right) h_1 \alpha d\eta \qquad\qquad \text{⑫}' = \int_0^1 C_{l_{\alpha,n}} B^2 \left(\frac{C_{l_{\alpha,n}}}{2\pi} + ac_n - a \right) h_2 \alpha d\eta$$

$$\text{⑬} = \int_0^1 B^3 a h_1 \alpha d\eta$$

$$\text{⑬′} = \int_0^1 B^3 a h_2 \alpha d\eta$$

$$\text{⑭} = \int_0^1 B^2 h_1 \alpha d\eta$$

$$\text{⑭′} = \int_0^1 B^2 h_2 \alpha d\eta$$

$$\text{⑮} = \int_0^1 C_{l_{\alpha,n}} B^2 \left(\frac{C_{l_{\alpha,n}}}{2\pi} + \right.$$

$$\text{⑮′} = \int_0^1 C_{l_{\alpha,n}} B^2 \left(\frac{C_{l_{\alpha,n}}}{2\pi} + \right.$$

$$\left. ac_n - a \right) \frac{d\alpha}{d\eta} h_1 d\eta$$

$$\left. ac_n - a \right) \frac{d\alpha}{d\eta} h_2 d\eta$$

$$\text{⑯} = \int_0^1 B^3 a \frac{d\alpha}{d\eta} h_1 d\eta$$

$$\text{⑯′} = \int_0^1 B^3 a \frac{d\alpha}{d\eta} h_2 d\eta$$

$$\text{⑰} = \int_0^1 C_{l_{\alpha,n}} B^2 \left(a - ac_n \right) h_1 \alpha d\eta$$

$$\text{⑰′} = \int_0^1 C_{l_{\alpha,n}} B^2 \left(a - ac_n \right) \alpha h_2 d\eta$$

$$\text{⑱} = \int_0^1 C_{l_{\alpha,n}} B^2 \left(a - \right.$$

$$\text{⑱′} = \int_0^1 C_{l_{\alpha,n}} B^2 \left(a - \right.$$

$$\left. ac_n \right) \frac{dh_1}{d\eta} \alpha d\eta$$

$$\left. ac_n \right) \frac{dh_2}{d\eta} \alpha d\eta$$

$$\text{⑲} = \int_0^1 B^3 a \frac{dh_1}{d\eta} \alpha d\eta$$

$$\text{⑲′} = \int_0^1 B^3 a \frac{dh_2}{d\eta} \alpha d\eta$$

$$\text{⑳} = \int_0^1 r_\alpha^2 m B^2 \alpha^2 d\eta$$

$$\text{㉑} = \int_0^1 C_{l_{\alpha,n}} B^2 \left(a - ac_n \right) \alpha^2 d\eta$$

$$\text{㉒} = \int_0^1 B^4\left(\frac{1}{8} + a^2\right)\alpha^2 d\eta \qquad\qquad \text{㉓} = \int_0^1 C_{l_{\alpha,n}} B^3\left(\frac{C_{l_{\alpha,n}}}{2\pi} + ac_n - a\right)\left(a - ac_n\right)\alpha^2 d\eta$$

$$\text{㉔} = \int_0^1 B^3\left(\frac{C_{l_{\alpha,n}}}{2\pi} + ac_n - a\right)\alpha^2 d\eta \qquad\qquad \text{㉕} = \int_0^1 C_{l_{\alpha,n}} B^3\left(\frac{C_{l_{\alpha,n}}}{2\pi} + ac_n - a\right)\left(a - ac_n\right)\frac{d\alpha}{d\eta}\,\alpha d\eta$$

$$\text{㉖} = \int_0^1 B^3\left(\frac{C_{l_{\alpha,n}}}{2\pi} + ac_n\right)\frac{d\alpha}{d\eta}\,\alpha d\eta \qquad\qquad \text{㉗} = \int_0^1 B^4\left(\frac{1}{8} + a^2\right)\frac{d\alpha}{d\eta}\,\alpha d\eta$$

These integrals are easily evaluated numerically. Only about one-half of these integrals contain $C_{l_{\alpha,n}}$ or ac_n. Hence, only these integrals change with Mach number. For a given wing the remaining integrals may be evaluted once for all. Note that the integrals are independent of density ρ. The density appears only as a multiplying factor in a_1, c_1, e_1, f_1, g_1, h_1, m_1, R_1, R_2, and R_3.

Solution of the Determinant

For a given wing at a given Mach number the three-by-three flutter determinant (eq. (A15)) was solved for Z on an electronic digital computer for various values of the parameter k_{nr} (and associated values of F and G). This evaluation of Z yielded values of $\frac{v_n}{b_r\omega_\alpha}$ and g corresponding to the various k_{nr} values. A plot of g against $\frac{v_n}{b_r\omega_\alpha}$

then gave the value of k_{nr} and $\dfrac{v_n}{b_r \omega_\alpha}$ for which $g = 0$. These values

$$k_{nr} = \frac{b_r \omega}{V_n}$$

and

$$\frac{v_n}{b_r \omega_\alpha} = \frac{V_n}{b_r \omega_\alpha}$$

define a flutter point. Then the flutter speed V is

$$V = \frac{V_n}{b_r \omega_\alpha} \times \frac{b_r \omega_\alpha}{\cos \Lambda_{ea}}$$

and the flutter frequency ω is

$$\omega = k_{nr} \times \frac{V_n}{b_r \omega_\alpha} \times \omega_\alpha$$

APPENDIX B

PROCEDURE FOR MAKING FLUTTER CALCULATIONS

The following procedure was used in making the calculations presented herein.

Summary of Required Information

First, a summary sheet is set up similar to that shown in table II. The entries on this sheet represent all the information necessary for the evaluation of integrals ① to ㉗, coefficients a_1 to m_5, and R_1, R_2, and R_3 listed in appendix A. These coefficients together with the circulation functions F and G (calculation of which is discussed at the end of this appendix) permit evaluation of the determinant elements A_{11} to E_{11} and, hence, solution of the flutter determinant as described in appendix A.

Columns (1) to (5) of the summary sheet contain wing mass and elastic parameters which, in the present case, were determined experimentally. All of the experimental flutter data shown herein were obtained with the wings mounted on a fuselage. (See refs. 30 to 34.) The calculations were therefore made considering the wings to be cantilevered from the side of the fuselage which was assumed fixed. The quantities ω_α, $\left(\dfrac{\omega_{h_1}}{\omega_\alpha}\right)^2$, $\left(\dfrac{\omega_{h_2}}{\omega_\alpha}\right)^2$, and l listed at the top of the summary sheet are also measured values. Column (6) contains values of $B = \dfrac{b}{b_r}$, the nondimensionalized semichord measured perpendicular to the elastic axis. The nondimensionalizing value b_r is the semichord b at station $\eta = 0.75$. Values of b may be obtained from the following equations:

$$\frac{b}{s} = \frac{\xi_{TE} - \xi_{LE}}{\left(K_1 + K_2\right) + \left(K_1 - K_2\right)a} \tag{B1}$$

where

$$\xi_{LE} = \eta \tan \Lambda_{LE} \qquad\qquad (B2)$$

$$\xi_{TE} = \frac{4}{A_p(1 + \lambda_p)} + \eta \tan \Lambda_{TE} \qquad (B3)$$

$$s = l \cos \Lambda_{ea}$$

$$\left. \begin{aligned} K_1 &= \frac{\cos\left(\Lambda_{LE} - \Lambda_{ea}\right)}{\cos \Lambda_{LE}} \\[2em] K_2 &= \frac{\cos\left(\Lambda_{ea} - \Lambda_{TE}\right)}{\cos \Lambda_{TE}} \end{aligned} \right\} \qquad (B4)$$

$$\left. \begin{aligned} \tan \Lambda_{LE} &= \tan \Lambda_{c/4} + \frac{1}{A}\frac{1 - \lambda}{1 + \lambda} \\[2em] \tan \Lambda_{TE} &= \tan \Lambda_{LE} - \frac{4}{A}\frac{1 - \lambda}{1 + \lambda} \end{aligned} \right\} \qquad (B5)$$

The geometrical quantities appearing in these equations are shown in figure 36. Note that in equation (B3) the values of aspect ratio A_p and taper ratio λ_p to be used are those obtained by considering the side of the fuselage to be a reflection plane. In equations (B5) it is immaterial whether A and λ are obtained by considering the reflection plane to be at the side of the fuselage or at the fuselage center line.

Columns (7) to (12) of the summary sheet (table II) are the amplitudes and slopes of the uncoupled vibration mode shapes. These mode shapes may be calculated for the particular wing by any of the methods given in references 36 and 37. However, since flutter speed is not highly

sensitive to slight changes in mode shape, the mode shapes for a uniform
cantilever beam may be used if aspect ratio and taper ratio are not too
small. All calculations in the present report were made by using the
first torsion and first and second bending mode shapes for a uniform canti-
lever beam as given in table III and figure .37. (Equations governing har-
monic bending or torsional oscillations of a uniform cantilever beam are
derived in ref. 37.) Table III contains all combinations of these mode
shapes which are required for the calculation of integrals ① to ㉗ .
Also presented in table III are the integrals of these mode-shape com-
binations which are useful in evaluating the integrals for untapered
wings.

   Columns (13) and (14) of table II represent the distributions of
static aerodynamic parameters at a given Mach number.

   Calculation of Static Aerodynamic Parameters $C_{l_{\alpha},n}$ and ac_n

   The values of local lift-curve slope $C_{l_{\alpha},n}$ are obtained for sec-
tions normal to the elastic axis by applying simple sweep theory to $C_{l_{\alpha}}$
values for streamwise sections. Thus,

$$C_{l_{\alpha},n} = \frac{C_{l_{\alpha}}}{\cos \Lambda_{ea}} \qquad (B6)$$

The use of simple sweep theory together with values of $C_{l_{\alpha}}$ for stream-
wise sections results in $C_{l_{\alpha},n}$ values different from those obtained by
direct integration of pressures over sections normal to the elastic axis.
However, the resulting discrepancies are negligibly small except near the
wing root where deflection amplitudes are small. (See fig. 27(e).) The
use of simple sweep theory should thus cause negligible errors in the
values of the integrals ① to ㉗ . The local aerodynamic centers ac_n
in units of semichord b and measured perpendicular to the elastic axis
are found from

$$ac_n = \left[ac\left(\frac{\xi_{TE} - \xi_{LE}}{b/s}\right) - (1 + a)K_1 \right] \cos \Lambda_{ea} + a$$

$$= \left\{ ac\left[(K_1 + K_2) + (K_1 - K_2)a \right] - (1 + a)K_1 \right\} \cos \Lambda_{ea} + a \qquad (B7)$$

Distributions of $C_{l_{\alpha,n}}$ and ac_n for all the wings calculated are shown in figures 27 to 35. As indicated in figures 27(e) and (f) the values of $C_{l_{\alpha,n}}$ and ac_n used in the flutter calculations do not always lie on the curves of $C_{l_{\alpha,n}}$ and ac_n distribution. The integrals ① to ㉗ (appendix A) are evaluated numerically by using values of mass, elastic, and aerodynamic parameters at $\eta = 0.05$ to 0.95, in increments of 0.10. The required values of $C_{l_{\alpha,n}}$ and ac_n therefore are average values over the η-intervals 0 to 0.10, 0.10 to 0.20, . . . 0.90 to 1.00. These values do not coincide with the $C_{l_{\alpha,n}}$ and ac_n distribution curves near points of sharp change.

Subsonic free stream.- In the case of subsonic free-stream velocity, the spanwise distribution of $C_{l_{\alpha}}$ is found by the method of reference 24. For these subsonic loading calculations, the full wing is considered. That is, the reflection plane is considered to be at the fuselage center line, and the presence of the fuselage is neglected. The effect of the fuselage on the actual loading is felt primarily near the wing root. Since deflection amplitudes are small near the root, the overall effect of the fuselage on the integrals ① to ㉗ should be negligible. Since the loading distribution is computed for the full wing including fuselage intercept and since the distribution only over the wing panel is required in the flutter calculation, the full-wing distribution of $C_{l_{\alpha}}$ is plotted, and values are read off at stations corresponding to $\eta = 0.05$, 0.15, . . . 0.95 of the wing panel. (See fig. 38.) For subsonic free-stream velocity, $ac_n = -0.5$ is used throughout. This value corresponds to the aerodynamic center at the quarter-chord of a section normal to the elastic axis.

Supersonic free stream.- For supersonic free stream, the cases of subsonic leading edge and supersonic leading edge are considered.

(1) Subsonic leading edge: In the case of supersonic free-stream velocity and subsonic leading edge, the spanwise distributions of C_{l_α} and ac are found by the method of reference 25. For these calculations, the wing is treated throughout as though the side of the fuselage is a reflection plane. This assumption seems reasonable since in the linearized theory of reference 25 the distribution of loading on the wing panel is dominantly affected by Mach waves emanating from the wing-fuselage juncture.

When the leading edge is subsonic and the trailing edge is supersonic, as in sketch 1,
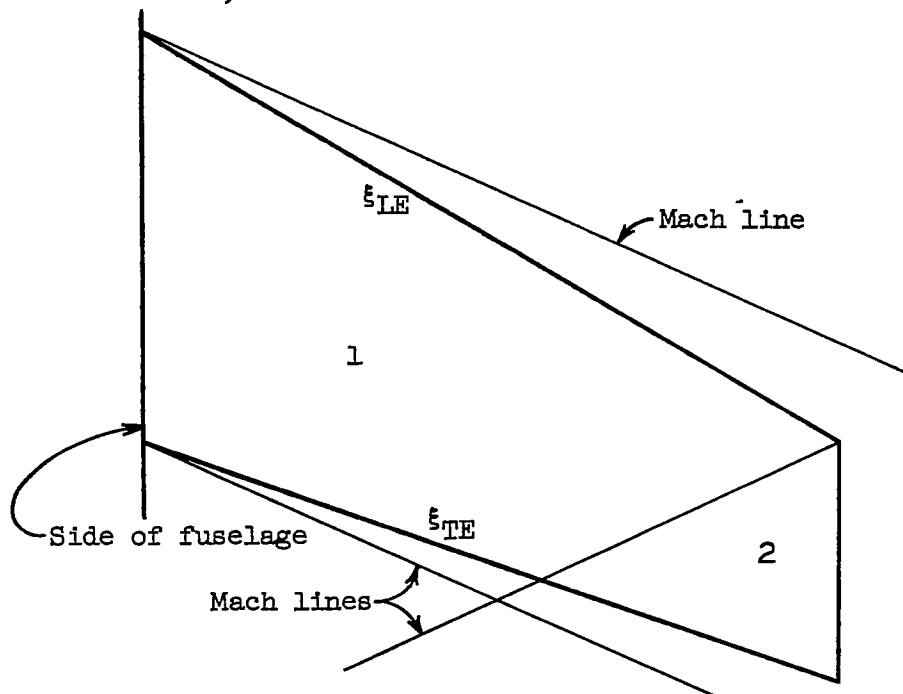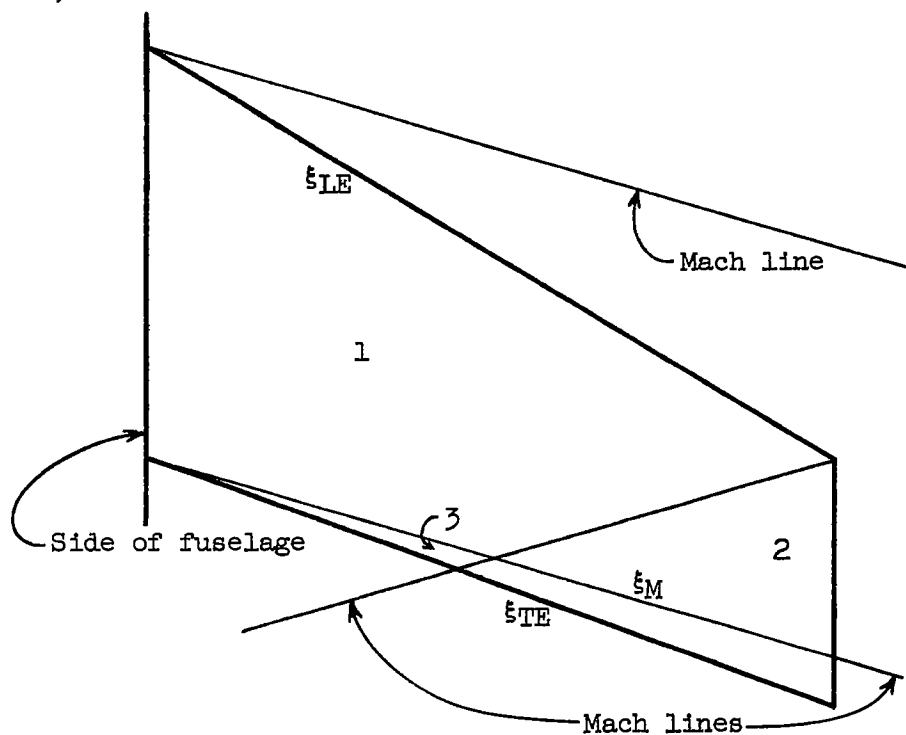

Sketch 1

the expressions for streamwise C_{l_α} and ac take a very simple form

$$C_{l_\alpha} = C_{l_\alpha,1} = \frac{4}{E \tan \Lambda_{LE}} \sqrt{\frac{\xi_{TE} + \xi_{LE}}{\xi_{TE} - \xi_{LE}}} \qquad (B8)$$

$$ac = \frac{C_{m_\alpha}}{C_{l_\alpha}} = \frac{C_{m_{\alpha,1}}}{C_{l_{\alpha,1}}} = \frac{1}{2\left(\xi_{TE} - \xi_{LE}\right)}\left(\xi_{TE} - 2\xi_{LE} + \frac{\xi_{LE}^2}{\sqrt{\xi_{TE}^2 - \xi_{LE}^2}} \log_e \frac{\xi_{TE} + \sqrt{\xi_{TE}^2 - \xi_{LE}^2}}{\xi_{LE}}\right) \quad (B9)$$

where $E = E\left(\sqrt{1 - \dfrac{\beta^2}{\tan^2\Lambda_{LE}}}\right)$ is the complete elliptic integral of the

second kind. Expressions for ξ_{LE}, ξ_{TE}, and $\tan\Lambda_{LE}$ are given by
equations (B2), (B3), and (B5). The numerical subscripts throughout
refer to the loading areas in the appropriate sketch. Note that for
this condition ac is a function only of wing geometry and that Mach
number affects C_{l_α} only through the function E. Equations (B8)

and (B9) contain no provision for accounting for the loss of loading
within the Mach cone from the tip leading edge. The procedure for
applying tip corrections is discussed subsequently.

When the leading edge and trailing edge are both subsonic, as in
sketch 2,

Sketch 2

the loadings indicated by equations (B8) and (B9) must be corrected to account for the loss of loading behind the root trailing-edge Mach line. For this condition

$$
\left.\begin{array}{l}
C_{l_\alpha} = C_{l_{\alpha,1}} + \Delta C_{l_{\alpha,3}} \\[2em]
C_{m_\alpha} = C_{m_{\alpha,1}} + \Delta C_{m_{\alpha,3}} \\[2em]
ac = \dfrac{C_{m_\alpha}}{C_{l_\alpha}}
\end{array}\right\} \tag{B10}
$$

where $C_{l_{\alpha,1}}$ and $C_{m_{\alpha,1}}$ are obtained from equations (B8) and (B9), and

$$
\left.\begin{array}{l}
\Delta C_{l_{\alpha,3}} = \dfrac{-4}{EK\tan\Lambda_{LE}\left(\xi_{TE} - \xi_{LE}\right)} \displaystyle\int_{\xi_M}^{\xi_{TE}} F\left(\varphi, \sqrt{1 - \dfrac{\beta^2}{\tan^2\Lambda_{TE}}}\right) d\xi \\[3em]
\Delta C_{m_{\alpha,3}} = \dfrac{-4}{EK\tan\Lambda_{LE}\left(\xi_{TE} - \xi_{LE}\right)^2} \displaystyle\int_{\xi_M}^{\xi_{TE}} \xi\, F\left(\varphi, \sqrt{1 - \dfrac{\beta^2}{\tan^2\Lambda_{TE}}}\right) d\xi - \dfrac{\xi_{LE}}{\xi_{TE} - \xi_{LE}} \Delta C_{l_{\alpha,3}}
\end{array}\right\} \tag{B11}
$$

where $K = K\left(\sqrt{1 - \dfrac{\beta^2}{\tan^2\Lambda_{TE}}}\right)$ is the complete elliptic integral of the

first kind, $F\left(\varphi, \sqrt{1 - \dfrac{\beta^2}{\tan^2\Lambda_{TE}}}\right)$ is the incomplete elliptic integral of

the first kind, and

$$
\xi_M = \frac{4}{A_p(1 + \lambda_p)} + \beta\eta \tag{B12}
$$

$$\varphi = \sin^{-1} \frac{\sqrt{1 - t_o^2}}{\sqrt{1 - \dfrac{\beta^2}{\tan^2 \Lambda_{TE}}}}$$

$$t_o = \frac{\beta \eta}{\xi - \dfrac{4}{A_p(1 + \lambda_p)}}$$

(B13)

Equations (B11) represent only the "symmetric" trailing-edge correction discussed in reference 25. However, this quantity is considered sufficiently accurate for present purposes. The integrals in equations (B11) are evaluated numerically.

For η stations near the wing tip the loadings given by equations (B8), (B9), or (B10) must be corrected to account for the loss of loading within the Mach cone from the tip leading edge. When the leading edge is subsonic, as in sketch 3,

Sketch 3

these corrections are made as follows: First, the spanwise locations of points P, S, and L (see sketch 3) are found from the equations

$$\eta_P = \frac{\tan \Lambda_{LE} + \beta - \dfrac{4}{A_p(1 + \lambda_p)}}{\tan \Lambda_{TE} + \beta} \tag{B14}$$

$$\eta_S = \eta_P + \left(\xi_{TE} - \xi_{ea}\right)_{\eta=\eta_P} \sin \Lambda_{ea} \cos \Lambda_{ea} \tag{B15}$$

where

$$\left(\xi_{TE} - \xi_{ea}\right)_{\eta=\eta_P} = \left(\frac{b}{s}\right)_{\eta=\eta_P}\left(1 - a_{\eta=\eta_P}\right)K_2$$

and

$$\eta_L = 1 - \left(\xi_{ea} - \xi_{LE}\right)_{\eta=1} \sin \Lambda_{ea} \cos \Lambda_{ea} \tag{B16}$$

where

$$\left(\xi_{ea} - \xi_{LE}\right)_{\eta=1} = \left(\frac{b}{s}\right)_{\eta=1}\left(1 + a_{\eta=1}\right)K_1$$

(See fig. 36.) The more inboard (measured parallel to the elastic axis) of the points S and L represents the η station at which the tip effect first begins to be felt.

The load intensity on the wing rises from trailing edge to leading edge and approaches infinity at the leading edge. Therefore, if $\eta_S < \eta_L$, the loss of loading caused by the tip will begin at the trailing edge where load intensity is relatively low and gradually extend forward into a region of high load intensity as·the tip is approached. The loss of loading outboard of η_S will thus produce a curve of $C_{l_{\alpha,n}}$ as a function of η which has negative curvature as well as negative slope. (See fig. 39(a).) Now the static aerodynamic loading parameters are introduced into the flutter equations through strip theory which implies that

the loading has a quasi-two-dimensional character. For a swept wing an
exact stripwise evaluation of loading near the tip would therefore have
questionable significance since neither the wing plan form nor the pres-
sure distribution is quasi-two-dimensional in that region. In view also
of the difficulty in performing an exact stripwise integration of loading
near the tip, a reasonable fairing of the $C_{l_{\alpha,n}}$ curve is considered
adequate, even though this fairing occurs at spanwise locations where
wing deflection is greatest. For the case of $\eta_S < \eta_L$ (fig. 39(a)),
the approximate curve used is geometrically derived from that obtained
by streamwise integration of loading in the tip region. The geometrical
derivation consists of applying a constant stretching factor to the curve
obtained by streamwise integration of the tip loading in order to fit
this curve to the known loading at $\eta = \eta_S$. The appropriate equations
for this streamwise calculation are equations (6), (15), and (26b) of
reference 25. No reflections of Mach lines from plan-form edges are con-
sidered. For wing 445, flutter speed determined by using this type of
fairing and that obtained by using exact stripwise integration of tip
loading differed by only 0.6 percent.

If $\eta_S = \eta_L$, the curve of $C_{l_{\alpha,n}}$ has a sharp discontinuity at
$\eta = \eta_S = \eta_L$. (See fig. 39(b).) In this case an accurate representation
of the loading in the tip region can be obtained with the aid of figure 7
of reference 25. This figure gives the loss of lift across the tip Mach
line. A straight line is used, as in figure 39(b), to fair the $C_{l_{\alpha,n}}$
curve to zero at η_T. The value of η_T is given by

$$\eta_T = 1 + \left(\xi_{TE} - \xi_{ea}\right)_{\eta=1} \sin \Lambda_{ea} \cos \Lambda_{ea} \qquad (B17)$$

If $\eta_S > \eta_L$, the region of high load intensity near the leading edge
is lost first, so that the curve of $C_{l_{\alpha,n}}$ against η has a steep nega-
tive slope just outboard of η_L but has also a positive curvature (as in
fig. 39(c)). In this case a straight line is used to fair the $C_{l_{\alpha,n}}$ curve
between η_L and $\eta = 1$. In no case is any loading outboard of $\eta = 1$
used in the flutter calculation.

In general, no tip correction was applied to ac_n since such cor-
rections would occur in only a small region. For wing 430, however, the
point η_S was so far inboard that it was considered necessary to apply
a tip correction to ac_n. (See figs. 28(d) and (e).) This correction

was obtained in the same manner as the correction for $C_{l_{\alpha,n}}$. That is, the correction was determined from streamwise integration of lift and pitching moment from which ac and hence ac_n were found.

(2) Supersonic leading edge: when the leading edge is supersonic, as in sketch 4,
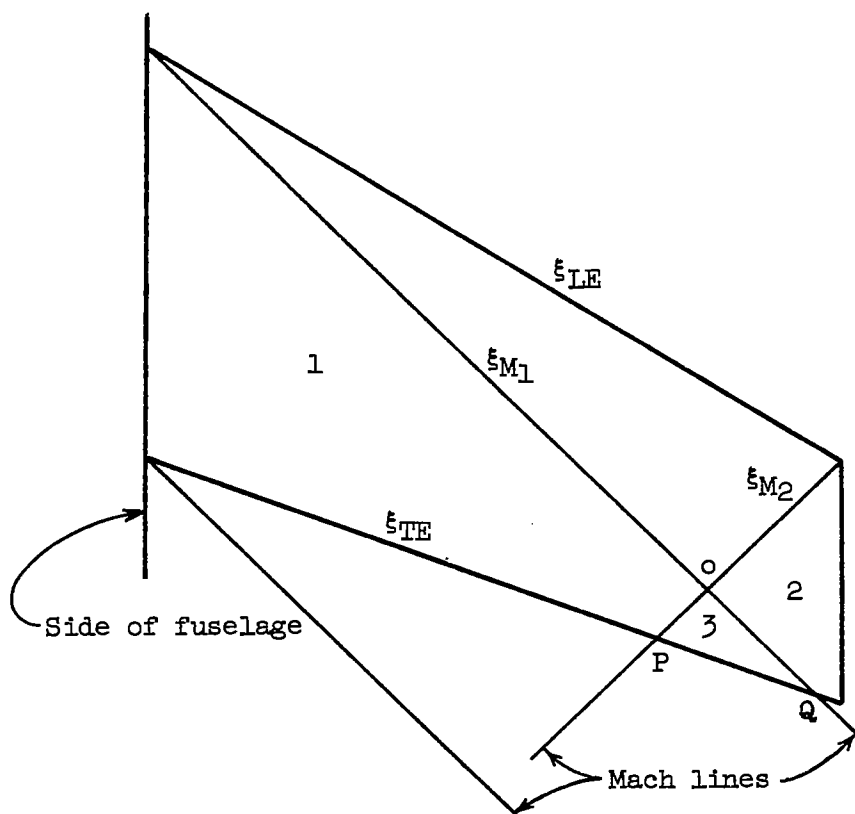
Sketch 4

the spanwise distributions of C_{l_α} and ac are found by the method of reference 26. Again the wing is treated as though the side of the fuselage is a reflection plane. Values of $C_{l_{\alpha,n}}$ and ac_n are found from C_{l_α} and ac by applying simple sweep theory as described previously. The procedure for finding C_{l_α} and ac is as follows: First, find the spanwise locations of points P, O, and Q (see sketch 4) by using the equations:

$$\eta_P = \frac{\tan \Lambda_{LE} + \beta - \dfrac{4}{A_p\left(1 + \lambda_p\right)}}{\tan \Lambda_{TE} + \beta} \qquad (B18)$$

$$\eta_O = \frac{\tan \Lambda_{LE} + \beta}{2\beta} \qquad (B19)$$

$$\eta_Q = \frac{4}{A_p\left(1 + \lambda_p\right)} \frac{1}{\beta - \tan \Lambda_{TE}} \qquad (B20)$$

If point O lies on the wing, then for $0 \leqq \eta \leqq \eta_P$,

$$c_{l_\alpha} = \frac{4}{\sqrt{\beta^2 - \tan^2\Lambda_{LE}}\left(\xi_{TE} - \xi_{LE}\right)}\left[\left(\xi_{M_1} - \xi_{LE}\right) + \int_{\xi_{M_1}}^{\xi_{TE}} \left(\frac{c_{p,1}}{c_{p,2D}}\right)d\xi\right] \qquad (B21)$$

and

$$c_{m_\alpha} = \frac{4}{\sqrt{\beta^2 - \tan^2\Lambda_{LE}}\left(\xi_{TE} - \xi_{LE}\right)^2}\left[\frac{1}{2}\left(\xi_{M_1}{}^2 - \xi_{LE}{}^2\right) + \int_{\xi_{M_1}}^{\xi_{TE}} \xi\left(\frac{c_{p,1}}{c_{p,2D}}\right)d\xi\right] - \frac{\xi_{LE}}{\xi_{TE} - \xi_{LE}}c_{l_\alpha} \qquad (B22)$$

For $\eta_P \leqq \eta \leqq \eta_O$,

$$c_{l_\alpha} = \frac{4}{\sqrt{\beta^2 - \tan^2\Lambda_{LE}}\left(\xi_{TE} - \xi_{LE}\right)}\left[\left(\xi_{M_1} - \xi_{LE}\right) + \int_{\xi_{M_1}}^{\xi_{M_2}} \left(\frac{c_{p,1}}{c_{p,2D}}\right)d\xi + \int_{\xi_{M_2}}^{\xi_{TE}} \left(\frac{c_{p,3}}{c_{p,2D}}\right)d\xi\right] \qquad (B23)$$

and

$$c_{m_\alpha} = \frac{4}{\sqrt{\beta^2 - \tan^2\Lambda_{LE}}\left(\xi_{TE} - \xi_{LE}\right)^2}\left[\frac{1}{2}\left(\xi_{M_1}{}^2 - \xi_{LE}{}^2\right) + \int_{\xi_{M_1}}^{\xi_{M_2}} \xi\left(\frac{c_{p,1}}{c_{p,2D}}\right)d\xi + \int_{\xi_{M_2}}^{\xi_{TE}} \xi\left(\frac{c_{p,3}}{c_{p,2D}}\right)d\xi\right] - \frac{\xi_{LE}}{\xi_{TE} - \xi_{LE}}c_{l_\alpha} \qquad (B24)$$

For $\eta_0 \leqq \eta \leqq \eta_Q$,

$$c_{l_\alpha} = \frac{4}{\sqrt{\beta^2 - \tan^2\Lambda_{LE}}\left(\xi_{TE} - \xi_{LE}\right)}\left[\left(\xi_{M2} - \xi_{LE}\right) + \int_{\xi_{M2}}^{\xi_{M_1}}\left(\frac{c_{p,2}}{c_{p,2D}}\right)d\xi + \int_{\xi_{M_1}}^{\xi_{TE}}\left(\frac{c_{p,3}}{c_{p,2D}}\right)d\xi\right] \quad \text{(B25)}$$

and

$$c_{m_\alpha} = \frac{4}{\sqrt{\beta^2 - \tan^2\Lambda_{LE}}\left(\xi_{TE} - \xi_{LE}\right)^2}\left[\frac{1}{2}\left(\xi_{M2}{}^2 - \xi_{LE}{}^2\right) + \int_{\xi_{M2}}^{\xi_{M_1}}\xi\left(\frac{c_{p,2}}{c_{p,2D}}\right)d\xi + \int_{\xi_{M_1}}^{\xi_{TE}}\xi\left(\frac{c_{p,3}}{c_{p,2D}}\right)d\xi\right] - \frac{\xi_{LE}}{\xi_{TE} - \xi_{LE}}c_{l_\alpha} \quad \text{(B26)}$$

For $\eta_Q \leqq \eta \leqq 1$,

$$c_{l_\alpha} = \frac{4}{\sqrt{\beta^2 - \tan^2\Lambda_{LE}}\left(\xi_{TE} - \xi_{LE}\right)}\left[\left(\xi_{M2} - \xi_{LE}\right) + \int_{\xi_{M2}}^{\xi_{TE}}\left(\frac{c_{p,2}}{c_{p,2D}}\right)d\xi\right] \quad \text{(B27)}$$

and

$$c_{m_\alpha} = \frac{4}{\sqrt{\beta^2 - \tan^2\Lambda_{LE}}\left(\xi_{TE} - \xi_{LE}\right)^2}\left[\frac{1}{2}\left(\xi_{M2}{}^2 - \xi_{LE}{}^2\right) + \int_{\xi_{M2}}^{\xi_{TE}}\xi\left(\frac{c_{p,2}}{c_{p,2D}}\right)d\xi\right] - \frac{\xi_{LE}}{\xi_{TE} - \xi_{LE}}c_{l_\alpha} \quad \text{(B28)}$$

where, as before,

$$\left.\begin{array}{c}\xi_{LE} = \eta\,\tan\Lambda_{LE} \\[3mm] \xi_{TE} = \dfrac{4}{A_p\left(1 + \lambda_p\right)} + \eta\,\tan\Lambda_{TE}\end{array}\right\} \quad \text{(B29)}$$

and

$$\left.\begin{array}{l} \xi_{M_1} = \beta\eta \\[2em] \xi_{M_2} = \tan\Lambda_{LE} + \beta(1-\eta) \end{array}\right\} \qquad (B30)$$

Also,

$$\left.\begin{array}{l} \left(\dfrac{C_{p,1}}{C_{p,2D}}\right) = \dfrac{1}{\pi}\cos^{-1}\left(R + \dfrac{S\eta^2}{\xi^2 - \tan^2\Lambda_{LE}\eta^2}\right) \\[2em] \left(\dfrac{C_{p,2}}{C_{p,2D}}\right) = \dfrac{1}{\pi}\cos^{-1}\left(\dfrac{\xi - T}{\xi - \tan\Lambda_{LE}\eta}\right) \\[2em] \left(\dfrac{C_{p,3}}{C_{p,2D}}\right) = \left(\dfrac{C_{p,1}}{C_{p,2D}}\right) + \left(\dfrac{C_{p,2}}{C_{p,2D}}\right) - 1 \end{array}\right\} \qquad (B31)$$

where

$$\left.\begin{array}{l} R = \dfrac{2}{\beta^2}\tan^2\Lambda_{LE} - 1 \\[2em] S = (R-1)\tan^2\Lambda_{LE} \\[2em] T = \tan\Lambda_{LE} + \left(2\beta + \tan\Lambda_{LE}\right)(1-\eta) \end{array}\right\} \qquad (B32)$$

If point O lies behind the trailing edge, then $\eta_P > \eta_Q$, and C_{l_α} and C_{m_α} are obtained as follows:

For $0 \leqq \eta \leqq \eta_Q$, C_{l_α} and C_{m_α} are given by equations (B21) and (B22); for $\eta_Q \leqq \eta \leqq \eta_P$,

$$C_{l_\alpha} = \frac{4}{\sqrt{\beta^2 - \tan^2\Lambda_{LE}}} \qquad (B33)$$

$$C_{m_\alpha} = \frac{4}{\sqrt{\beta^2 - \tan^2\Lambda_{LE}}} \times \frac{1}{2} \qquad (B34)$$

For $\eta_P \lesseqgtr \eta \lesseqgtr 1$, C_{l_α} and C_{m_α} are given by equations (B27) and (B28).

All of the integrals in the foregoing expressions for C_{l_α} and C_{m_α} are evaluated numerically.

It should be noted that for the case of supersonic leading edge if $\eta_S < \eta_L$, no separate tip correction is necessary. Approximately correct values of $C_{l_{\alpha,n}}$ and ac_n in the tip region ($\eta > \eta_S$) are obtained by applying simple sweep theory to the values of C_{l_α} and ac resulting from equations (B23) to (B28). Loadings of this type are shown in figures 28(e) and 34(d). If $\eta_S > \eta_L$, then the $C_{l_{\alpha,n}}$ curve is faired with a straight line between η_L and $\eta = 1$. (See fig. 39(c).) In this latter case, equations (B23) to (B28) need not be evaluated.

Circulation Functions

As mentioned in the body of this paper, the circulation functions F and G, which appear in the determinant elements listed in appendix A, are obtained from aerodynamic coefficients given in reference 27 for two-dimensional airfoils oscillating in compressible flow. (Similar coefficients for supersonic speeds only are also given in ref. 38.) These coefficients l_α, l_z, m_α, m_z are defined in reference 27 so that

$$P = -2b\rho v^2\left(h_{LE}l_z + \theta l_\alpha\right) \qquad (B35)$$

and

$$M_\alpha = (2b)^2\rho v^2\left(h_{LE}m_z + \theta m_\alpha\right) \qquad (B36)$$

in the notation of the present paper, where h_{LE} is the value of translation deflection at the leading edge. Now another expression for lift in the case of two-dimensional compressible flow may be obtained from equation (6) by deleting the terms containing σ and τ. Thus,

$$P = -\pi\rho b^2(v\dot{\theta} + \ddot{h} - ba\ddot{\theta}) - C_{l_{\alpha,n}}\rho vbC\left[v\theta + \dot{h} + b\left(\frac{C_{l_{\alpha,n}}}{2\pi} + ac_n - a\right)\dot{\theta}\right] \quad (B37)$$

where

$$\left.\begin{aligned} C_{l_{\alpha,n}} &= \frac{2\pi}{\beta} \\[2mm] ac_n &= -\frac{1}{2} \end{aligned}\right\} \quad \text{for} \quad M < 1$$

and

$$\left.\begin{aligned} C_{l_{\alpha,n}} &= \frac{4}{\beta} \\[2mm] ac_n &= 0 \end{aligned}\right\} \quad \text{for} \quad M > 1$$

Expressions for the circulation functions in terms of the aerodynamic coefficients of reference 29 may be obtained by equating expressions (B35) and (B37). Equating the two expressions for P (eqs. (B35) and (B37)), using

$$\dot{\theta} = i\omega\theta$$

$$\dot{h} = i\omega h$$

$$\ddot{\theta} = -\omega^2\theta$$

$$\ddot{h} = -\omega^2 h$$

for simple harmonic oscillation, and noting that

$$h_{LE} = \frac{h}{2b} - \frac{\theta}{2}(1 + a)$$

lead to

$$C_{l_{\alpha,n}}F_C\theta - C_{l_{\alpha,n}}G_C k_{nr}\left[\frac{h}{b} + \theta\left(\frac{C_{l_{\alpha,n}}}{2\pi} + ac_n - a\right)\right] = \pi k_{nr}^2\left(\frac{h}{b} - a\theta\right) + \left[\frac{h}{b} - \theta(1 + a)\right]l_z{}' + 2\theta l_\alpha{}'$$

and

$$C_{l_{\alpha,n}}F_C k_{nr}\left[\frac{h}{b} + \theta\left(\frac{C_{l_{\alpha,n}}}{2\pi} + ac_n - a\right)\right] + C_{l_{\alpha,n}}G_C\theta = -\pi\theta k_{nr} + \left[\frac{h}{b} - \theta(1 + a)\right]l_z{}'' + 2\theta l_\alpha{}''$$

where

$$l_\alpha = l_\alpha(M, k_{nr}) = l_\alpha{}' + il_\alpha{}''$$

$$l_z = l_z(M, k_{nr}) = l_z{}' + il_z{}''$$

Considering only the pitching oscillation, that is, putting $h = 0$, permits simplification to

$$F_C - k_{nr}\left(\frac{C_{l_{\alpha,n}}}{2\pi} + ac_n - a\right)G_C = \frac{1}{C_{l_{\alpha,n}}}\left[2l_\alpha{}' - (1 + a)l_z{}' - \pi k_{nr}^2 a\right]$$

and

$$k_{nr}\left(\frac{C_{l_{\alpha,n}}}{2\pi} + ac_n - a\right)F_C + G_C = \frac{1}{C_{l_{\alpha,n}}}\left[2l_\alpha{}'' - (1 + a)l_z{}'' - \pi k_{nr}\right]$$

or

$$F_C = \frac{\left[2l_\alpha' - (1+a)l_z'\right] + k_{nr}\left(\frac{C_{l_\alpha,n}}{2\pi} + ac_n - a\right)\left[2l_\alpha'' - (1+a)l_z''\right] - \pi k_{nr}^2\left(\frac{C_{l_\alpha,n}}{2\pi} + ac_n\right)}{C_{l_\alpha,n}\left[1 + k_{nr}^2\left(\frac{C_{l_\alpha,n}}{2\pi} + ac_n - a\right)^2\right]}$$ (B38)

and

$$G_C = \frac{\left[2l_\alpha'' - (1+a)l_z''\right] - k_{nr}\left(\frac{C_{l_\alpha,n}}{2\pi} + ac_n - a\right)\left[2l_\alpha' - (1+a)l_z'\right] - \pi k_{nr} + \pi k_{nr}^3 a\left(\frac{C_{l_\alpha,n}}{2\pi} + ac_n - a\right)}{C_{l_\alpha,n}\left[1 + k_{nr}^2\left(\frac{C_{l_\alpha,n}}{2\pi} + ac_n - a\right)^2\right]}$$ (B39)

Analogous expressions for F_C and G_C could be obtained by equating expressions for pitching moment M_α instead of lift P. It was indicated previously in this report that use of the present method for predicting flutter characteristics should probably be restricted to cases for which k_{nr} is moderately small. Therefore, the k_{nr}^3 term in equation (B39) may be dropped. Furthermore, the factor $\left(\frac{C_{l_\alpha,n}}{2\pi} + ac_n - a\right)$ does not vary greatly with Mach number except in the immediate vicinity of $M = 1$, and this vicinity is inaccessible to the present method. Therefore, since this factor is always multiplied by k_{nr} or k_{nr}^2, only small error will be introduced into the circulation functions by taking throughout $\left(\frac{C_{l_\alpha,n}}{2\pi} + ac_n - a\right) = \frac{1}{2}$, which is the incompressible flow value with $a = 0$. The value $a = 0$ implies torsional oscillation about the midchord. Equations (B38) and (B39) then reduce to

$$F_C = \frac{\left(2l_\alpha' - l_z'\right) + \frac{k_{nr}}{2}\left(2l_\alpha'' - l_z''\right) - \pi \frac{k_{nr}^2}{2}}{C_{l_\alpha,n}\left[1 + \left(\frac{k_{nr}}{2}\right)^2\right]}$$ (B40)

$$G_C = \frac{\left(2l_\alpha'' - l_z''\right) - \frac{k_{nr}}{2}\left(2l_\alpha' - l_z'\right) - \pi k_{nr}}{c_{l_{\alpha,n}}\left[1 + \left(\frac{k_{nr}}{2}\right)^2\right]} \tag{B41}$$

These expressions for F_C and G_C are independent of wing parameters and depend only on Mach number M and reduced frequency k_{nr}. As mentioned in the body of this report, when the two-dimensional circulation functions F_C and G_C are used in flutter calculations for three-dimensional wings, the functions are defined by the Mach number normal to the leading edge. Thus C_C becomes

$$C_C = C_C\left(M_{LE}, k_{nr}\right) = F_C\left(M_{LE}, k_{nr}\right) + iG_C\left(M_{LE}, k_{nr}\right)$$

A typical comparison of F_C and G_C calculated from equations (B40) and (B41) with those obtained from equations (B38) and (B39) is shown in figure 40. Values of F_C and G_C were obtained from equations (B38) and (B39) for two positions of aerodynamic center: $ac_n = 0$ (the two-dimensional supersonic value) and $ac_n = -0.325261$ (the value at the station $\eta = 0.75$ of wing 445 at $M = 1.75$). The results in both cases closely approximate the results from equations (B40) and (B41). The differences between the three sets of F_C and G_C curves shown in figure 40 would result in less than 1 percent difference in the calculated flutter speed for wing 445. Since calculated flutter speed is only moderately sensitive to small changes in the circulation function values (see fig. 3), the circulation functions used throughout this investigation were calculated from the simplified equations (B40) and (B41).

Some typical curves of F_C and G_C are shown in figure 41, and the combinations $\left(2l_\alpha' - l_z'\right)$ and $\left(2l_\alpha'' - l_z''\right)$ used in equations (B40) and (B41) are plotted in figures 42 and 43, respectively.

REFERENCES

1. Cicala, P.: Comparison of Theory With Experiment in the Phenomenon
     of Wing Flutter. NACA TM 887, 1939.

2. Dengler, M. A., and Goland, Martin: The Subsonic Calculation of
     Circulatory Spanwise Loadings for Oscillating Airfoils by Lifting-
     Line Techniques. Jour. Aero. Sci., vol. 19, no. 11, Nov. 1952,
     pp. 751-759.

3. Goland, Martin, Luke, Y. L., and Dengler, M. A.: Theoretical Studies
     of the Effects of Aspect Ratio on Flutter. Wright Air Development
     Center, WADC Tech. Rep. 54-29 (Contract Nos. AF18(600)-129 and
     AF33(038)-10400), Wright Air Dev. Center, U. S. Air Force, June 1954.

4. Biot, M. A., and Boehnlein, C. T.: Aerodynamic Theory of the Oscil-
     lating Wing of Finite Span. GALCIT Rep. No. 5, Sept. 1942.

5. Dingel, [M.], and Kuessner, [H. G.]: Contributions to Nonstationary
     Wing Theory. VIII - The Vibrating Wing of Large Aspect Ratio.
     Translation No. F-TS-935-RE, Air Materiel Command, U. S. Army Air
     Force, May 1947.

6. Lawrence, H. R., and Gerber, E. H.: The Aerodynamic Forces on Low
     Aspect Ratio Wings Oscillating in an Incompressible Flow. Jour.
     Aero. Sci., vol. 19, no. 11, Nov. 1952, pp. 769-781. (Errata issued,
     vol. 20, no. 4, Apr. 1953, p. 296.)

7. Schade, Th., and Krienes, K.: The Oscillating Circular Airfoil on
     the Basis of Potential Theory. NACA TM 1098, 1947.

8. Jones, Robert T.: The Unsteady Lift of a Wing of Finite Aspect Ratio.
     NACA Rep. 681, 1940.

9. Wasserman, L. S.: Aspect Ratio Corrections in Flutter Calculations.
     MR. No. MCREXA5-4595-8-5, Air Materiel Command, Eng. Div., U. S. Air
     Force, Aug. 26, 1948.

10. Reissner, Eric: Effect of Finite Span on the Airload Distributions
     for Oscillating Wings. I - Aerodynamic Theory of Oscillating Wings
     of Finite Span. NACA TN 1194, 1947.

11. Reissner, Eric, and Stevens, John E.: Effect of Finite Span on the
     Air-Load Distributions for Oscillating Wings. II - Methods of Cal-
     culation and Examples of Application. NACA TN 1195, 1947.

12. Runyan, Harry L., and Woolston, Donald S.: Method for Calculating the Aerodynamic Loading on an Oscillating Finite Wing in Subsonic and Sonic Flow. NACA TN 3694, 1956.

13. Nelson, Herbert C.: Lift and Moment on Oscillating Triangular and Related Wings With Supersonic Edges. NACA TN 2494, 1951.

14. Watkins, Charles E., and Berman, Julian H.: Air Forces and Moments on Triangular and Related Wings With Subsonic Leading Edges Oscillating in Supersonic Potential Flow. NACA Rep. 1099, 1952.

15. Nelson, Herbert C., Rainey, Ruby A., and Watkins, Charles E.: Lift and Moment Coefficients Expanded to the Seventh Power of Frequency for Oscillating Rectangular Wings in Supersonic Flow and Applied to a Specific Flutter Problem. NACA TN 3076, 1954.

16. Nelson, Herbert C., and Rainey, Ruby A.: Comparison of Flutter Calculations Using Various Aerodynamic Coefficients With Experimental Results for Some Rectangular Cantilever Wings at Mach Number 1.3. NACA TN 3301, 1954.

17. Froehlich, Jack E.: Nonstationary Motion of Purely Supersonic Wings. Jour. Aero. Sci., vol. 18, no. 5, May 1951, pp. 298-310.

18. Pines, S., and Dugundji, J.: Aerodynamic Flutter Derivatives of a Flexible Wing With Supersonic Edges. ATC Rep. No. ARTC-7, Aircraft Industries Assoc. (Washington, D. C.), Feb. 15, 1954.

19. Pines, Samuel, Dugundji, John, and Neuringer, Joseph: Aerodynamic Flutter Derivatives for a Flexible Wing With Supersonic and Subsonic Edges. Jour. Aero. Sci., vol. 22, no. 10, Oct. 1955, pp. 693-700.

20. Pines, S., and Dugundji, J.: Application of Aerodynamic Flutter Derivatives to Flexible Wings With Supersonic and Subsonic Edges. Rep. No. E-SAF-2, Republic Aviation Corp., Apr. 15, 1954.

21. Li, Ta: Aerodynamic Influence Coefficients for an Oscillating Finite Thin Wing in Supersonic Flow. Preprint No. 500, S.M.F. Pub. Fund Preprint, Inst. Aero. Sci., Inc., Jan. 1955.

22. Barmby, J. G., Cunningham, H. J., and Garrick, I. E.: Study of Effects of Sweep on the Flutter of Cantilever Wings. NACA Rep. 1014, 1951. (Supersedes NACA TN 2121.)

23. Smilg, Benjamin, and Wasserman, Lee S.: Application of Three-Dimensional Flutter Theory to Aircraft Structures. ACTR No. 4798, Materiel Div., Army Air Corps, July 9, 1942.

24. DeYoung, John, and Harper, Charles W.: Theoretical Symmetric Span
      Loading at Subsonic Speeds for Wings Having Arbitrary Plan Form.
      NACA Rep. 921, 1948.

25. Cohen, Doris: Formulas for the Supersonic Loading, Lift, and Drag
      of Flat Swept-Back Wings With Leading Edges Behind the Mach Lines.
      NACA Rep. 1050, 1951.

26. Lagerstrom, P. A., Wall, D., and Graham, M. E.: Formulas in Three-
      Dimensional Wing Theory. Rep. No. SM 11901, Douglas Aircraft Co.,
      Inc. July 8, 1946.

27. Jordan, P. F.: Aerodynamic Flutter Coefficients for Subsonic, Sonic
      and Supersonic Flow (Linear Two-Dimensional Theory). Rep. No.
      Structures 141, British R.A.E., Apr. 1953.

28. Bursnall, William J.: Initial Flutter Tests in the Langley Transonic
      Blowdown Tunnel and Comparison With Free-Flight Flutter Results.
      NACA RM L52K14, 1953.

29. Ruhlin, Charles L.: Experimental Transonic Flutter Characteristics
      of an Untapered, 45° Sweptback, Aspect-Ratio-4 Wing. NACA RM L55L22,
      1956.

30. Unangst, John R., and Jones, George W., Jr.: Some Effects of Sweep
      and Aspect Ratio on the Transonic Flutter Characteristics of a
      Series of Thin Cantilever Wings Having a Taper Ratio of 0.6. NACA
      RM L55I13a, 1956.

31. Jones, George W., Jr., and Unangst, John R.: Investigation To
      Determine Effects of Center-of-Gravity Location on Transonic Flutter
      Characteristics of a 45° Sweptback Wing. NACA RM L55K30, 1956.

32. Pratt, George L.: Experimental Flutter Investigation of a Thin
      Unswept Wing at Transonic Speeds. NACA RM L55A18, 1955.

33. Theodorsen, Theodore: General Theory of Aerodynamic Instability and
      the Mechanism of Flutter. NACA Rep. 496, 1935.

34. Woolston, Donald S., and Runyan, Harry L.: Appraisal of Method of
      Flutter Analysis Based on Chosen Modes by Comparison With Experi-
      ment for Cases of Large Mass Coupling. NACA TN 1902, 1949.

35. Theodorsen, Theodore, and Garrick, I. E.: Mechanism of Flutter - A
      Theoretical and Experimental Investigation of the Flutter Problem.
      NACA Rep. 685, 1940.

36. Houbolt, John C., and Anderson, Roger A.: Calculation of Uncoupled
    Modes and Frequencies in Bending or Torsion of Nonuniform Beams.
    NACA TN 1522, 1948.

37. Scanlan, Robert H., and Rosenbaum, Robert: Introduction to the Study
    of Aircraft Vibration and Flutter. The Macmillan Co., 1951.

38. Garrick, I. E., and Rubinow, S. I.: Flutter and Oscillating Air-
    Force Calculations for an Airfoil in a Two-Dimensional Supersonic
    Flow. NACA Rep. 846, 1946. (Supersedes NACA TN 1158.)

TABLE I

SUMMARY OF CALCULATED FLUTTER CHARACTERISTICS FOR SEVERAL WINGS

$$\left[\text{Calculations made by use of the complex circulation function} \quad C = \frac{F_C}{F_I}\left(F_I + iG_I\right)\right]$$

(a) Wings with taper ratio $\lambda = 0.6$

M	Wing 445			Wing 445F			Wing 445R			Wing 245			Wing 645		
	$A=4$; $\Lambda_{c/4}=45°$; $\rho=0.003800\,\frac{slug}{cu\ ft}$; $V_R=735.0\,\frac{ft}{sec}$; $\omega_\alpha=2,192\,\frac{radians}{sec}$			$A=4$; $\Lambda_{c/4}=45°$; $\rho=0.003000\,\frac{slug}{cu\ ft}$; $V_R=840.0\,\frac{ft}{sec}$; $\omega_\alpha=1,144\,\frac{radians}{sec}$			$A=4$; $\Lambda_{c/4}=45°$; $\rho=0.002378\,\frac{slug}{cu\ ft}$; $V_R=928.7\,\frac{ft}{sec}$; $\omega_\alpha=2,306\,\frac{radians}{sec}$			$A=2.4$; $\Lambda_{c/4}=45°$; $\rho=0.003900\,\frac{slug}{cu\ ft}$; $V_R=650.4\,\frac{ft}{sec}$; $\omega_\alpha=1,665\,\frac{radians}{sec}$			$A=6.4$; $\Lambda_{c/4}=45°$; $\rho=0.003500\,\frac{slug}{cu\ ft}$; $V_R=901.1\,\frac{ft}{sec}$; $\omega_\alpha=3,173\,\frac{radians}{sec}$		
	$\frac{V}{V_R}$	$\frac{\omega}{\omega_\alpha}$	k_{nr}	$\frac{V}{V_R}$	$\frac{\omega}{\omega_\alpha}$	k_{nr}	$\frac{V}{V_R}$	$\frac{\omega}{\omega_\alpha}$	k_{nr}	$\frac{V}{V_R}$	$\frac{\omega}{\omega_\alpha}$	k_{nr}	$\frac{V}{V_R}$	$\frac{\omega}{\omega_\alpha}$	k_{nr}
0	1.150	0.434	0.1408	1.125	0.605	0.0895	1.132	0.299	0.0781	------	------	--------	1.070	0.337	0.1063
.5	1.129	.436	.1444	1.103	.606	.0915	1.106	.299	.0800	------	------	-------	1.045	.338	.1092
.75	1.092	.438	.1496	1.065	.610	.0954	1.062	.300	.0833	1.244	0.918	0.2005	1.004	.340	.1142
1.15470	1.300	.467	.1347	1.363	.676	.0831	1.186	.315	.0794	1.668	.953	.1549	1.064	.360	.1136
1.41421	1.724	.473	.1019	-----	------	-------	1.479	.328	.0656	2.198	1.055	.1302	1.366	.362	.0893
1.75	1.866	.785	.1576	-----	-----	-------	-----	-----	-------	-----	-----	-------	-----	-----	------

TABLE I.- Continued

SUMMARY OF CALCULATED FLUTTER CHARACTERISTICS FOR SEVERAL WINGS

(a) Concluded

M	Wing 452 $A = 4;\ \Lambda_{c/4} = 52.5^\circ;$ $\rho = 0.002700\ \frac{slug}{cu\ ft};$ $V_R = 988.7\ \frac{ft}{sec};$ $\omega_\alpha = 2,300\ \frac{radians}{sec}$			Wing 430 $A = 4;\ \Lambda_{c/4} = 30^\circ;$ $\rho = 0.003700\ \frac{slug}{cu\ ft};$ $V_R = 694.7\ \frac{ft}{sec};$ $\omega_\alpha = 2,158\ \frac{radians}{sec}$			Wing 400 $A = 4;\ \Lambda_{c/4} = 0;$ $\rho = 0.002378\ \frac{slug}{cu\ ft};$ $V_R = 976.5\ \frac{ft}{sec};$ $\omega_\alpha = 2,463\ \frac{radians}{sec}$			Wing 400R $A = 4;\ \Lambda_{c/4} = 0;$ $\rho = 0.003100\ \frac{slug}{cu\ ft};$ $V_R = 852.5\ \frac{ft}{sec};$ $\omega_\alpha = 1,982\ \frac{radians}{sec}$		
	$\frac{V}{V_R}$	$\frac{\omega}{\omega_\alpha}$	k_{nr}	$\frac{V}{V_R}$	$\frac{\omega}{\omega_\alpha}$	k_{nr}	$\frac{V}{V_R}$	$\frac{\omega}{\omega_\alpha}$	k_{nr}	$\frac{V}{V_R}$	$\frac{\omega}{\omega_\alpha}$	k_{nr}
0	-----	-----	------	1.250	0.530	0.1646	1.398	0.586	0.1278	1.389	0.480	0.0974
.5	-----	-----	------	1.228	.530	.1676	1.362	.585	.1309	1.350	.480	.1000
.75	1.061	0.438	0.1189	1.186	.527	.1729	1.297	.584	.1373	1.283	.480	.1052
1.15470	-----	-----	------	1.608	.511	.1233	2.640	.753	.0870	1.549	.549	.0995
1.18415	1.113	.455	.1185	-----	-----	------	-----	-----	------	-----	-----	------
1.41421	1.340	.470	.1017	1.882	.680	.1403	4.100	1.469	.1093	1.919	.564	.0827
1.6	1.570	.479	.0885	-----	-----	------	-----	-----	------	-----	-----	------

TABLE I.- Concluded

SUMMARY OF CALCULATED FLUTTER CHARACTERISTICS FOR SEVERAL WINGS

(b) Wings with taper ratio $\lambda = 1.0$

M	Wing 4451 $A = 4;\ \Lambda_{c/4} = 45°;$ $\rho = 0.003200\ \frac{slug}{cu\ ft};$ $V_R = 944.7\ \frac{ft}{sec};$ $\omega_\alpha = 2,352\ \frac{radians}{sec}$			Wing 4001 $A = 4;\ \Lambda_{c/4} = 0;$ $\rho = 0.002378\ \frac{slug}{cu\ ft};$ $V_R = 828.5\ \frac{ft}{sec};$ $\omega_\alpha = 2,048\ \frac{radians}{sec}$			Wing 7001 $A = 7.38;\ \Lambda_{c/4} = 0;$ $\rho = 0.005500\ \frac{slug}{cu\ ft};$ $V_R = 844.8\ \frac{ft}{sec};$ $\omega_\alpha = 2,271\ \frac{radians}{sec}$		
	$\frac{V}{V_R}$	$\frac{\omega}{\omega_\alpha}$	k_{nr}	$\frac{V}{V_R}$	$\frac{\omega}{\omega_\alpha}$	k_{nr}	$\frac{V}{V_R}$	$\frac{\omega}{\omega_\alpha}$	k_{nr}
0	1.166	0.309	0.0961	1.475	0.412	0.0575	1.310	0.398	0.0755
.5	1.142	.308	.0978	1.430	.411	.0592	1.257	.398	.0787
.75	1.100	.307	.1013	1.353	.411	.0625	1.168	.400	.0851
1.15470	1.224	.339	.1005	1.860	.500	.0553	2.264	.756	.0831
1.3	-----	-----	------	2.330	.533	.0470	3.945	.768	.0485
1.35	1.566	.381	.0883	-----	-----	------	-----	-----	------

TABLE II

SAMPLE SUMMARY SHEET SHOWING INFORMATION REQUIRED FOR FLUTTER CALCULATIONS

Summary Sheet - Wing 400R

$A = 4; \lambda = 0.6; \Lambda_{c/4} = 0;$

$A_p = 3.30; \lambda_p = 0.657; \tan \Lambda_{ea} = 0$

$\left(\dfrac{\omega_{h_1}}{\omega_\alpha}\right)^2 = 0.082736; \left(\dfrac{\omega_{h_2}}{\omega_\alpha}\right)^2 = 2.00956; \omega_\alpha = 1982.3 \text{ radians/sec};$

$l = 0.4458333 \text{ ft}; b_r = 0.1209635 \text{ ft}; \rho = 0.003100 \text{ slug/cu ft}$

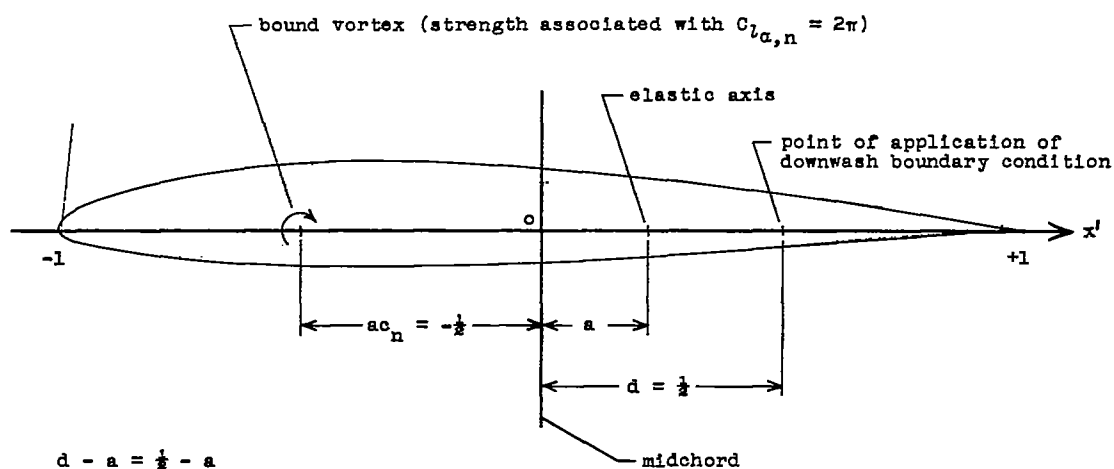| Station	Wing mass and stiffness parameters				Nondimensional semichord	Wing vibration mode shapes (a)						Static aerodynamic parameters for $M = \sqrt{2}$	
(1)	(2)	(3)	(4)	(5)	(6)	(7)	(8)	(9)	(10)	(11)	(12)	(13)	(14)
η	$\dfrac{m_y}{\text{slugs/ft}}$	r_α^2	x_α	a	$B = \dfrac{b}{b_r}$	α	$\dfrac{d\alpha}{d\eta}$	h_1	$\dfrac{dh_1}{d\eta}$	h_2	$\dfrac{dh_2}{d\eta}$	$c_{l_{\alpha,n}}$	ac_n
0.05	0.01451	0.340	0.223	-0.0500	1.322497	0.07846	1.56596	0.0042924	0.16974	-0.025351	-0.97005	3.863575	-0.0032564
.15	.01382	.337	.221	-.0499	1.276426	.23345	1.52740	.036832	.47295	-.18879	-2.12604	3.895958	-.0074113
.25	.01298	.330	.219	-.0494	1.230355	.38268	1.45123	.097280	.72805	-.41726	-2.28648	3.926802	-.0086348
.35	.01197	.300	.217	-.0485	1.184284	.52250	1.33933	.18086	.93588	-.61768	-1.59857	3.955474	-.0076147
.45	.01093	.284	.215	-.0465	1.138213	.64945	1.19444	.28293	1.09814	-.71699	-.31353	3.957912	-.0105307
.55	.01002	.278	.213	-.0441	1.092142	.76041	1.02015	.39907	1.21770	-.67127	1.24454	3.844466	-.0358626
.65	.00927	.284	.211	-.0409	1.046071	.85264	.82074	.52519	1.29879	-.47029	2.73860	3.615055	-.0776133
.75	.00853	.308	.209	-.0370	1.000000	.92388	.60110	.65773	1.34710	-.13507	3.89150	3.246949	-.1338290
.85	.00770	.306	.207	-.0323	.953929	.97237	.36669	.79367	1.36998	.29154	4.55626	2.670658	-.2024901
.95	.00668	.284	.205	-.0270	.907858	.99692	.12322	.93117	1.37634	.76093	4.77088	1.631485	-.2817228

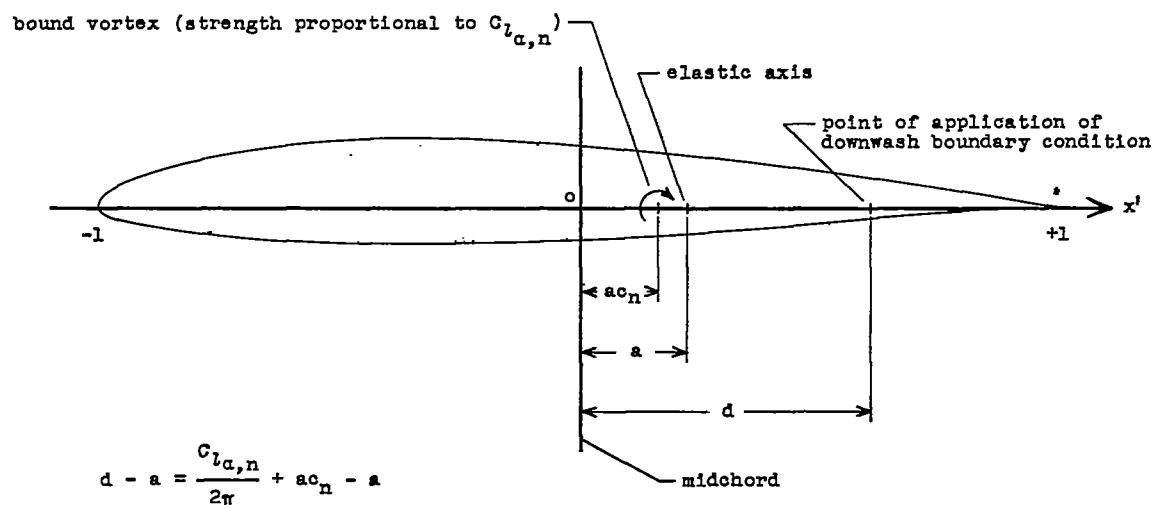^aValues listed are for uniform cantilever beam.

TABLE III

MODE-SHAPE COMBINATIONS FOR UNIFORM CANTILEVER BEAM

USED IN FLUTTER CALCULATIONS

[First torsion and first and second bending modes]

(1)	(2)	(3)	(4)	(5)	(6)	(7)	(8)	(9)	(10)	(11)	(12)	(13)	(14)	(15)	(16)	(17)	(18)	(19)	(20)	(21)	(22)
η	α	$\frac{d\alpha}{d\eta}$	h_1	$\frac{dh_1}{d\eta}$	h_2	$\frac{dh_2}{d\eta}$	α^2	$\frac{d\alpha}{d\eta}\alpha$	$h_1\alpha$	$\frac{dh_1}{d\eta}\alpha$	$h_2\alpha$	$\frac{dh_2}{d\eta}\alpha$	$\frac{d\alpha}{d\eta}h_1$	$\frac{d\alpha}{d\eta}h_2$	h_1^2	$\frac{dh_1}{d\eta}h_1$	h_1h_2	$\frac{dh_2}{d\eta}h_1$	h_2^2	$\frac{dh_2}{d\eta}h_2$	$\frac{dh_1}{d\eta}h_2$
0.05	0.07846	1.56596	0.00429	0.16974	-0.02555	-0.97005	0.00616	0.12287	0.00034	0.01532	-0.00199	-0.07611	0.00672	-0.03570	0.00002	0.00073	-0.00011	-0.00416	0.00064	0.02459	-0.00450
.15	.23345	1.52740	.03683	.47295	-.18879	-2.12604	.05450	.35657	.00860	.11041	-.04407	-.49632	.05626	-.28856	.00136	.01742	-.00695	-.07831	.03564	.40138	-.08929
.25	.38268	1.45123	.09728	.78805	-.41726	-2.88648	.14644	.55536	.03723	.27861	-.15968	-.87499	.14118	-.60554	.00946	.07062	-.04059	-.22243	.17411	.95406	-.30579
.35	.52250	1.33553	.18086	.99588	-.61768	-1.59857	.27301	.69980	.09450	.48900	-.32274	-.83525	.24223	-.82728	.03271	.16926	-.11171	-.28912	.38153	.98740	-.57807
.45	.64945	1.19444	.28293	1.09814	-.71699	-.50353	.42179	.77573	.18375	.71319	-.46565	-.20362	.33794	-.85640	.08005	.31070	-.20286	-.08871	.51407	.22480	-.78736
.55	.76041	1.00015	.39907	1.21770	-.67127	1.24454	.57822	.77573	.30346	.92595	-.51044	.94636	.40711	-.68480	.15926	.48595	-.26788	.49666	.45060	.83542	-.81741
.65	.85264	.82074	.52519	1.29879	-.47029	2.73860	.72699	.69980	.44780	1.10740	-.40099	2.33504	.43104	-.38599	.27582	.68211	-.24699	1.43849	.22117	-1.28794	-.61081
.75	.92588	.60110	.65773	1.34710	-.13307	3.89050	.85755	.55554	.60766	1.24456	-.12479	3.59528	.39536	-.08119	.43261	.88603	-.08884	2.55956	.01824	-.52562	-.18195
.85	.97257	.36669	.79576	1.36998	.29154	4.55626	.94550	.35656	.77185	1.33213	.28548	4.43037	.29106	.10690	.63305	1.08744	.23141	3.61658	.08500	1.32853	.39940
.95	.99692	.12362	.95117	1.37634	.76093	4.77088	.99385	.12284	.94830	1.37210	.75859	4.75609	.11474	.09376	.86708	1.28161	.70656	4.44230	.57901	3.63031	1.04730
$\frac{\Sigma}{10}$							.50000	.50206	.33835	.75867	-.09883	1.35769	.24236	-.35686	.24884	.49921	-.00260	1.18709	.24600	.49019	-.19263

bound vortex (strength associated with $C_{l_{\alpha,n}} \approx 2\pi$)

elastic axis

point of application of
downwash boundary condition

o

x'

-1   +1

$ac_n = -\frac{1}{2}$ a

$d = \frac{1}{2}$

$d - a = \frac{1}{2} - a$ midchord

(a) Relations used in references 22 and 33.

bound vortex (strength proportional to $C_{l_{\alpha,n}}$)

elastic axis

point of application of
downwash boundary condition

o

x'

-1   +1

ac_n

a

d

$d - a = \dfrac{C_{l_{\alpha,n}}}{2\pi} + ac_n - a$ midchord

(b) Relations used in present method.

Figure 1.- Geometric relations associated with the application of the
downwash boundary condition.
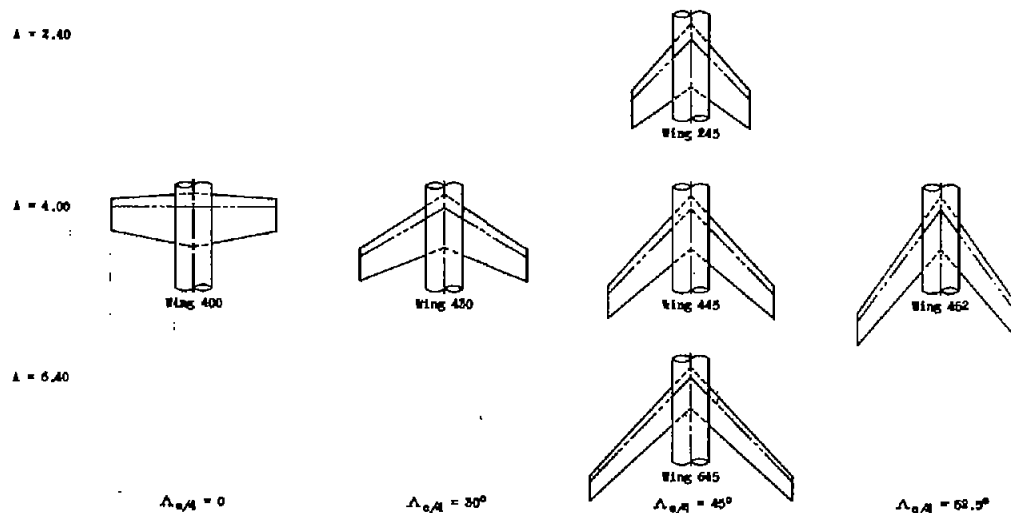
(a) Wings with $\lambda = 0.6$.
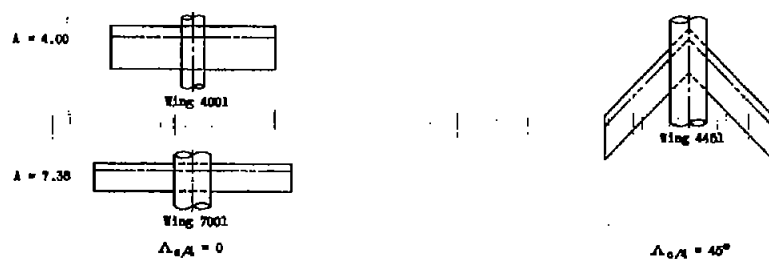
(b) Wings with $\lambda = 1.0$.

Figure 2.- Plan forms of wings for which flutter characteristics were calculated.
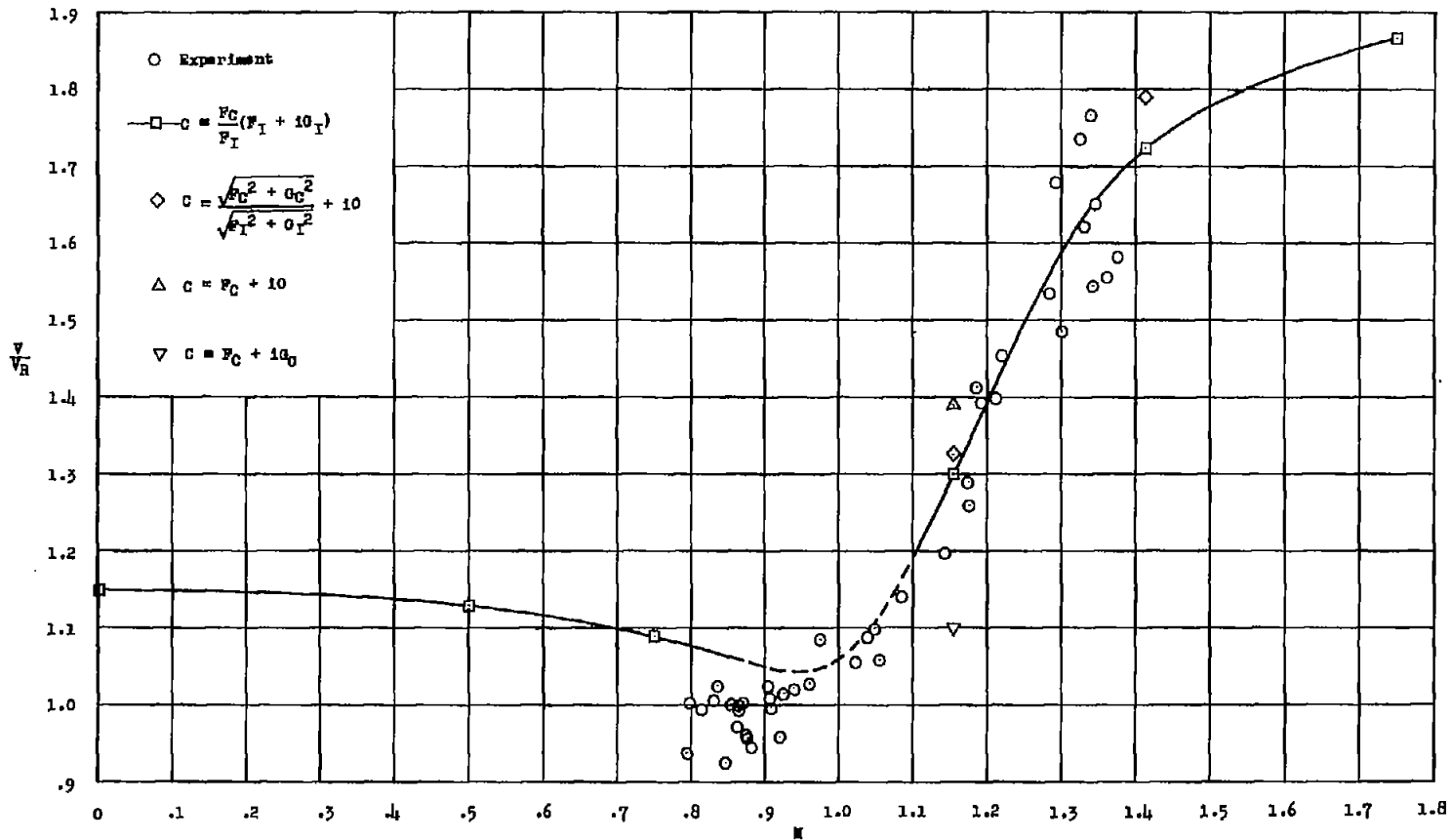
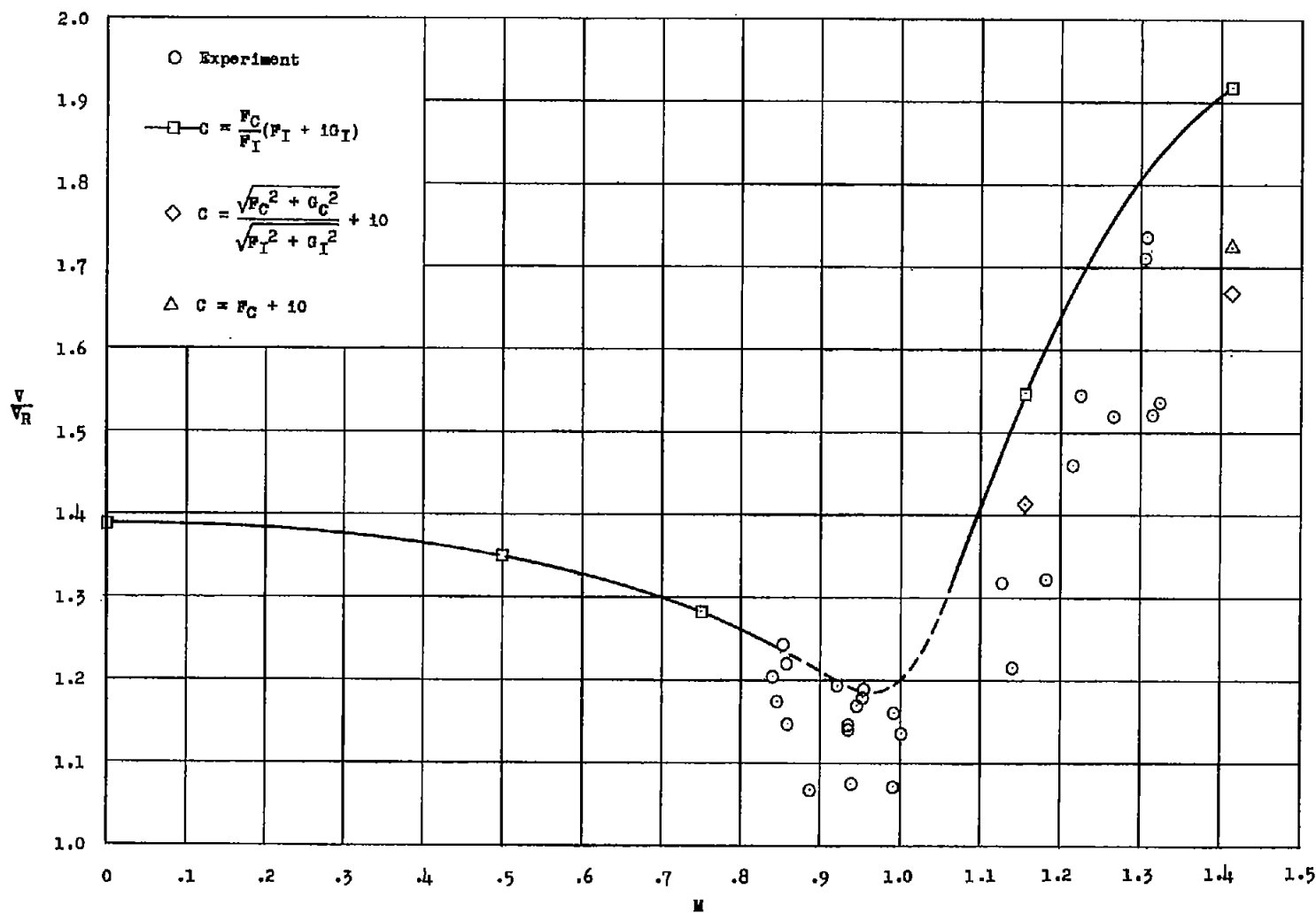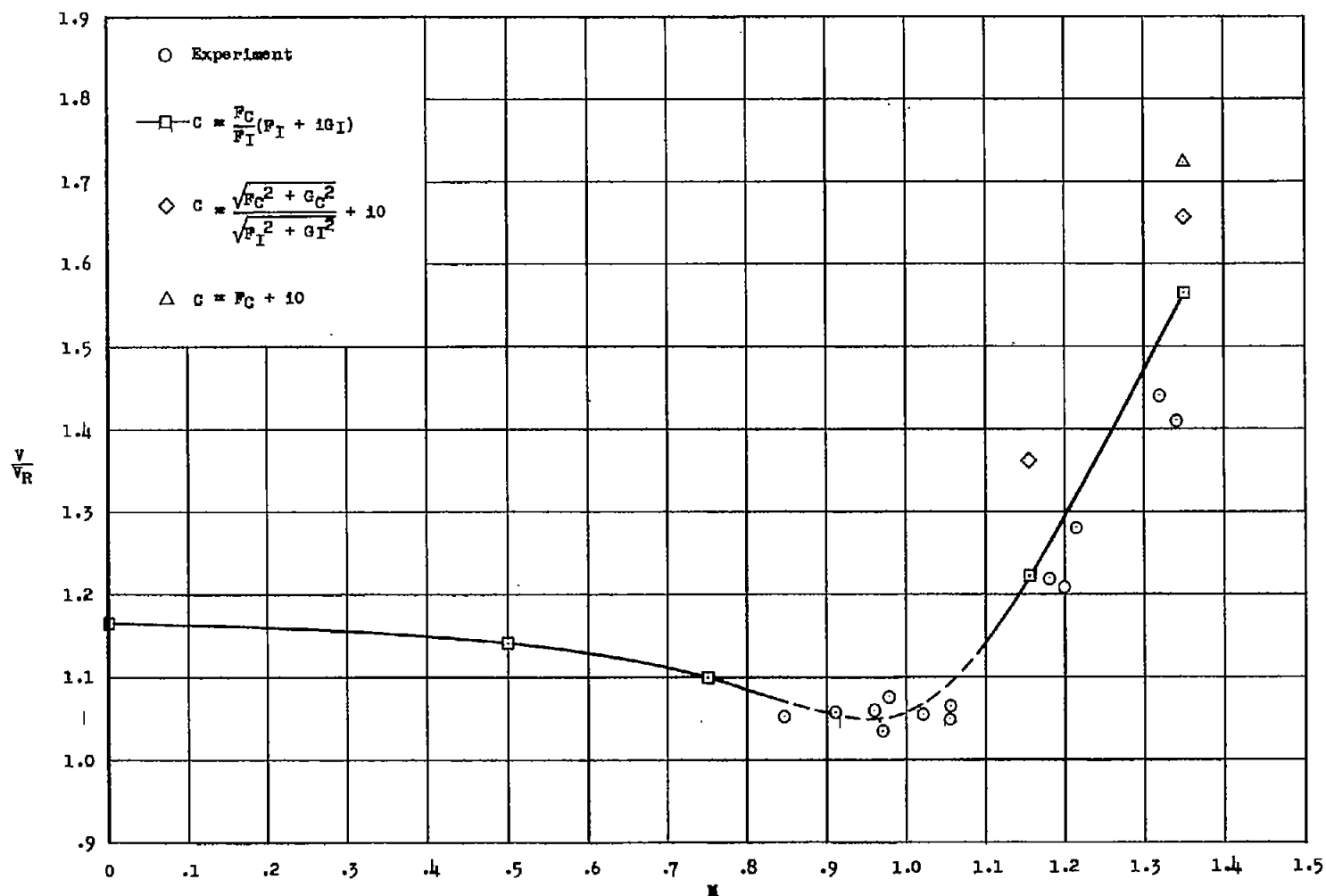Figure 3.- Variation of flutter speed with Mach number for wing 445. For calculated points ρ = 0.003800 slugs/cu ft.

Figure 4.- Variation of flutter speed with Mach number for wing 445F. For calculated points $\rho = 0.003000$ slugs/cu ft.
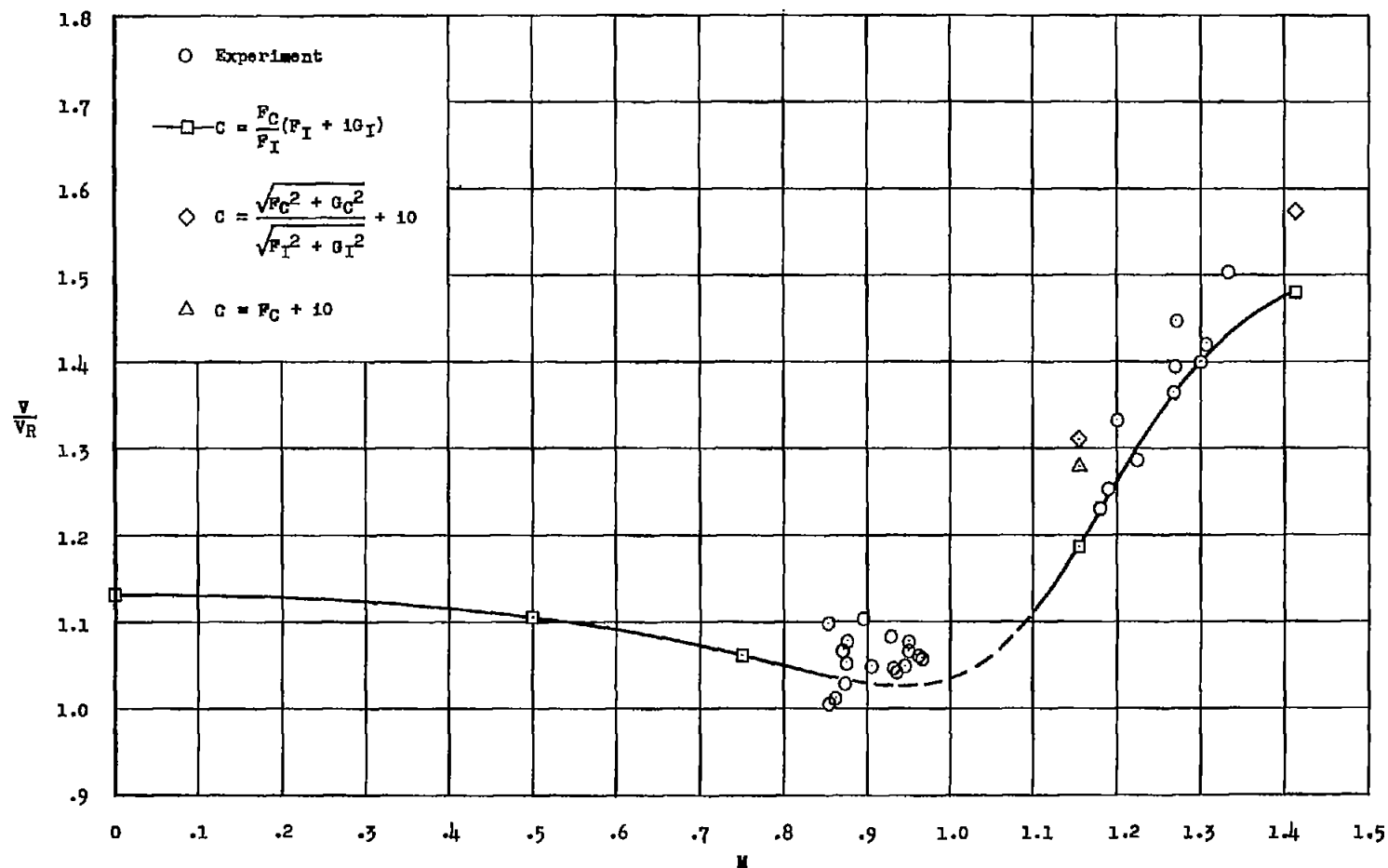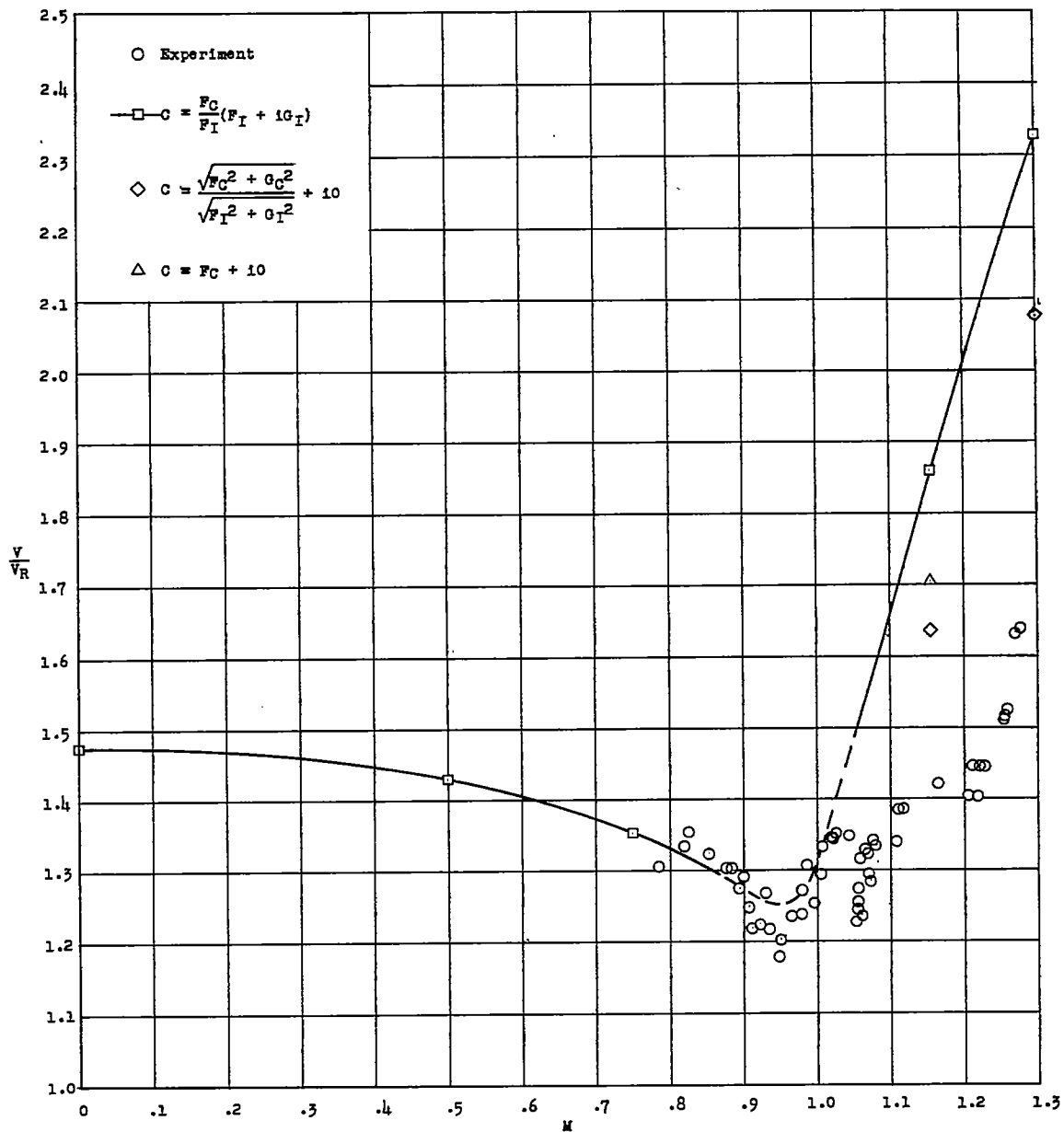
Figure 5.- Variation of flutter speed with Mach number for wing 445R. For calculated points $\rho = 0.002378$ slugs/cu ft.
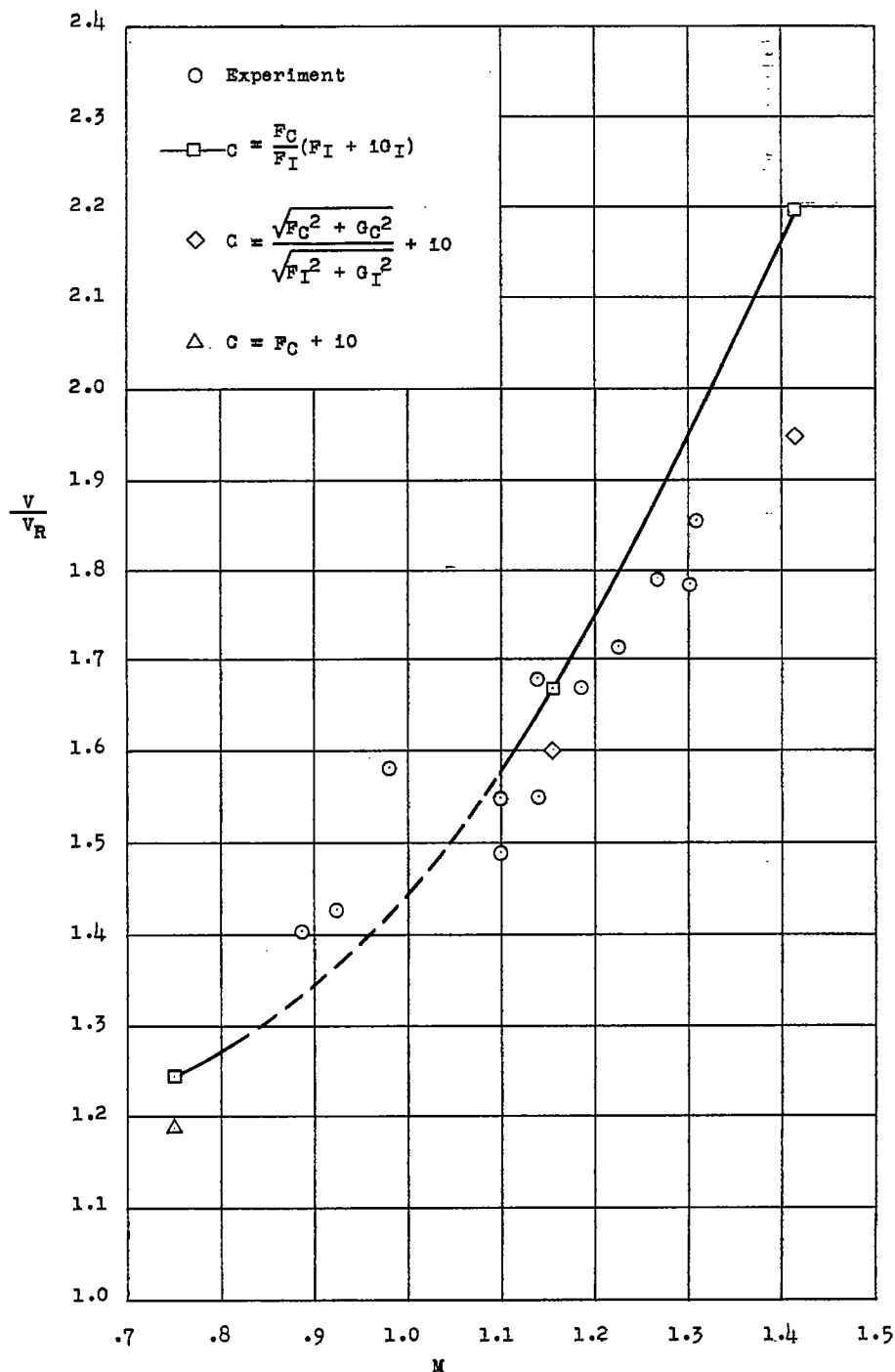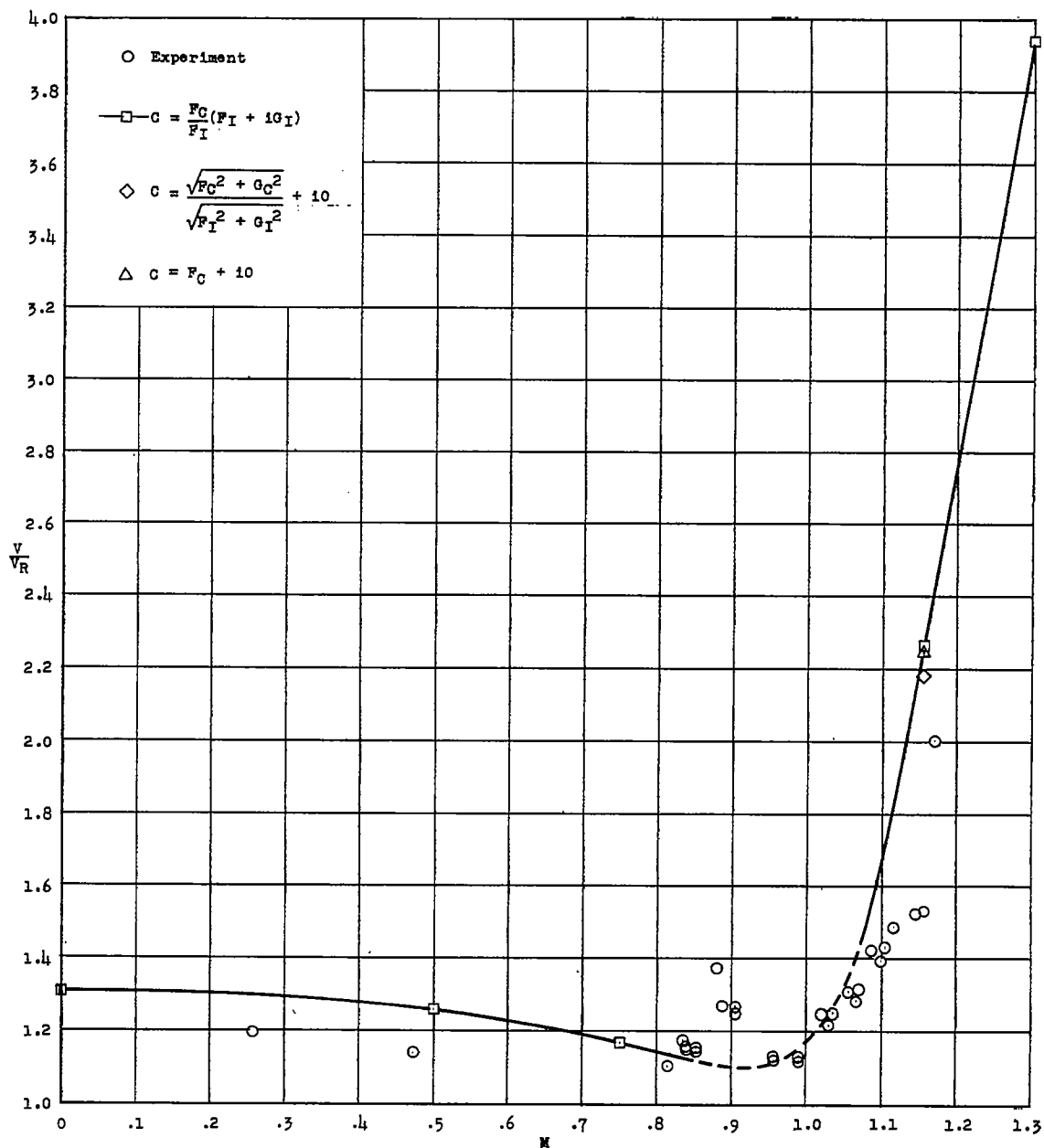
Figure 6.- Variation of flutter speed with Mach number for wing 245. For calculated points $\rho = 0.003900$ slugs/cu ft.
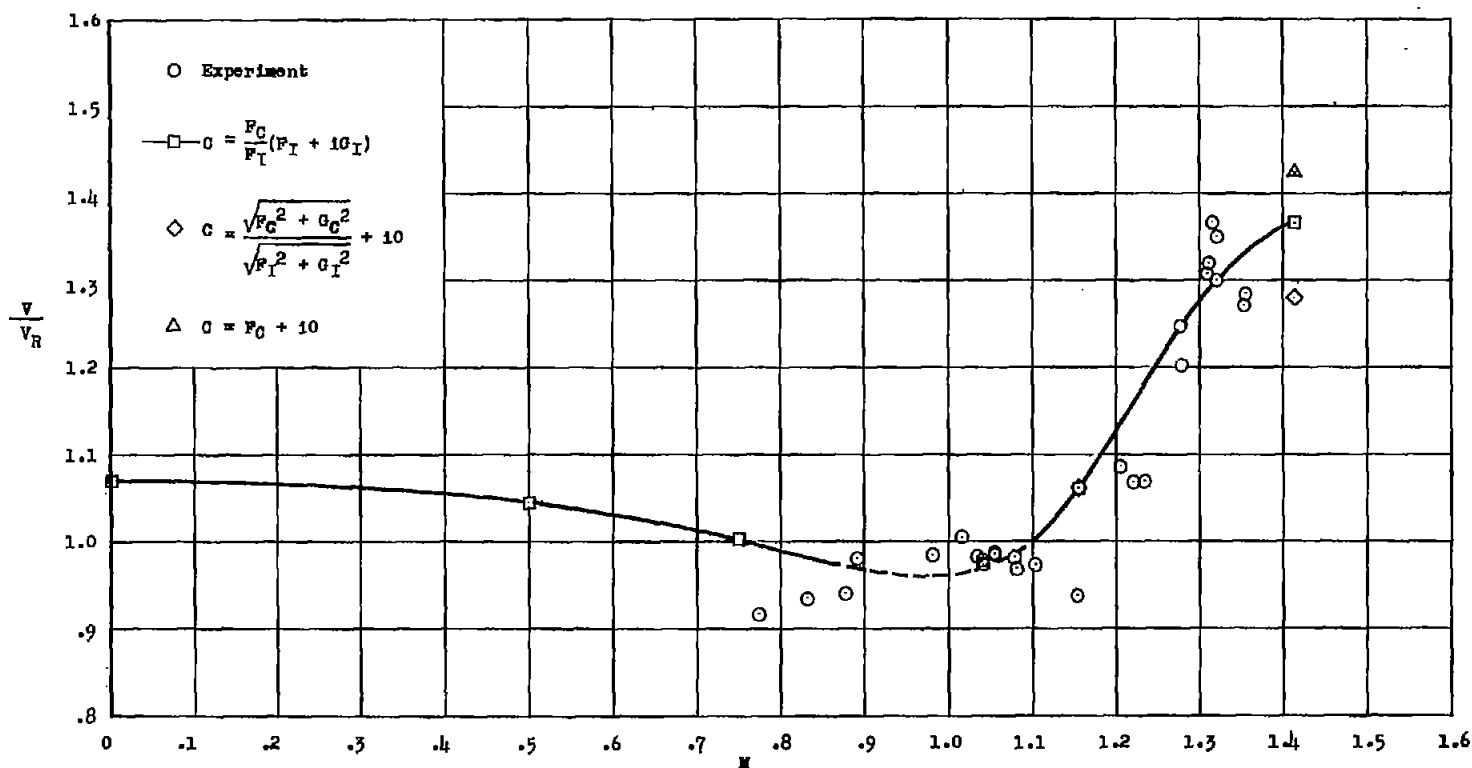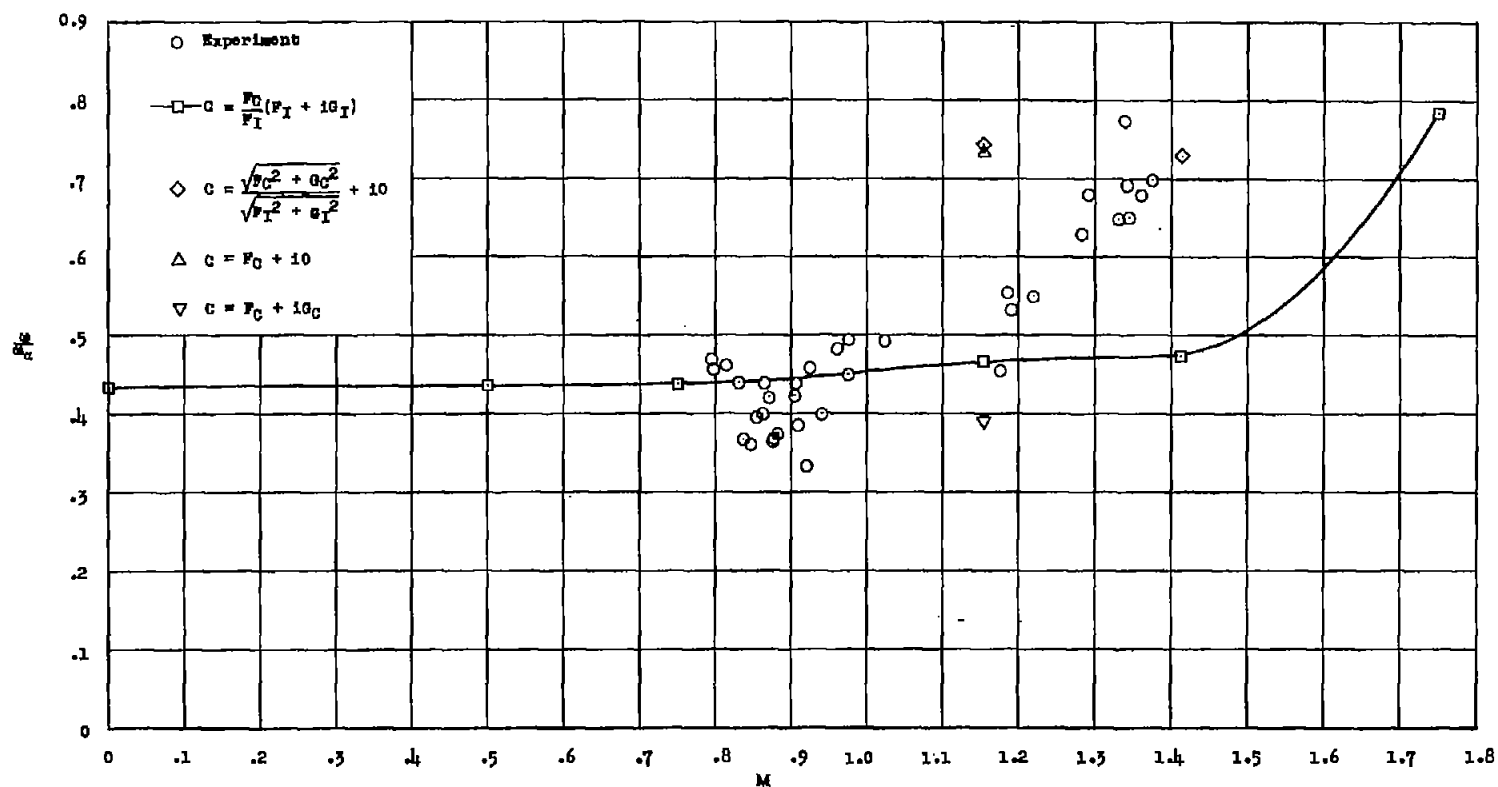
Figure 7.- Variation of flutter speed with Mach number for wing 645.   For calculated points
$\rho = 0.003500$ slugs/cu ft.
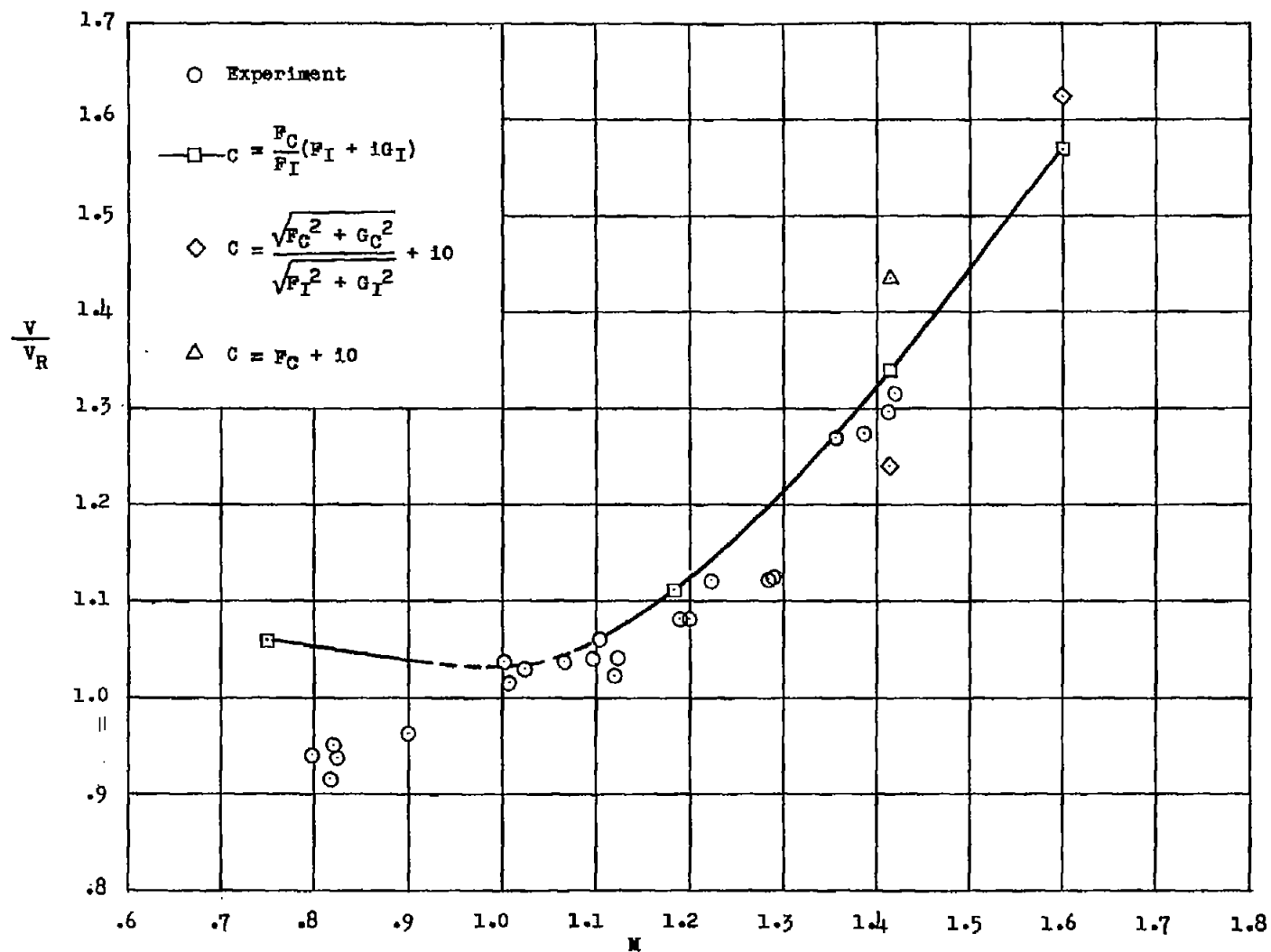
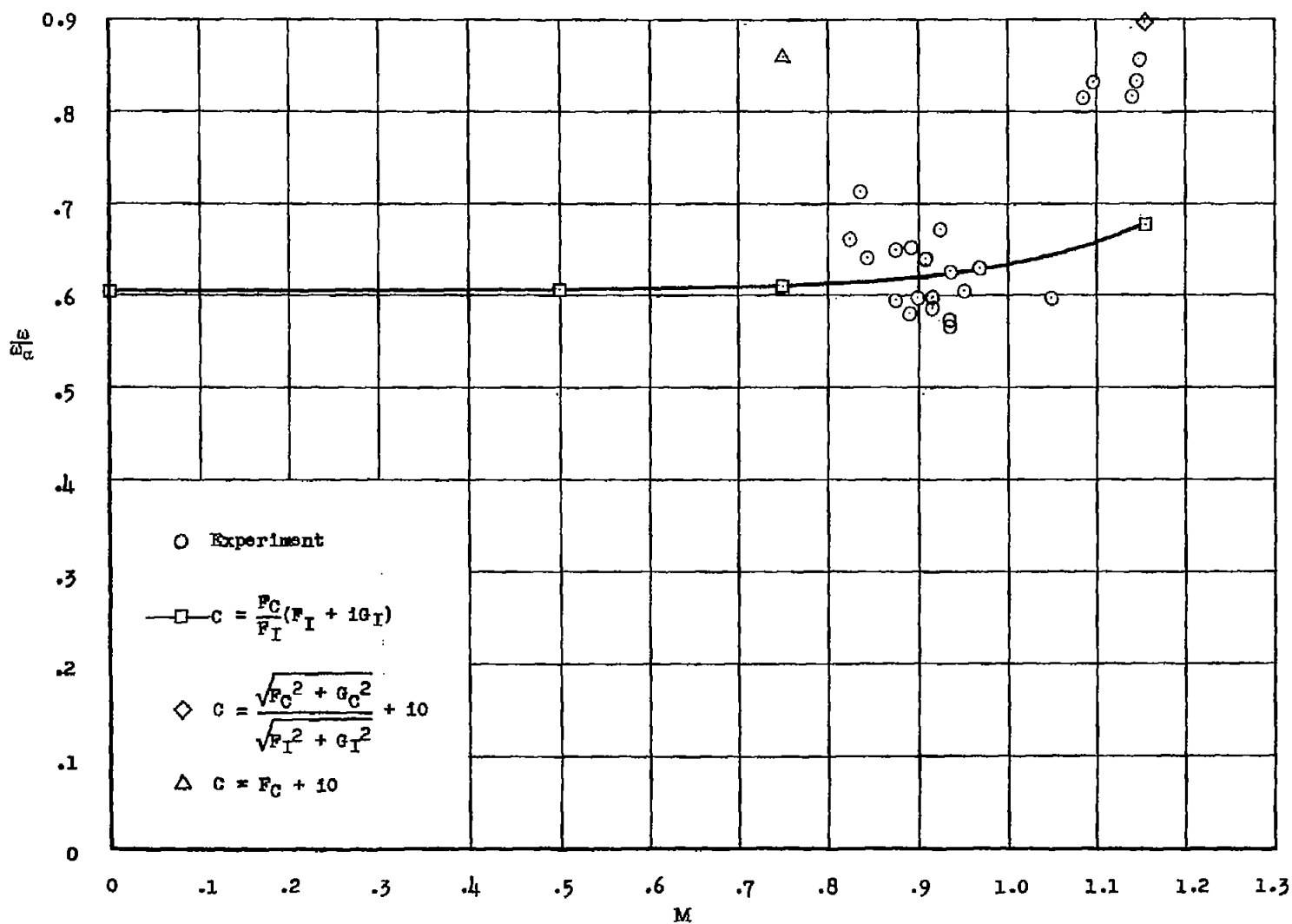Figure 8.- Variation of flutter speed with Mach number for wing 452. For calculated points ρ = 0.002700 slugs/cu ft.
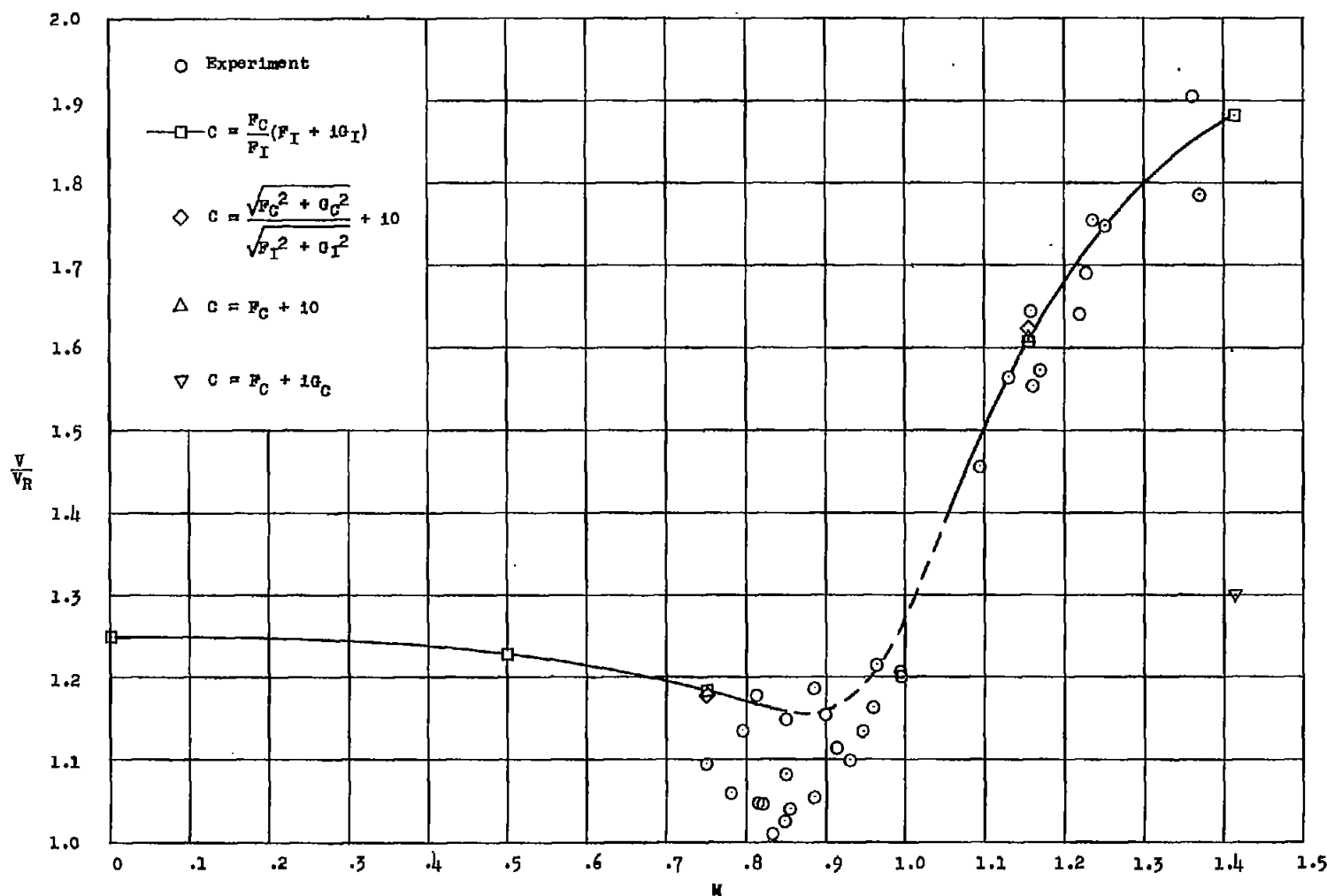
Figure 9.- Variation of flutter speed with Mach number for wing 430. For calculated points $\rho = 0.003700$ slugs/cu ft.
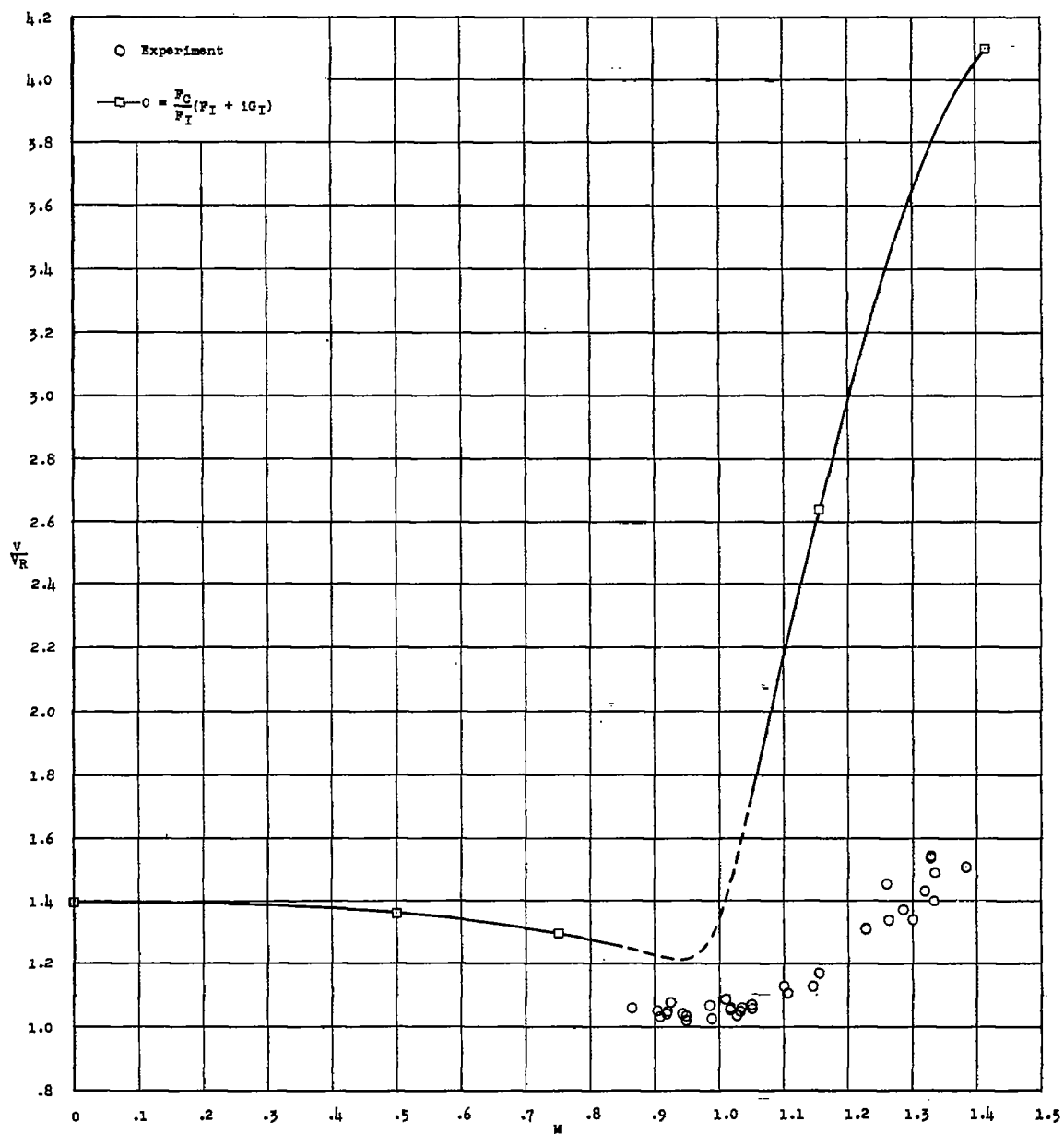
Figure 10.- Variation of flutter speed with Mach number for wing 400.
For calculated points $\rho = 0.002378$ slugs/cu ft.

Figure 11.- Variation of flutter speed with Mach number for wing 400R. For calculated points
ρ = 0.003100 slugs/cu ft.

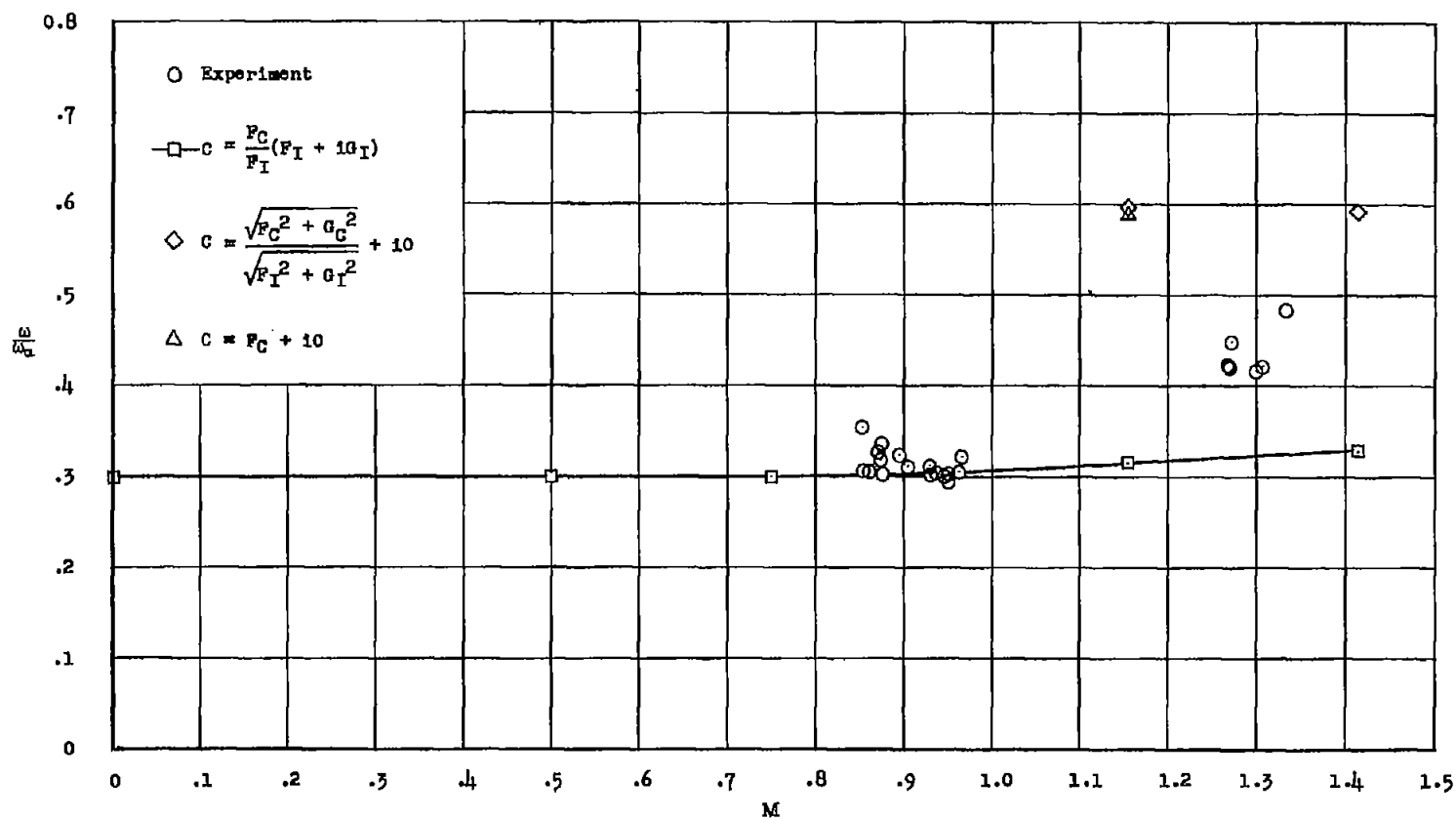Figure 12.- Variation of flutter speed with Mach number for wing 4451. For calculated points ρ = 0.003200 slugs/cu ft.

Figure 13.- Variation of flutter speed with Mach number for wing 4001. For calculated points $\rho = 0.002378$ slugs/cu ft.

Figure 14.- Variation of flutter speed with Mach number for wing 7001.
For calculated points $\rho = 0.005500$ slugs/cu ft.

Figure 15.- Variation of flutter frequency with Mach number for wing 445. For calculated points $\rho = 0.003800$ slugs/cu ft.
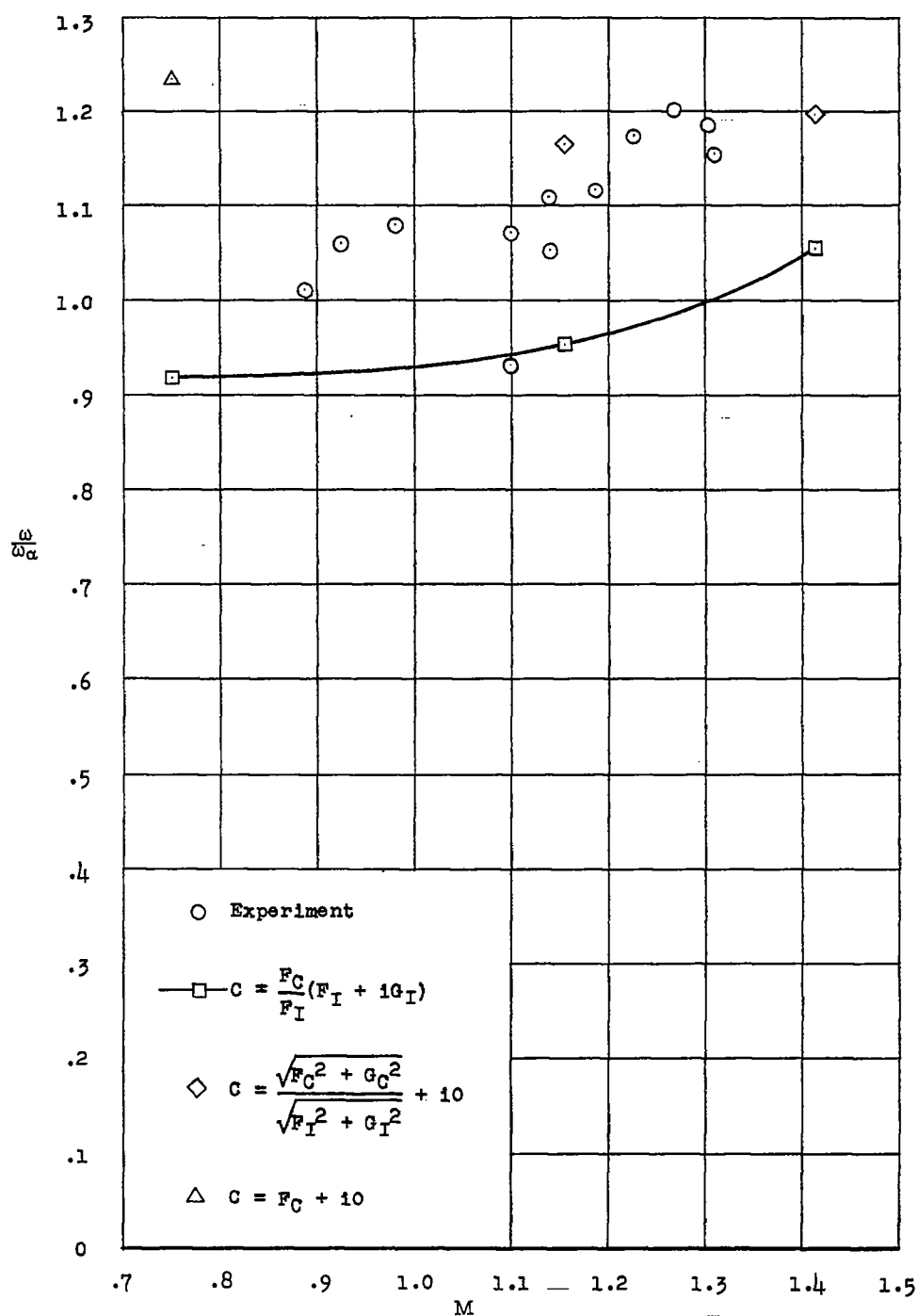
0.9

.8

.7

$\frac{\omega}{\omega_\alpha}$ .6

.5

.4

.3

.2

.1

0

O Experiment

—□— $c = \dfrac{F_C}{F_I}(F_I + iG_I)$

◇ $c = \dfrac{\sqrt{F_C{}^2 + G_C{}^2}}{\sqrt{F_I{}^2 + G_I{}^2}} + 10$

△ $c = F_C + 10$

0   .1   .2   .3   .4   .5   .6   .7   .8   .9   1.0   1.1   1.2   1.3

M

Figure 16.- Variation of flutter frequency with Mach number for wing 445F. For calculated points $\rho = 0.003000$ slugs/cu ft.

Figure 17.- Variation of flutter frequency with Mach number for wing 445R. For calculated points $\rho = 0.002378$ slugs/cu ft.

Figure 18.- Variation of flutter frequency with Mach number for
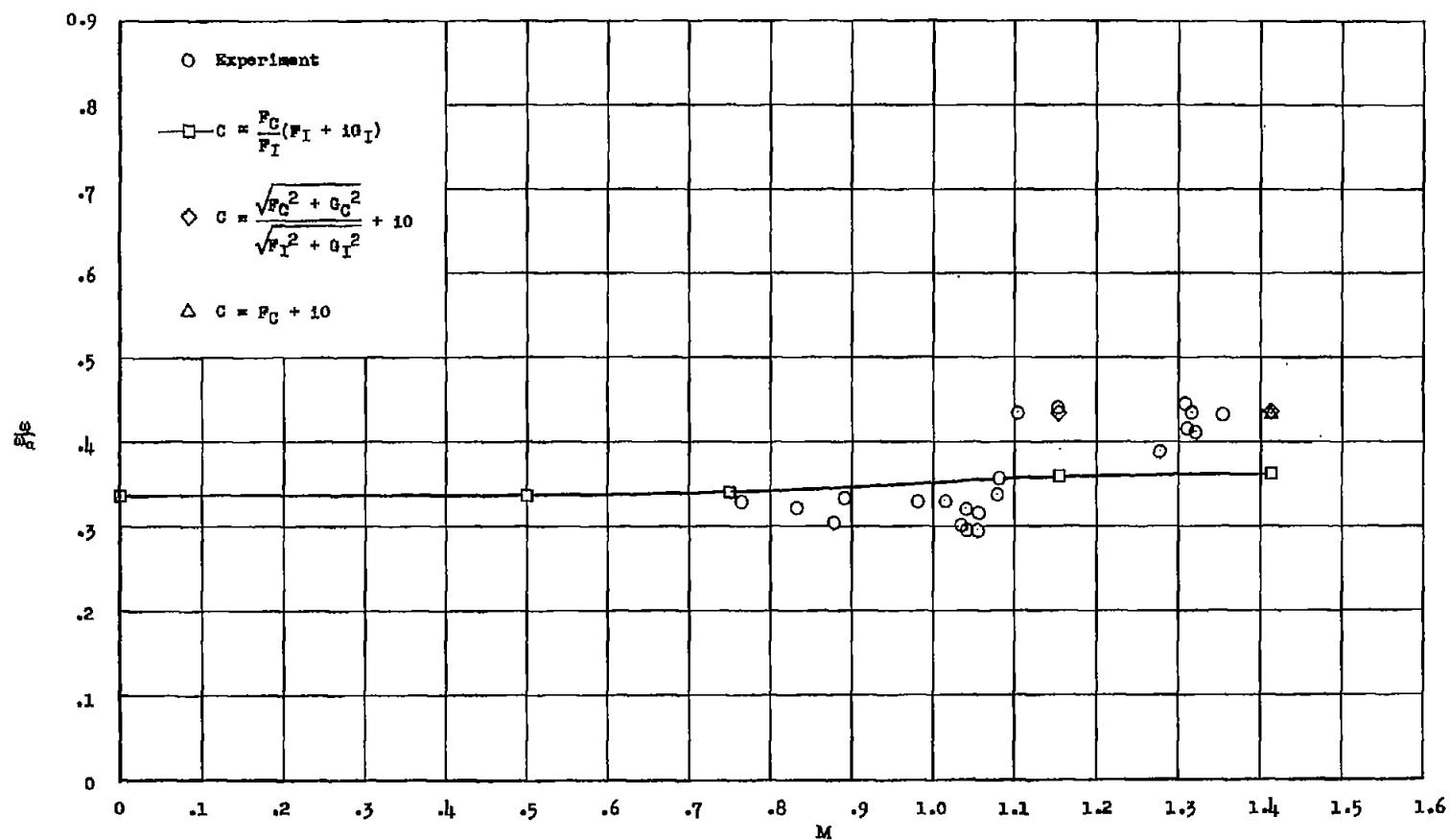wing 245. For calculated points $\rho = 0.003900$ slugs/cu ft.

Figure 19.- Variation of flutter frequency with Mach number for wing 645. For calculated points $\rho = 0.003500$ slugs/cu ft.
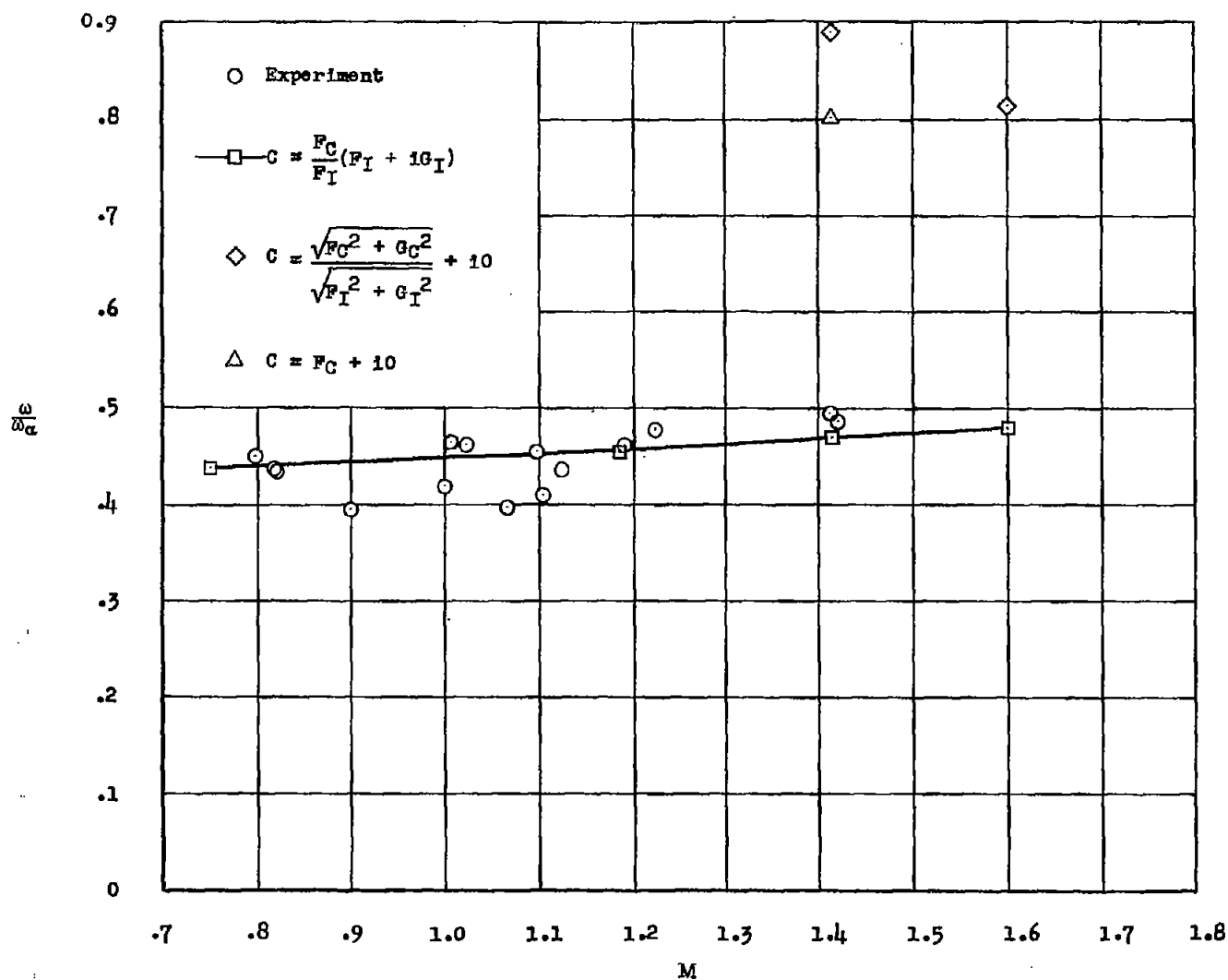
Figure 20.- Variation of flutter frequency with Mach number for wing 452. For calculated points ρ = 0.002700 slugs/cu ft.
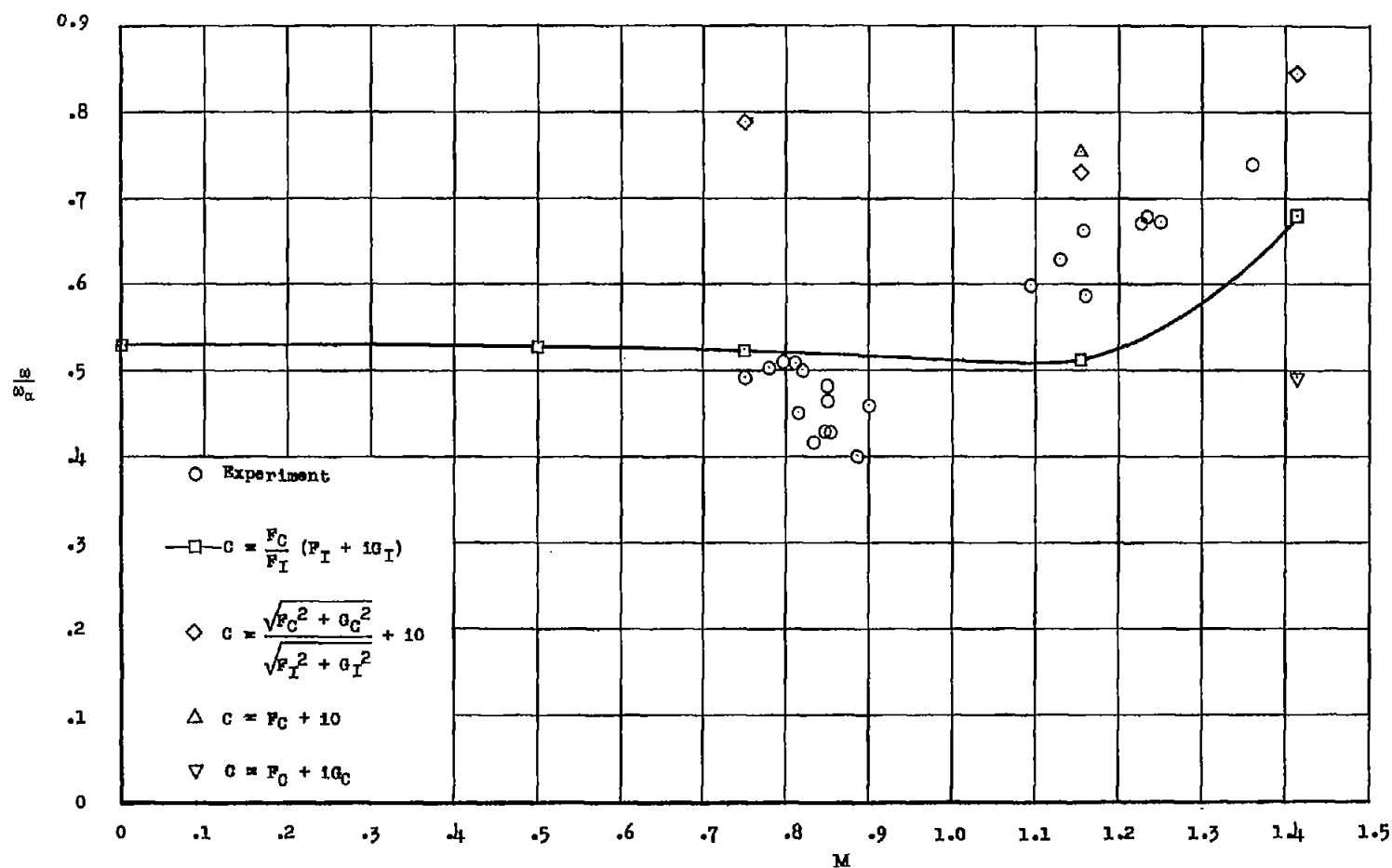
Figure 21.- Variation of flutter frequency with Mach number for wing 430. For calculated points $\rho = 0.003700$ slugs/cu ft.
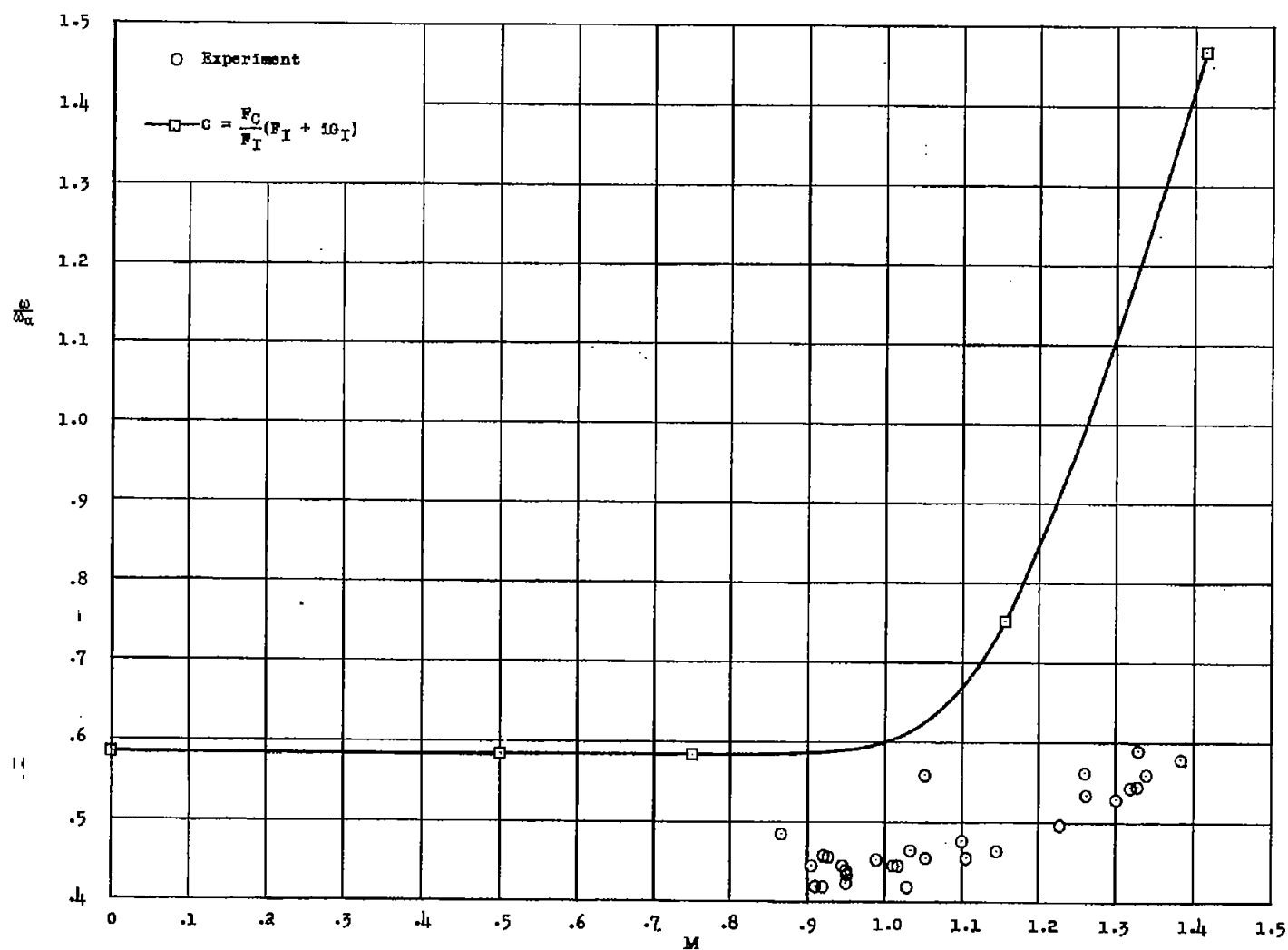
Figure 22.- Variation of flutter frequency with Mach number for wing 400. For calculated points
ρ = 0.002378 slugs/cu ft.